Accounting for the geometrical complexity of structural models in Voronoi-based meshing methods

PhD Thesis

Specialty Geosciences

Jeanne PELLERIN

Note that the original version of this thesis is written in French.

PhD defended the March 20, 2014.

Thesis committee:

Pascal Frey	Professor, Université Paris 06	Reviewer
Hamdi Tchelepi	Professor, Stanford University	Reviewer
Stephan Matthäi	Professor, University of Leoben	Examiner
Jean-François Remacle	Professor, Université de Louvain	Examiner
Jean Virieux	Professor, Université Grenoble 01	Examiner
Bruno Lévy	Research director, INRIA	Adviser
Guillaume Caumon	Professor, Université de Lorraine	Adviser
David Ledez	Total	Invited

To my parents,

Abstract

Depending on the specific method used to build a 3D structural model, and on the exact purpose of this model, its mesh must be adapted so that it enforces criteria on element types, maximum number of elements, and mesh quality. Meshing methods developed for applications others than geomodeling forbid any modification of the input model, that may be desirable in geomodeling to better control the number of elements in the final mesh and their quality.

The objective of this thesis is to develop meshing methods that fulfill this requirement to better manage the geometrical complexity of B-Rep geological structural models. An analysis of the sources of geometrical complexity in those models is first proposed. The introduced measures are a first step toward the definition of tools allowing objective comparisons of structural models and permit to characterize the model zones that are more complicated to mesh. We then introduce two original meshing methods based on Voronoi diagrams: the first for surface remeshing, the second for hybrid gridding. The key ideas of these methods are identical: (1) the use of a centroidal Voronoi optimization to have a globally controlled number of elements of good quality, and (2) combinatorial considerations to locally build the final mesh while sometimes modifying the initial model. The surface remeshing method is automatic and permits to simplify a model at a given resolution. The gridding method generates a hybrid volumetric mesh. Prisms and pyramids fill the very thin layers of the model while the remaining regions are filled with tetrahedra.

Contents

Introduction

From 2D models to 3D structural models

Understanding the 3D organization of subsurface rock units is crucial in domains such as the exploration, the exploitation, and the protection of natural resources: water, minerals, oil and gas. Except on outcrops, we cannot see the subsurface, and restricted information is available to understand its organization. That is often why a geological map is determined. This map gives at each point of Earth's surface the outcropping rock type (figure 1a). It is established by geologists from the interpolation of localized field observations. The depth organization of the rock units is characterized by vertical cross-sections. We can see that, in the area represented on figure 1b, subsurface rocks are organized in layers. These layers are separated by lines called horizons and are cut by faults. Layers 2, 3 et 4 are partly eroded. This current configuration is the result of an history that geologists reconstitute when they determine these maps and cross-sections (figure 2).

Geological maps and cross-sections are models of real settings, representing them schematically in two dimensions. However, subsurface rock organization is volumetric. The corresponding models are called structural models, they are 3D geological maps which give one rock type for each point of the subsurface (figure 3). Like a digital picture in which each pixel is associated to a color, a structural model may be cut into voxels, each of them being associated to a rock type (figure 3a). Another possibility is to only represent the surfaces (horizons, faults, erosions, *etc*) delimiting the different rock volumes. This boundary representation (B-Rep) allows the modeling of almost all natural complex configurations.

Goals of meshes in geomodeling

Whichever the representation of a structural model, a mesh is used to store and visualize this model on a computer. A mesh is a set of elementary geometrical shapes (squares, triangles, cubes, tetrahedra, *etc*) that do not intersect and which union approximate the studied object. It is defined by the vertices of these shapes and by the rules used to link these vertices. For example, the model on figure 3a is meshed by cubes. If the size of these cubes is too big, the image of the geological structures is, like a low resolution digital picture, not precise.

Meshes are also necessary to answer engineering problems, such as the evaluation of the impact of a tunnel on the stability of the surrounding rocks. Using the adequate physic theories, this problem can be transformed into a mathematical problem. In most cases, this mathematical problem cannot be solved, and a mesh is used to determine an approximated version of the problem that is then solved numerically. This
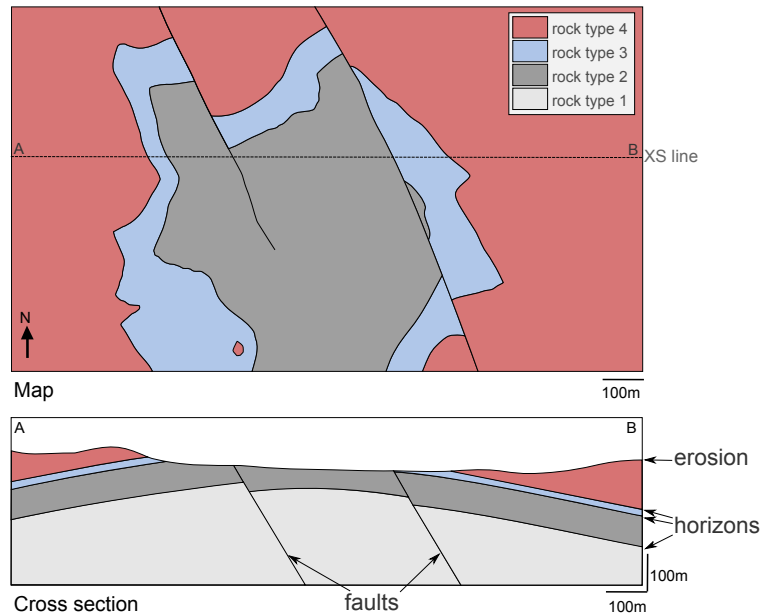
Figure 1: 2D MODELS: A MAP AND A CROSS SECTION. The map gives a top view on the outcropping rock type, while the cross section give a view on their depth organization. The lines (surfaces in 3D figure 3) delimiting two different layers are called horizons. These horizons are folded and cut by two faults. The erosion line determines the topography of the area.
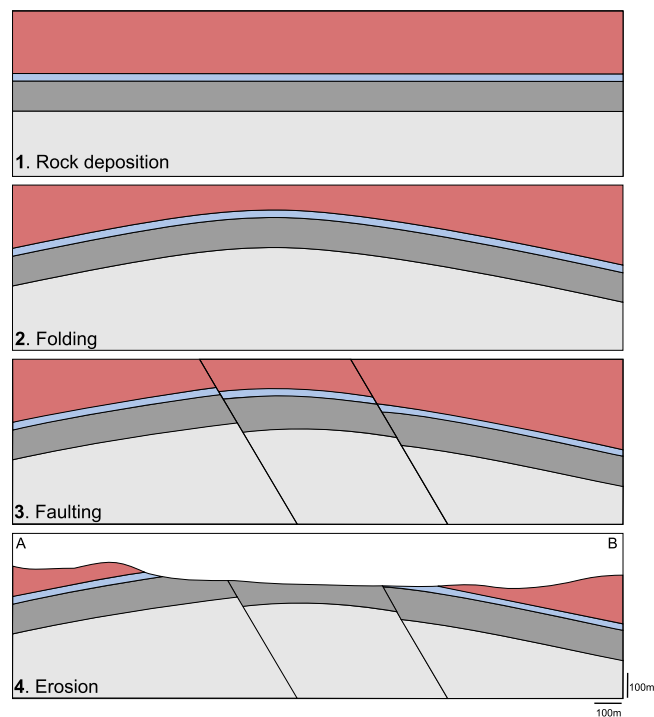
Figure 2: CROSS-SECTION VIEW ON THE DEFORMATIONS OF THE LAYERS FROM FIGURE 1 SINCE THEIR DEPOSITION.
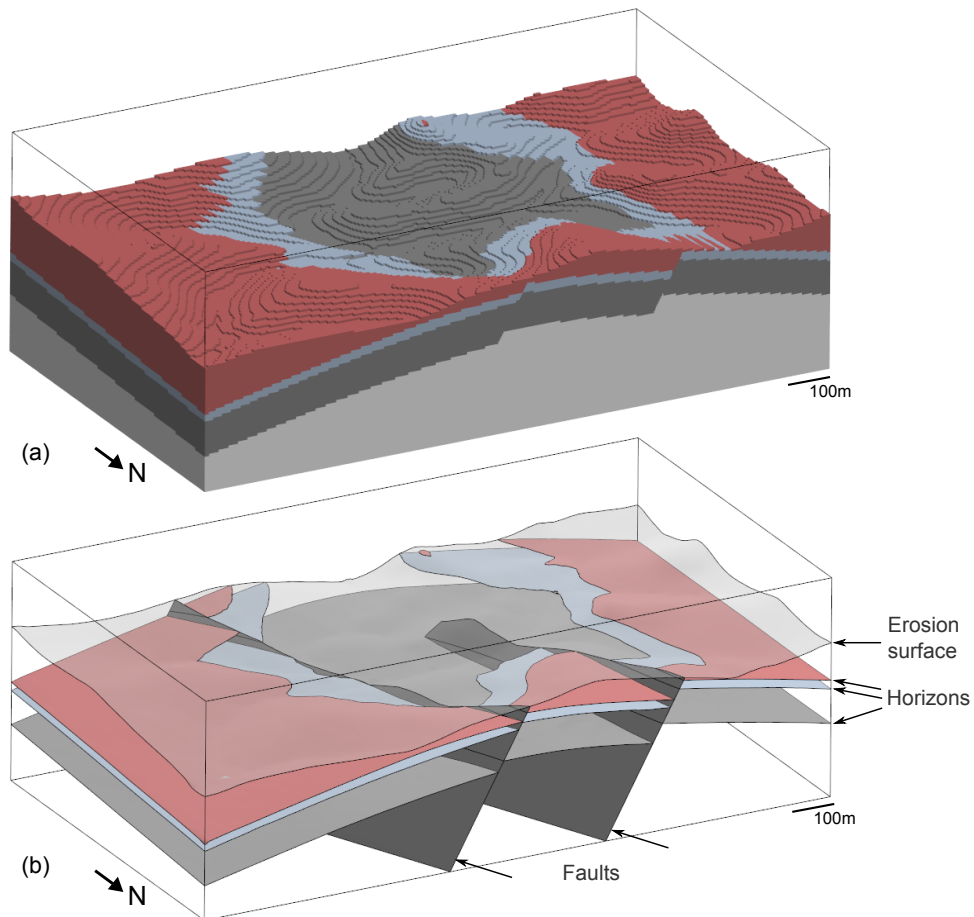
Figure 3: TWO REPRESENTATIONS FOR A 3D STRUCTURAL MODEL. This synthetic model corresponds to the map and the cross-section from figure 1. (a) Volumetric representation: the model is cut into cubes, each one having the color of the associated rock unit. (b) Boundary representation: only the surfaces delimiting rock units are represented. The surfaces delimiting the area of interest (box) are not displayed.
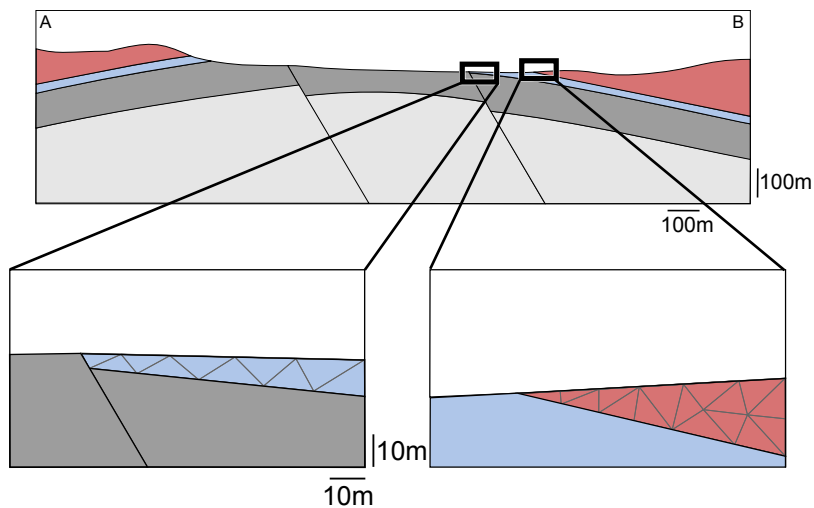
Figure 4: TWO CHALLENGES FOR STRUCTURAL MODEL MESHING. (a) The blue layer is very thin and cannot be meshed with triangles whose edge lengths are above 5m in this area. (b) The angle in the red layer is 16 degrees, so to respect its the layer boundaries at least one triangle in the mesh must have an angle of 16 degrees.

is the second objective of meshes : allow numerical simulations aiming at mimicking a natural behavior.

Challenges for mesh generation

When the hypotheses on which rely the transformation of the engineering problem to the numerical simulation result are not verified, this result may be significantly different from the real behavior. To obtain reliable results in a reasonable time, the mesh must represent the model precisely enough and respect a set of quality criteria on the number, aspect, and size of its elements. These two requirements are contradictory. It is not always possible to mesh all model components having an impact on the solution and, at the same time, respect these quality criteria. For example, a model in which a layer has locally a thickness of 5m cannot be meshed with triangles that have edges measuring at least 10m (figure 4a). Similarly it will not be possible to generate elements with angles above 30 degrees if the model contains an angle of 16 degrees (figure 4b).

In those cases, a choice must be made to obtain the best compromise between the precision, reliability, and robustness of the results, and the memory needs, and computational time. A priori, decreasing the constraints on mesh quality (greater number of elements, smaller elements) increases computational time and memory needs, but increases the result precision. Modifying the model geometry (lower level of detail) allows meshing it with less elements while simplifying components that may have a negative effect on the numerical solution, but the risk is to decrease the result precision. Ideally, to take a decision, results obtained for different meshes for different model resolutions should be compared. This requires to have automatic tools to (1) modify and mesh a model at a given resolution with elements having the desired quality, and (2) evaluate the differences between the result and the real behavior. This thesis is related to the first point and gives possible answers to the following questions:
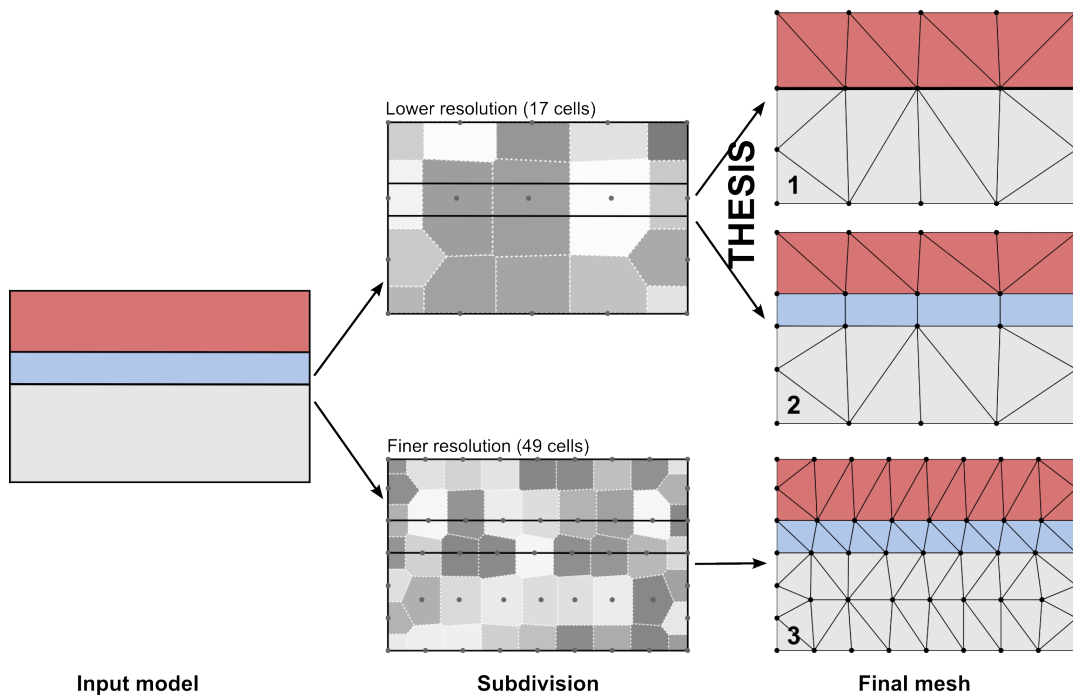
Figure 5: USE OF A VORONOI DIAGRAM SUBDIVISION TO ANALYZE, MODIFY AND MESH A BOUNDARY MODEL. This thesis focuses on the building of a mesh in the cases where the model subdivision by the Voronoi diagram is coarse, i.e. when the intersections with model boundaries may be complex. The objective is to generate either a mesh of the simplified model (1) or a mesh of the initial model (2) in which the number of elements is controlled.

- How to characterize the level of detail of a geological model in three dimensions and how to identify its small characteristics ?

- How to automatically modify the level of detail of a model and simplify its small characteristics ?

- How to mesh a model (surfaces and volumes) when the required elements size is bigger than the model resolution ?

Strategy

We use a subdivision of the model by a Voronoi diagram to analyze its geometry and its connectivity, and to generate a mesh of its surfaces and volumetric regions (figure 5). A Voronoi diagram is defined for a set of points, to each point it associates the part of the model (the Voronoi cell) closer to this point than to any other point. From the Voronoi diagram and its intersections with the model boundaries a meshes of the surfaces and of the volumetric regions can be built (figure 5).

We propose strategies to build a mesh in all possible configurations for the intersections of a model with a Voronoi diagram. Indeed, according to the Voronoi cell resolution, the intersections with the model boundaries are more or less complicated (figure 5). This approach allows us to control the number of elements in the final mesh and to modify the model (figure 5). The difference between the model resolution and the mesh resolution can thus be reduced.

After the definitions of the geometrical objects on which this work is based (chapter 1), we describe the objectives of meshes and the available meshing methods (chapter 2). In chapter 3, we propose measures of the geometrical complexity of structural models. Then we propose a surface remeshing method (chapter 4) that permits to control the number of elements in the mesh, to simplify the model, and to generate triangles as equilateral as possible. This method is extended in chapter 5 to generate a hybrid volumetric mesh of a structural model. Prisms and pyramids are used to fill the thin layers of the model, while the rest of it is meshed with tetrahedra.

Contributions

The contributions presented in this thesis are:

- measures helping the identification of small geometrical characteristics in geological models. They are described in chapter 3. This work is not published at this time.

- a mesh building method to remesh the surfaces defining a boundary model from the intersection of a Voronoi diagram with these boundaries. This work is presented in chapter 4, and published in Pellerin *et al.* [2014], a preliminary version was presented in Pellerin *et al.* [2011] ;

- a strategy to build a hybrid mesh (prisms, pyramids et tetrahedra) of the regions of a boundary model from a Voronoi diagram and its intersections with the model boundaries that is described in chapter 5. A short version of this work was presented in Pellerin *et al.* [2012].

Publications

J. Pellerin, B. Lévy et G. Caumon : Topological control for isotropic remeshing of nonmanifold surfaces with varying resolution: application to 3D structural models. *In Proc. IAMG.* cogeo@oeaw-giscience, sept. 2011.

J. Pellerin, B. Lévy et G. Caumon : A Voronoi-based hybrid meshing method. *In International Meshing Roundtable, Research Notes*, oct. 2012.

J. Pellerin, B. Lévy, G. Caumon et A. Botella : Automatic surface remeshing of 3D structural models at specified resolution: A method based on Voronoi diagrams. *Computers & Geosciences*, 62(0):103 – 116, 2014.

Chapter 1

Fundamental geometrical objects

In this chapter we define the geometrical objects that are used by many meshing methods and on which this work is based. They are related to the Voronoi diagram, a fundamental structure of geometry, see Aurenhammer [1991] and Okabe *et al.* [2009].

1.1 Voronoi diagram and Delaunay triangulation

1.1.1 Voronoi diagram

A Voronoi diagram [Voronoï, 1908] is a space subdivision into several regions defined from a set of points, called sites and denoted S. Each site, $p \in S$, corresponds to one region, called Voronoi cell, that includes all the points of the space that are closer of this site p than to any other site q (figure 1.1). Formally, when the considered space is $\mathbb{R}^2$, and when the proximity between a point x and a site p is measured by the Euclidean distance between these two points $||x - p||$, the Voronoi cell of p is defined by:

$$V_p = \{x \in R^2, ||x - p|| \leq ||x - q||, q \in S\} \tag{1.1}$$

The set of the Voronoi cells is the Voronoi diagram of S (figure 1.1a). Voronoi cells are convex closed polygons that are bounded or not, and cover the space without overlapping. Their edges, called Voronoi edges, are the points equidistant from two neighboring sites. Cell vertices, or Voronoi vertices, are the points equidistant from three neighboring sites (figure 1.2). These definitions can be generalized to higher dimensions. In this thesis, we stop at three, in $\mathbb{R}^3$, the regions corresponding to the sites are polyhedra (figure 1.3). Their facets, Voronoi facets, are the points equidistant from two neighbor sites; they are included in the mid plane of these two sites. Edges are shared by three Voronoi cells and vertices by four cells (figure 1.4a).

It is important to note that the above given definition is only correct when all sites S are in general position, i.e. there is no four cocircular sites, and no five cospherical points. These degenerated cases disappear with an extremely small perturbation of site positions, that may only be symbolic [Edelsbrunner et Mücke, 1990]. In the following of this thesis, we assume that the sites are in general position.

Remark : A lot of Voronoi diagram generalizations have bee developed changing the distance measure between two points, changing site nature *etc*, see the reviews of
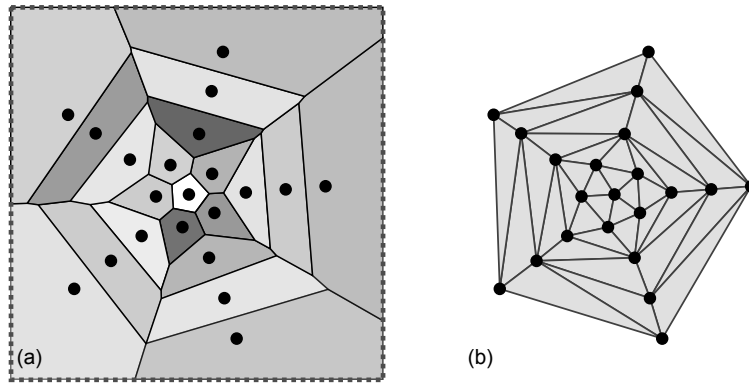
Figure 1.1: Voronoi diagram and corresponding Delaunay triangulation in the plane. (a) The Voronoi diagram of the 21 sites (black dots) is a set of 21 convex polygons that covers the plane, the 5 cells intersecting the border are indeed infinite. (b) The corresponding Delaunay triangulation triangulates the convex envelope of the sites.
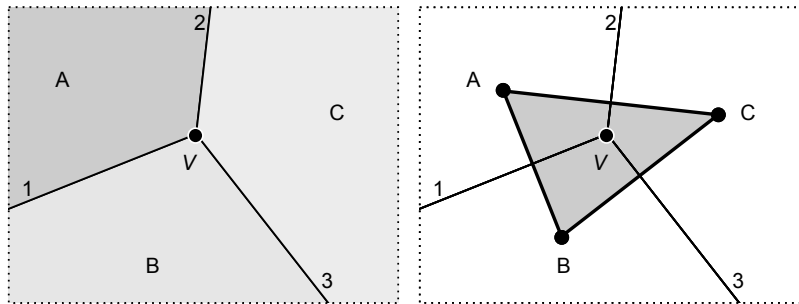
Figure 1.2: 2D Voronoi-Delaunay dual relationship. Voronoi vertex V is shared by three Voronoi cells: A, B, and C. It corresponds to a Delaunay triangle ABC, which vertices are sites and which edges correspond to Voronoi edges (number 1 to 3).

[Okabe *et al.*, 2009] and Aurenhammer [1991]. It is also possible to work in non Euclidean spaces, for example the one defined by a surface embedded in a 3D space.

1.1.2 Delaunay triangulation

A second object extremely interesting in a meshing context can be built from a Voronoi diagram: the Delaunay triangulation. We saw that, in the plane, in general position, each Voronoi vertex is equidistant from three sites. The triangle connecting these sites is a Delaunay triangle and the Delaunay triangulation is the set of the triangles corresponding to Voronoi vertices (figure 1.1b). The Delaunay triangulation of sites S is said dual of the Voronoi diagram of sites S because, to each Voronoi cell corresponds a triangulation vertex, to each Voronoi edge corresponds a triangulation edge, and to each Voronoi vertex corresponds a Delaunay triangle (figure 1.2). Delaunay triangulation definition can also be generalized in higher dimensions. In a three dimensional space, Delaunay tetrahedralization has one edge for each Voronoi facet, one triangle for each Voronoi edge and one tetrahedron for each Voronoi vertex (figure 1.4).

The Delaunay triangulation of a point set S is also defined independently of the Voronoi diagram by the empty ball or Delaunay criteria [Delaunay, 1934] that states that, in $\mathbb{R}^2$, a triangle is Delaunay if its circumscribed circle does not contain any
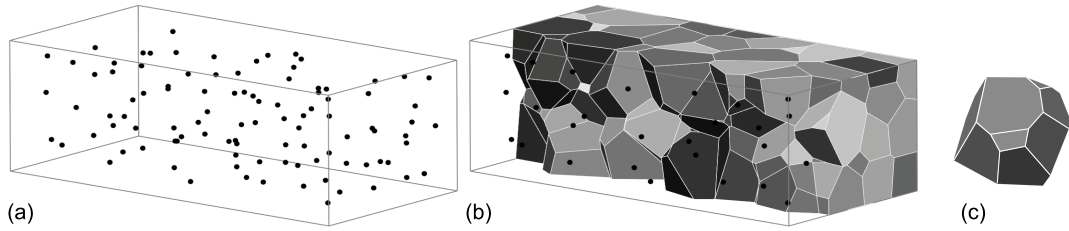
Figure 1.3: 3D Voronoi diagram. (a) 200 sites are distributed in a box. (b) Solid slice in the Voronoi diagram of the sites cut by the box. (c) One Voronoi cell.
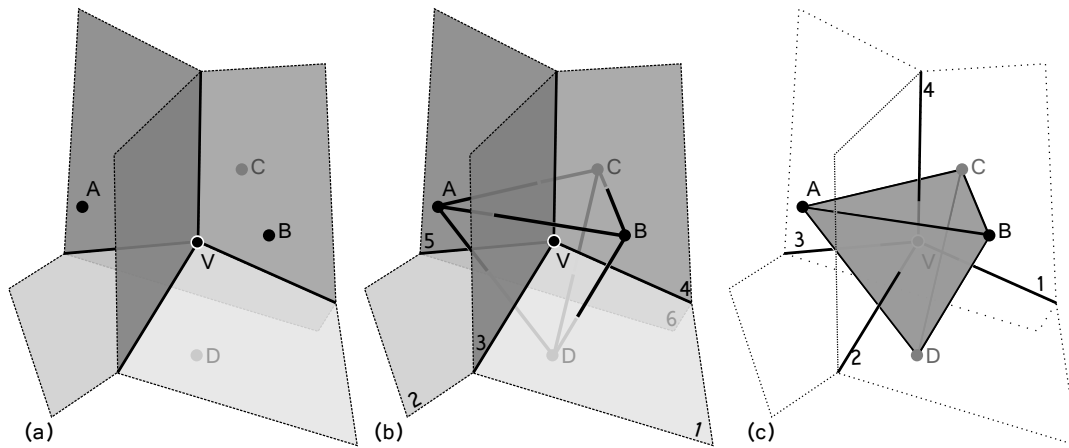
Figure 1.4: 3D Voronoi-Delaunay dual relationship. (a) Voronoi vertex V is equidistant from the sites of cells A, B, C and D. (b) To each Voronoi facet containing V (numbers 1 to 6) corresponds one segment linking the sites of the 2 cells sharing the facet. (c) To each Voronoi edge containing V (numbers 1 to 4) corresponds a triangle linking the sites of the 3 cells sharing this edge.

other point of S than its own vertices. The mathematical properties of Delaunay triangulation made it a favored object of study in meshing (partie 2.3).

1. The open circumscribed balls to Delaunay triangulation simplices[1] do not contain any point of S. This empty ball (also called Delaunay) criterion is connected with a lemma that gives that, for any triangulation of S, if the empty ball criterion is true for each pair of adjacent elements, then it is true for all its elements [Delaunay, 1934].

2. For any point set S in general position, its Delaunay triangulation exists and is unique.

3. The Delaunay triangulation maximizes the minimal angle of the triangulation of S.

1.1.3 Voronoi diagram computation

Computing the Voronoi diagram of a point set can be done either directly, or by computing the dual Delaunay triangulation. See the reviews of Fortune [1992], Okabe et al. [2009], Boissonnat et Yvinec [1995] for a description of the main methods, and the implementations of TetGen[2] or CGAL[3].

1.2 Restricted Voronoi diagram and restricted Delaunay triangulation

1.2.1 Restricted Voronoi diagram

Definitions

A Voronoi diagram subdivides the space in which it is defined into convex regions. So it also subdivides any object included in that space. This subdivision is called the restricted Voronoi diagram. For a set of sites S and an object Ω the restricted Voronoi diagram is defined as the intersection of the Voronoi diagram of S with Ω[4]. Two examples are given figures 1.5b and 1.5e. The intersection of a Voronoi cell, V_p, with the object Ω is called the restricted Voronoi cell of p to Ω and is defined by $V_{p\cap\Omega} = V_p \cap \Omega$. Restricted cell dimension depends on the object dimension, restricted cells to the star are surfaces (figure1.5b), while restricted cells to its contour are lines (figure 1.5e).

The intersection of a Voronoi edge with the object is a restricted Voronoi edge, the intersection of a Voronoi facet with the object is a restricted Voronoi facet, and the intersection of a Voronoi vertex and the object is a restricted Voronoi vertex. To the contrary of Voronoi diagram elements, the ones of a restricted Voronoi diagram do not always have only one connected component, i.e. there are at least two points in the same element that cannot be connected by a path included in that element. For

---

[1]Triangles in $\mathbb{R}^2$ and tetrahedra in $\mathbb{R}^3$.

[2]http://wias-berlin.de/software/tetgen/

[3]http://www.cgal.org/

[4]In other papers, when the object and the space containing it have the same dimension (figure 1.5c) the restricted Voronoi diagram is also called clipped Voronoi diagram.
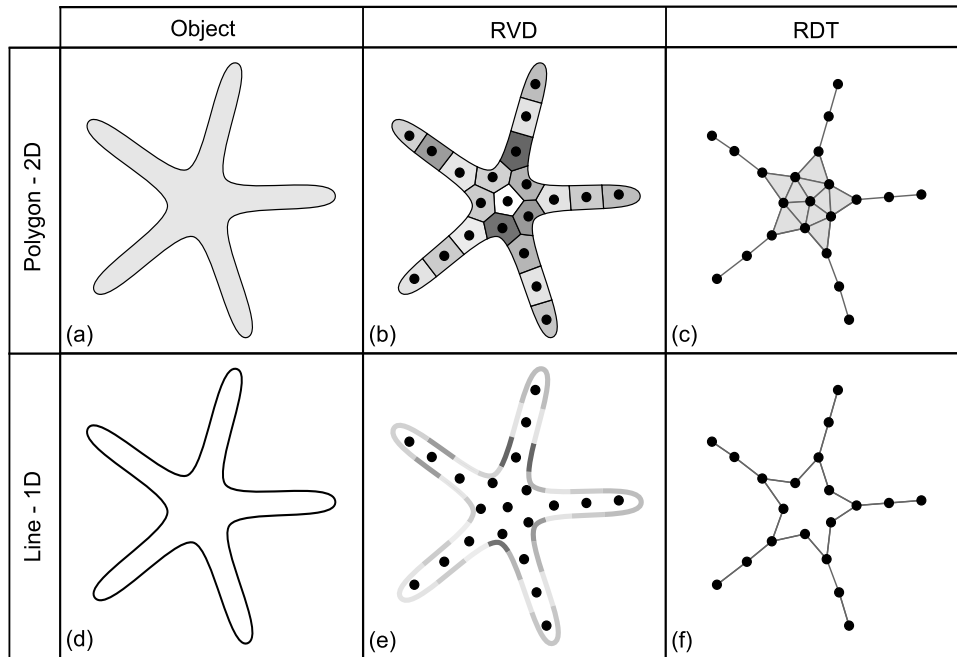
Figure 1.5: RESTRICTED VORONOI DIAGRAM AND RESTRICTED DELAUNAY TRIANGULATION. (b) Restricted Voronoi diagram to a star (a). (c) The corresponding restricted Delaunay triangulation meshes the star. (e) Restricted Voronoi diagram to the star contour (d). (f) The corresponding restricted Delaunay triangulation is a sub-set of the one for the star (c). As the Voronoi cell of the site at the star center does not intersect the contour, the restricted Delaunay triangulation does not contain this site.

example, for the restricted Voronoi diagram to the star contour, figure 1.5e, restricted cell in star branch center have two connected components- two segments.

Degenerated cases

On the star example, figure 1.5, restricted Voronoi cell dimension is the same one than the star's, that is three. This equality is only true if degenerated intersections between the Voronoi cell and the object, i.e. intersections restricted to a unique point or to an edge, are excluded (figure 1.6). This should also be true for the intersections of all Voronoi diagram elements (cell, facet, edge, and vertex) with the object. In a d dimensional space, a Voronoi diagram element of dimension l generically intersects an object of dimension m, if this intersection has the expected dimension: $m + l - d$. In $\mathbb{R}^3$, intersections of Voronoi cells, facets, edges, vertices with a surface must respectively be of dimension two (surface parts), one (line parts), zero (points), and empty [Edelsbrunner et Shah, 1997]. The intersections between a Voronoi vertex and any line or surface are excluded. According to Edelsbrunner et Shah [1997], these assumptions are reasonable and we suppose them true in this thesis. Nevertheless we will see at the end of chapter 4 that the most part of issues encountered when computing a mesh from a restricted Voronoi diagram are connected with configurations close to degenerated ones.
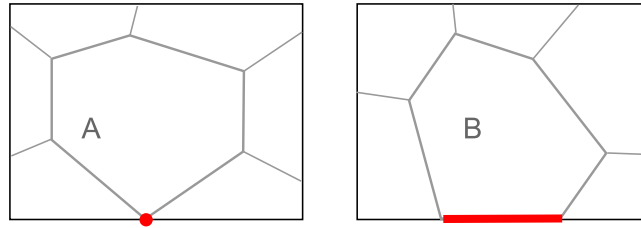
Figure 1.6: Degenerated intersections between a Voronoi cell and a rectangle. Cell A intersects the rectangle at a unique point. Cell B intersects the rectangle along one of its edges.

1.2.2   Restricted Voronoi diagram computation

When the object is defined by its boundaries, the computation of its intersection with a Voronoi diagram is complex. Lévy et Liu [2010] propose a method valid for volumes defined by their boundary surface in 3D, but it lacks robustness to degenerated configurations [Merland, 2013]. When the object is meshed, the restricted Voronoi diagram computation is easier.

In this thesis, we are interested by the restricted Voronoi diagram to a 3D surface. To compute it, we use the method originally developed by Yan *et al.* [2009], that was improved by Nivoliers [2012]. The fundamental operation is to compute the intersection between one surface triangle and one Voronoi cell. As a Voronoi cell can be defined by the intersection of mid planes between its site and its closest neighbor sites, it is sufficient to cut the triangle by each of these planes. To compute only once the intersection between one triangle and one Voronoi cell and improve the performances two propagations strategies through triangle-site pairs are possible, they are detailed by Nivoliers [2012].

1.2.3   Restricted Delaunay triangulation

Restricted Delaunay triangulation is defined as the restricted Voronoi diagram dual, similarly to the dual definition of the Delaunay triangulation. In $\mathbb{R}^2$, the restricted Delaunay triangulation has one vertex for each restricted cell, one segment for each restricted edge, and one triangle for each restricted Voronoi vertex (figures 1.5c and f).

A restricted Delaunay triangulation is then constituted of the Delaunay triangulation elements that are dual of Voronoi diagram elements intersecting the considered object. Its triangles, edges, and vertices (figure 1.5c) are a subset of the Delaunay triangulation (figure 1.1). Indeed, the restricted Voronoi diagram is by definition a subset of the Voronoi diagram.

Let's consider the restricted Voronoi diagrams to two objects A and B such that A is included in B. The restricted Voronoi diagram to A is a subset of the restricted Voronoi diagram to B and the same is true for the restricted Delaunay triangulations. So, the same sites can be used to conformably triangulate, i.e. the interiors of the two triangulations do not intersect, two objects of possibly different dimensions. For example, segments of the restricted Delaunay triangulation to the star contour (figure 1.5f) are included in the restricted Delaunay triangulation to the star (figure 1.5c).

When restricted Delaunay triangulation elements are not in the boundary of an
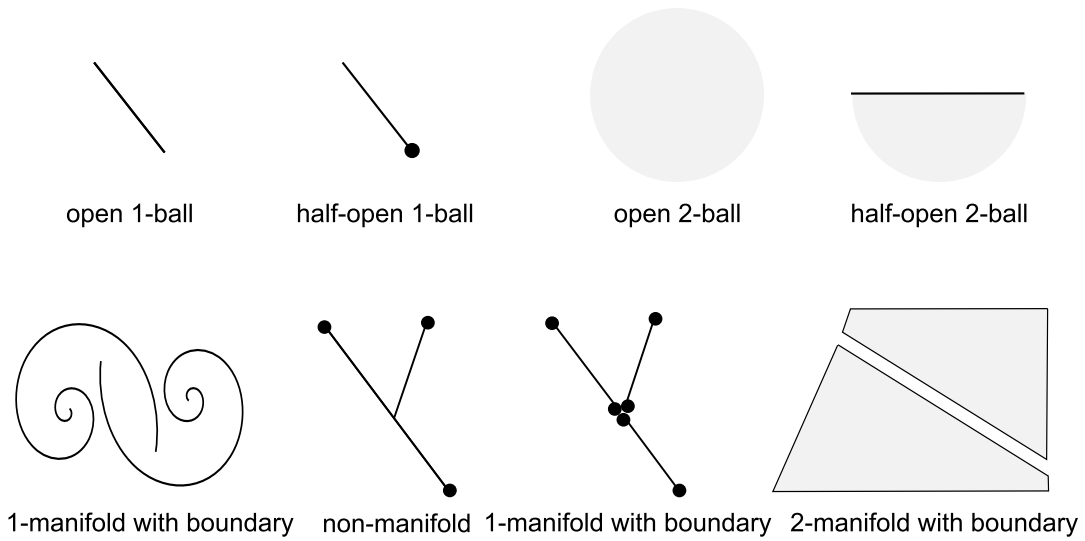
Figure 1.7: TOPOLOGICAL BALLS AND MANIFOLD SPACES IN THE PLANE.

element of higher dimension, for example segments in star branches, figure 1.5c, the restricted Delaunay triangulation is then a multi-dimensional object that may be seen as a simplified version of the initial object.

1.2.4   Restricted Delaunay triangulation topology

The topological ball property introduced by Edelsbrunner et Shah [1997], give a criterion to guarantee that the restricted Delaunay triangulation has the same topology (is homeomorphic) than the input object and is not a simplified version of it.

Preliminary definitions

Two topological spaces X and Y are homeomorphic, if a continuous bijective application from X to Y which inverse is continuous exists. An open k-ball is a space homeomorphic to $\mathbb{R}^k$ (figure 1.7). A open k-half ball is a space homeomorphic to the half space $\mathbb{H}^k = \{x = (\xi_i) \in \mathbb{R}^k \mid \xi_i \geq 0\}$. A closed k-ball is a space homeomorphic to $\mathbb{B}^k = \{x \in \mathbb{R}^k \mid ||x - O|| \leq 1\}$. The neighborhood of a subset Y included in X is a subset of X that contains Y. The space X included in $\mathbb{R}^d$ is k-manifold without boundary if all its points have an open k-ball neighborhood, it is an open k-manifold with boundary if all its points have a k-ball or a k-half ball neighborhood (figure 1.7). The set of points that do not have an open k-ball neighborhood is the boundary of X, and the set of points that do constitute its interior.

Topological ball property

A finite non-degenerated point set of $\mathbb{R}^d$, S, has the topological ball property [Edelsbrunner et Shah, 1997] for the bounded closed m-manifold, $\mathsf{X} \subseteq \mathbb{R}^d$, if for each $l \leq m$ and each subset of $m + 1 - l$ points $T \subseteq S$:

- the intersection between X and the points shared by the Voronoi cells of sites T is either empty, or a closed l-ball;
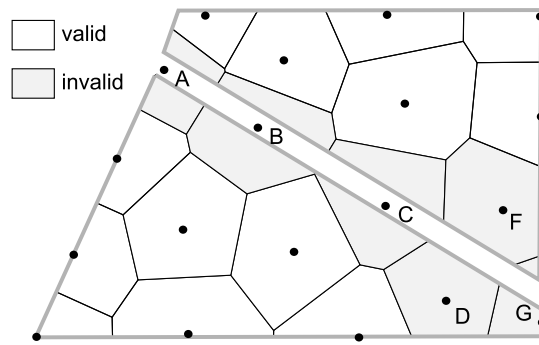
Figure 1.8: Voronoi cells verifying or not the topological ball property. Cells A, B, C, G have two connected components. Cells D and F are disks, but their intersection with the model boundaries (gray line) have two connected components.

- the intersection between X boundary and the points shared by the Voronoi cells of sites T is either empty, or a closed $l-1$-ball.

This means that a non-degenerated point set S has the topological ball property for a manifold surface Ω embedded in $\mathbb{R}^3$ if: all restricted Voronoi cells (respectively facets and edges) of S to Ω are closed 2-balls, (respectively 1-balls and points) and if all restricted Voronoi cells (respectively facets and edges) of S to Ω boundary are closed 1-balls (respectively points and the empty space) (figure1.8).

The theorem proved by Edelsbrunner et Shah [1997] gives that: for a compact manifold $X \subseteq \mathbb{R}^d$ with or without border, and for a finite non-degenerated point set $S \subseteq \mathbb{R}^d$ which Voronoi diagram intersects X generically; if S has the topological ball property for X then the restricted Delaunay triangulation of S to X is homeomorphic to X. A generalization to non-manifold spaces is also proposed in that paper, it is however much less used.

Epsilon sampling

Introduced by Amenta et Bern [1999], the ϵ-sampling theory gives a geometrical mean to guarantee that a point set has the topological ball property for a surface. Its definition is based on the medial axis notion. The medial axis of an object is the set of points that have more than one closest point on the border of the object. The *lfs*, for local feature size, is defined by Amenta et Bern [1999] as the minimal (Euclidean) to the medial axis (or surface of the object)[5]. A point set S is an ϵ-sampling of the manifold surface Ω if for each points x of Ω, there is a point of S at a distance inferior to $\varepsilon \times lfs(x)$. When $\varepsilon < 0.1$, Amenta et Bern [1999] show then that S has the topological ball property for the surface Ω.

The exact computation of the medial axis and so the computation of the *lfs* is a complicated problem (see for example Attali *et al.* [2009]) and remains a research subject. It is however possible to determine an approximation from the vertices of the Voronoi diagram of a dense enough point set sampling the object.

---

[5]A fist version of *lfs* was proposed Ruppert [1995].

1.3   Voronoi diagram optimization

Space subdivision into Voronoi cells determined from sites randomly distributed is also random, and its optimization appears in numerous statistics, image processing, or mesh generation problems. The goal is then to optimize site placement to reach a specific objective, for example, minimize the distances between each one of the sites and points inside their Voronoi cell. This optimization tends toward a specific Voronoi diagram: a centroidal Voronoi diagram.

1.3.1   Centroidal Voronoi diagram

The Voronoi diagram of a site set is centroidal if each site is at the centroid $p*$ of its Voronoi cell V_p:

$$p* = \frac{\int_{V_p} y dy}{\int_{V_p} dy} \tag{1.2}$$

When a density function ρ is defined, the centroid becomes:

$$p* = \frac{\int_{V_p} y\rho(y)dy}{\int_{V_p} \rho(y)dy} \tag{1.3}$$

Let's consider the problem of the computation of the partition of a domain Ω in k regions Ω_i and the positions of k points s_i that minimizes the function:

$$F((s_i, \Omega_i)_{i=1...k}) = \sum_{i=1}^{k} \int_{y \in \Omega_i} \rho(y)||y - s_i||^2 dy \tag{1.4}$$

This function evaluates the sum of the square distance between points s_i and points of the region Ω_i with the same index. Du *et al.* [1999] show that, to minimize this function, it is necessary that the regions Ω_i are the Voronoi cells of points s_i and that each point must be at the centroid of its Voronoi cell. They also show that this function has the same minimums than the function:

$$F_{CVT}((s_i)_{i=1...k}) = \sum_{i=1}^{k} \int_{y \in V_i} \rho(y)||y - s_i||^2 dy \tag{1.5}$$

where V_i is the Voronoi cell corresponding to point s_i. Function F_{CVT} parameters are only point positions, the integration being done on the Voronoi cells V_i. To compute a centroidal Voronoi diagram it is then sufficient to minimize this function of the site positions. In practice, it is very difficult to obtain a global minimum, and a local minimum is often considered satisfactory.

Remark : In the same space, for a given number of sites, there are several centroidal Voronoi diagrams, all of them minimizing the function F_{CVT}.

1.3.2   Centroidal restricted Voronoi diagram

The restricted Voronoi diagram of a point set S to a domain Ω is centroidal if each site p is at the centroid of its restricted Voronoi cell. A property, similar to the one of the classical centroidal Voronoi diagram, is established by integrating function F_{CVT}
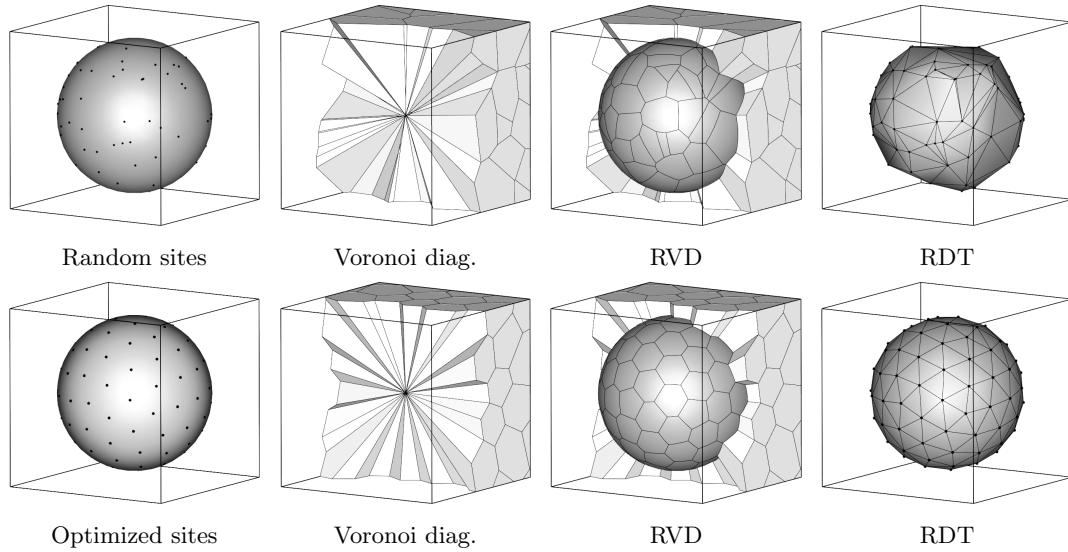
Figure 1.9: OPTIMIZATION OF 100 SITES NEAR A SPHERE. After the optimization, the restricted Voronoi diagram cells have shapes close to regular hexagons and the restricted Delaunay triangulation triangles are almost equilateral.

only on the restricted Voronoi cells:

$$F_\Omega = \sum_{i=1}^{k} \int_{y \in V_i \cap \Omega} \rho(y)||y - s_i||^2 dy \tag{1.6}$$

When points s_i belong to domain Ω, the centroidal restricted Voronoi diagram is constrained [Du *et al.*, 2003]. Because we use the sites to subdivide the volumetric regions and the surfaces of a model, we use non constrained centroidal restricted Voronoi diagrams. An site optimization example on a sphere is given figure 1.9. After the optimization restricted Delaunay triangulation triangle are almost equilateral.

1.3.3   Centroidal Voronoi diagram and centroidal restricted Voronoi diagram computation

To optimize site positions and obtain a centroidal Voronoi diagram or a centroidal restricted Voronoi diagram the principle is the same than for numerous optimizations:

1. Randomly distribute sites S
2. Build the Voronoi diagram (restricted) of S to the object
3. Determine new site positions S'
4. If a convergence criterion is reached, terminate, else replace S by new sites S' and go back to step 2.

The question is then to compute the new site positions S'. The classical strategy is to take the centroids of the Voronoi cells. The resulting algorithm, called Llyod algorithm [Lloyd, 1982], converge relatively slowly, i.e. many iterations are needed before reaching any minimum, the site displacement to their optimal positions being too slow.

Liu *et al.* [2009] propose to compute a centroidal Voronoi diagram using a Newton-like algorithm to minimize F_{CVT} and its restricted version. However this optimization

needs function F_{CVT} to be C^2 it is almost always the case, except in configurations where two points collide [Zhang *et al.*, 2012] or when a mid plane coincides with a boundary facet [Liu *et al.*, 2009]. Practice show that Newton-;like methods can be used to compute a centroidal Voronoi diagram or a centroidal restricted Voronoi diagram [Liu *et al.*, 2009, Yan *et al.*, 2009, Lévy et Liu, 2010, Merland, 2013].

Chapter 2

State of the art: objective and generation of meshes

2.1 Meshing and geomodeling

Understanding the three dimensional organization of subsurface rocks is crucial in fields such as the exploration, the exploitation, and the protection of mineral and energetic natural resources. Geological modeling, or geomodeling, provides tools to build and analyze subsurface models. Meshes are fundamental for most part of these tools.

2.1.1 What is a mesh?

Definition

A mesh is a way to represent an object numerically by approximating it with a set of simple elements. Take for example the star drawn in the plane and defined by an infinite number of points (figure 2.1a). By placing ten points on its contour and by linking these points in an adequate manner, we build a mesh of the star contour (figure 2.1b) or of its interior (figure 2.1c).

In a more general case, the mesh of an object is defined by a set of vertices and a set of elements linking these vertices. To have a valid mesh, these elements must
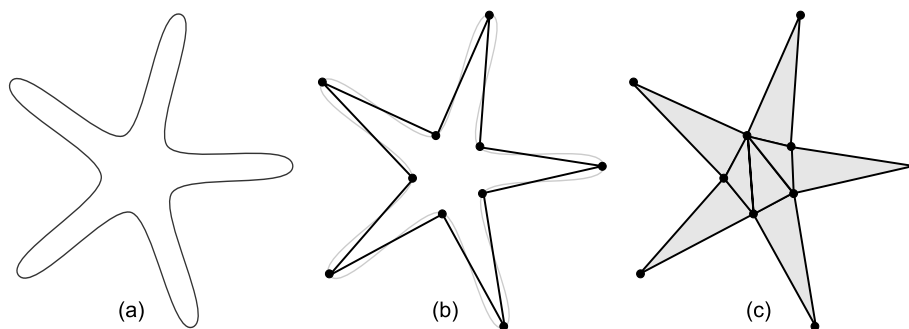

Figure 2.1: ONE STAR MESH. (a) Star defined by an infinite number of points. (b) Mesh of the star border line with 10 vertices and 10 segments. (c) Mesh of the interior of the star with 8 triangles.

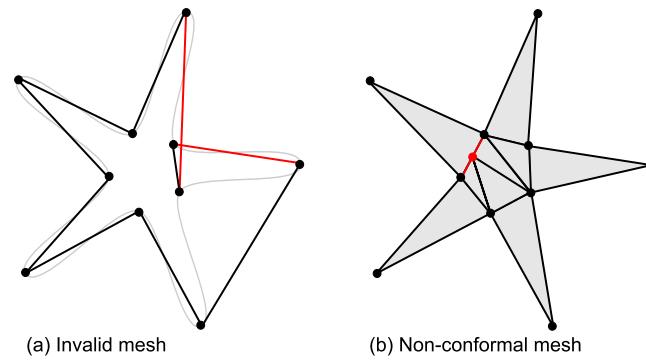(a) Invalid mesh   (b) Non-conformal mesh

Figure 2.2: Invalid and non-conformal meshes. (a) Invalid mesh, two segments intersect. (b) Valid non-conformal mesh.

enforce three conditions: the union of all elements is an approximation of the object, the interior of each element is not empty, and the intersection of the interiors of two elements is empty [Frey et George, 1999]. The meshes of figures 2.1b, 2.1c and 2.2b are valid while the one on figure 2.2a is invalid. Segments linking two vertices are the elements of dimension 1. The elements of dimension 2, the facets, are polygons, the most simple are triangles and quadrangles. Elements of dimension 3 are polyhedra, for example hexahedra or tetrahedra, they are the cells of the mesh.

The mesh is conformal if the intersection of two elements is either empty, either an element common the border of these two elements (figure 2.2c). The mesh is constrained if some of its elements were imposed at its building, very often elements meshing the domain boundaries. We say that two meshes are conformal if the mesh produced by the union of their elements is conformal. For example, the mesh of the star interior (figure 2.1c) is conformal to the mesh of its contour (figure 2.1b).

Mesh types

A mesh type is defined from the types of its elements and by their connectivity[1]. The last determines two mesh classes, structured meshes which have a regular connectivity, i.e. all their vertices have the same number of neighbors, and unstructured meshes which do not have a regular connectivity. Due to the many options for constitutive elements, the diversity of unstructured meshes is large ; either these elements are any polyhedra, or their type is known. When all the elements have the same type, the mesh type name is built from the element name: quadrangular mesh, triangular mesh, hexahedral mesh, tetrahedral mesh, prismatic mesh, *etc*. When the mesh is constituted of elements of different types, it is said hybrid or mixed element.

A simplicial mesh is exclusively constituted of simplices. We recall that a d-simplex is an element corresponding to the convex hull of a set of $d + 1$ points of $\mathbb{R}^n$ ($d \leq n$) that are affine independent[2]. The convex hull is defined as the smallest set that includes these points, i.e. a set that includes all the segments linking each pair of points of the set. In $\mathbb{R}^3$, 0-simplices are points, 1-simplices are segments, 2-simplices are triangles, and 3-simplices are tetrahedra (figure 2.3). In a simplicial mesh, the advantage is that all its elements are convex and that all its facets are

---

[1]The connectivity of an element being defined as the connections between its vertices.
[2]This excludes configurations where three points are aligned and where four points are coplanar.
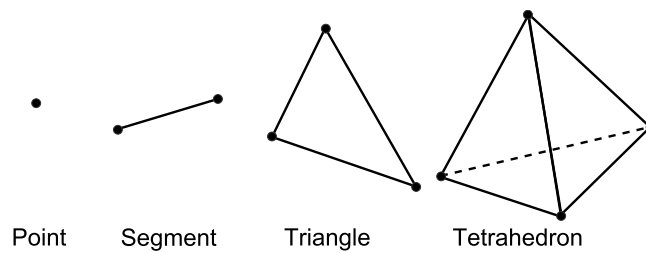
Figure 2.3: SIMPLICES IN $\mathbb{R}^3$.

planar.

2.1.2   Mesh objectives in geomodeling

Meshes to represent models

As we saw in the previous section, meshes are before all a way to represent objects with the union of a finite number of bounded simple elements. The object we are interested in this work are geological structural models delimiting the different subsurface rock volumes. There are two main options to represent these models.

Volumetric meshing   In a volumetric meshed representation, the regions of the model are meshed, and each cell is associated to a rock type. The simplest mesh is a regular subdivision of the model in cubes, which is similar to a 3D digital picture (figure 3a). As we will see in section 2.1.3, meshes constituted of hexahedra or tetrahedra are the most commonly used.

Boundary representation   In a boundary representation (or B-Rep), the model is described by the surfaces delimiting its volumetric regions (figures 2.4 and 3b). This representation has a lighter memory print, is more flexible, and permit to represent the most part of natural configurations. It is also particularly adapted to structural models that are generally built from the geological surfaces delimiting rock layers (horizons, faults, unconformities, *etc*). The question is then to mesh these surfaces that are generally triangulated[3] [Caumon *et al.*, 2009]. In this work, we only consider models which surface meshes are conformal (figure 2.5). A consequence is that the intersections between surfaces can be determined from their geometry.

Meshes to run numerical simulations

In geomodeling as well as in conception, a model is built to answer questions depending on its application domain, for example: How were rock deformed since their formation? What is the amount of recoverable oil? What is the impact of a tunnel on a zone stability? Processes modeling mechanical rock deformation, fluid flows, heat or wave propagation are themselves modeled by partial differential equations, that cannot be solved exactly (analytically) in the general case, and for which an approximated solution is computed numerically. Since their beginning, numerical solving

---

[3]Surfaces as a set of points of coordinates (x, y, z), can also be defined implicitly $f(x, y, z) = 0$, parametrically $(x, y, z) = \sigma(u, v)$, or explicitly $z = f(x, y)$.
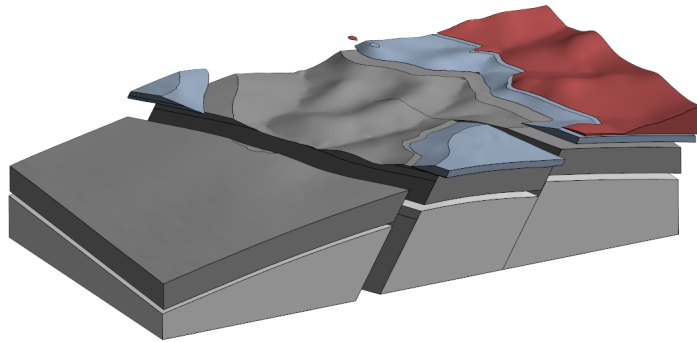
Figure 2.4: VOLUMETRIC REGIONS IN A B-REP MODEL. Each region is defined by its boundary surfaces. Several regions are hidden (see also figure 3).
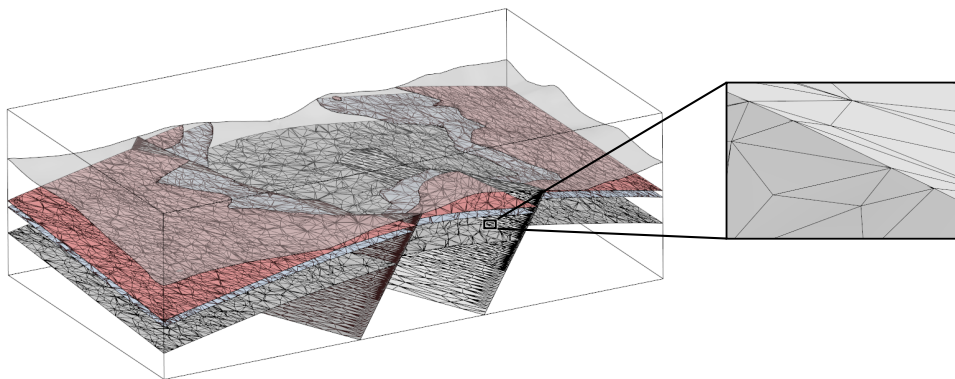
Figure 2.5: TRIANGULATED SURFACES OF A B-REP MODEL. The surfaces defining the volume of interest are not displayed. Meshes of intersecting surfaces are conformal.
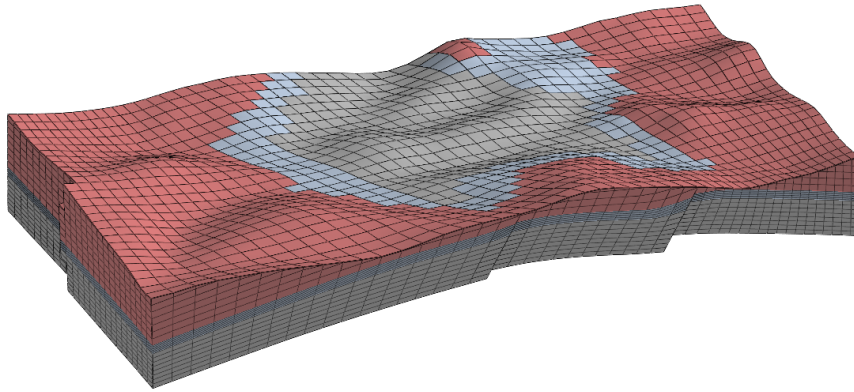
Figure 2.6: CURVILINEAR GRID. Mesh hexahedra are deformed to fit horizons and faults. The cells that are adjacent to the erosion surface (see figure 3) are degenerated, inactive cells are created to have a regular grid.

methods have been associated to meshes that are a mean to discretize space [Baker, 2005]. Meshes are a prerequisite for any numerical simulation. Because rock properties (composition, porosity, permeability, *etc*) vary inside a model region, meshes in geomodeling are also used to store these properties.

We will not detail typical geosciences equations. Flow in porous medium equations are described in Farmer [2005], geomechanical equations and heat propagation in Turcotte [2002], wave propagation equations in Aki et Richards [2009] and basin process equations in Mello *et al.* [2009]. We will not give any detail on the different numerical resolution schemes for partial differential equations, the reader is referred to Allaire [2005] and Saad [2003] for a detailed description of the main approaches: finite difference, finite element, and finite volume.

2.1.3   Volumetric meshes used in geomodeling

If geological model surfaces are often meshed with triangles, volumetric meshes are more diverse.

Meshes for flow simulations

The most part of meshes in geomodeling are developed for flow simulations in hydrocarbon reservoirs, the main objective being to predict hydrocarbon production. The simplest volumetric mesh is probably a Cartesian grid that subdivides regularly the model into identical rectangular parallelepipeds (figure 3). On this structured meshes, finite difference like numerical schemes that are simpler to implement and very efficient can be used. On the other hand, as all their elements have the same geometry and the same connectivity, the approximation of the modeled geological objects is often too coarse to get reliable simulation results.

Curvilinear grids   Curvilinear grids, or stratigraphic grids, or corner-point grids, are regular meshes constituted of deformed hexahedra that are aligned on layers boundaries, horizons, and faults (figure 2.6). However, in the areas where these boundaries intersect, cells cannot generally be aligned with them all. Degenerated cells and/or inactive cells are created, and some geological boundaries are removed
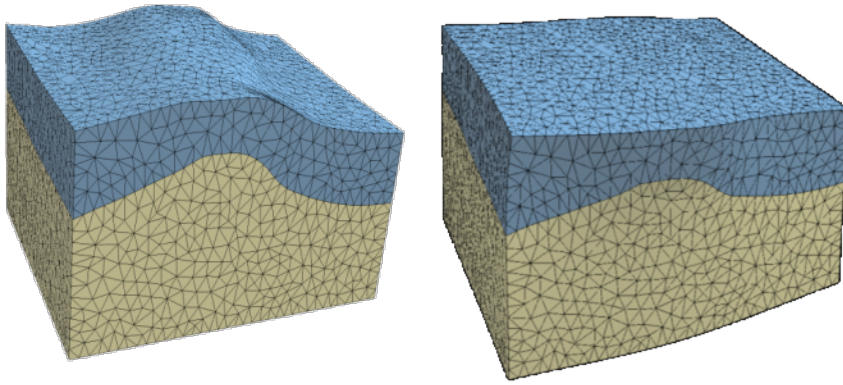
Figure 2.7: FOLD RESTORATION RUN ON A TETRAHEDRAL MESH (FROM DURAND-RIARD [2010]). The folded top horizon is restored to its original state - horizontal.

or approximated by stair steps (typically faults). These grids are generally generated by extruding a quadrangular mesh of one of the horizons, and creating the desired number of hexahedra layers. They are massively used in an oil exploration-production context for geostatistical rock property filling and reservoir fluid flow simulations (e.g. [Farmer, 2005]).

Unstructured meshes   Unstructured meshes, for which element connectivity, size, aspect, and orientation vary, permit to better capture model complicated geometries. They are not much used for flow simulation, because the matrix resulting of the discretization do not generally have a regular pattern making them more expansive to store and to inverse. Nevertheless, recently developed simulators like GPRS [Cao, 2002] and IX [DeBaun *et al.*, 2005], and works on new discretization schemes (see for example Eymard *et al.* [2012]) might change that.

Unstructured mesh diversity is very large, we only describe here a selection of the ones used for flow simulations. Truncated grids are obtained by truncating structured grids, generally by faults on which the grid is not aligned [Lasseter et Jackson, 2004]. These grids can be refined around specific zones of interest [Sword *et al.*, 2013] which give them a nice flexibility. Semi-structured meshes, i.e. structured in at least one direction, are similar to stratigraphic grids. The difference is that the cells are built by extruding Voronoi cells, triangles, or a mix of several elements, instead of quadrangles (see for example Lepage [2003]). Modular meshes, directly dependent on the decomposition of the model in several blocks, the modules, are constituted of the meshes of these blocks. Regular grids can be used to mesh non-crucial areas, and to adapt mesh elements in more important areas for the simulation, see for example Flandrin *et al.* [2006] and Lepage [2003]. The difficulty is then to generate the mesh linking the modules. The last important type of unstructured meshes is the grid constituted of any convex polygons, see for example Merland [2013].

Meshes for other applications

For other applications than reservoir simulation, the diversity of meshes is much more limited. A great part of mechanical, heat, wave propagation problems are solved using finite element type methods. Meshes are often simplicial meshes, because they can
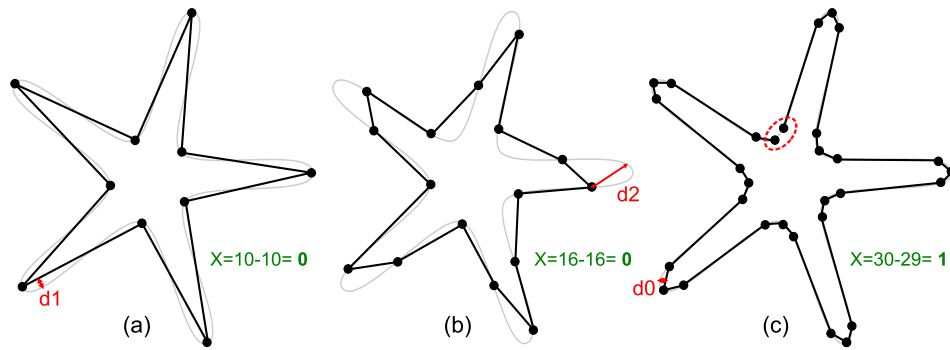
Figure 2.8: STAR APPROXIMATION QUALITY. Three meshes of the same star are more or less satisfactory approximations. Hausdorff distance between the initial model and each mesh (d0 < d1 < d2) indicate that the best geometrical approximation is mesh (c). But its Euler characteristic is not correct because one segment is missing. The topology of meshes (a) and (b) is correct but approximation is not good for mesh (b).

represent any geometry. Tetrahedron meshes are used for geomechanical restoration to check model consistency and understand the evolution of given structures (see for example Durand-Riard *et al.* [2011] and Vidal-Royo *et al.* [2012]), for computing heat or seismic wave propagation [Lelievre *et al.*, 2012], heat transfer [Liu *et al.*, 2012], or flows in fracture media [Mustapha et Mustapha, 2007]. They are also used to implicitly model stratigraphic horizons in the deposit space [Mallet, 2004]. Moretti [2008] and [Moretti *et al.*, 2006] use a curvilinear grid aligned on horizons and faults (without any degenerated or inactive cell) for restoration computation. The use of unstructured hexahedra mesh is limited since it is very difficult to generate them automatically [Owen et Shelton, 2014].

2.2   Mesh quality and generation challenges

We saw in the previous section that meshes have two main objectives in geomodelling: (1) represent approximately subsurface models and (2) run numerical simulations on these models. To have reliable, fast, and robust results the mesh must respect criteria on the number, the size, and the shape of its elements. In this section, we will see how these criteria may be contradictory, how the zones where they do can be identified, and how they can be adequately taken into account in meshing.

2.2.1   Mesh quality

The quality of a mesh is a set of criteria that evaluate its influence on the precision and the efficiency of the applications by which it is used. For example mesh on figure 2.8b give a less precise estimation of the perimeter of the star than meshes on figures 2.8a and c. The optimal mesh is the one which for a given application permit to reach the desired precision while keeping the number of elements at a minimum.

Model approximation quality

B-Rep model approximation quality is reduced to the approximation quality of its boundaries. The firsts criteria to measure the fidelity of the representation of an

Figure 2.9: HAUSDORFF DISTANCE BETWEEN TWO LINES X AND Y. $sup(F)$ is the superior bound of F and $inf(F)$ its inferior bound.

object (model) by a given mesh are geometrical, i.e. evaluate the differences of geometrical properties between the model and its mesh: distance, normal, c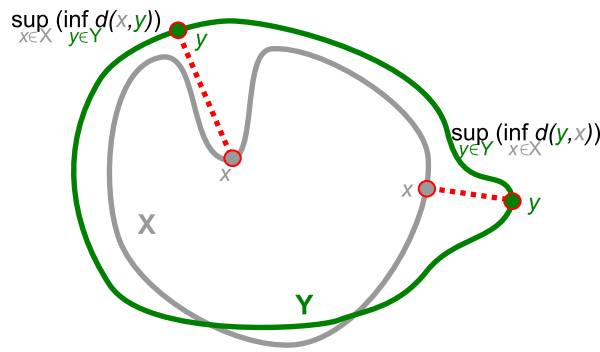urvature, *etc.* [Frey et George, 1999]. These differences can either be locally evaluated for each vertex, edge, or triangle, or globally. Hausdorff distance evaluates the proximity of two models. For two objects X and Y it is defined as (figure 2.9):
$d_H(X,Y) = \max \{\sup_{x \in X} \inf_{y \in Y} d(x,y) \,|\, \sup_{y \in Y} \inf_{x \in X} d(y,x)\}$.

Topological criteria evaluate the fidelity of the mesh to the initial model independently of its geometry. In a B-Rep models, this means verifying that the connections between the surfaces are the same and that the topology of each one of the surfaces is the same. Generally, in computational graphics, stating that two domains have the same topology means that they are homeomorphic (section 1.2.4). If it is possible to prove that the result of a meshing algorithm is homeomorphic to a input model (section 1.2.4), it is, to our knowledge, not possible to actually compute that is is. In the case where the initial model is meshed, weaker properties may be compared: the Euler-Poincare characteristic: $\mathsf{X} = S - A + F$, where S is the number of vertices, A the number of edges, and F the number of facets, or the homology [Boltcheva *et al.*, 2011]. For example, the star mesh on figure 2.8c is not correct, because its Euler characteristic is 1, while it should be 0, same as the star contour, a closed line.

Mesh quality for numerical simulations

The influence of a mesh on the precision and the efficiency of numerical simulations aiming at solving partial differential equations may be important. This influence depends on several factors among which the simulated physical process, the discretization method, the geometrical mesh properties (distances, curvatures, angles, *etc.*), see Knupp [2007], Berzins [1999] and references therein. Mesh quality is defined by Knupp [2007] as the characteristics of the mesh that permit that the computations linked to a numerical simulation are efficient, faithful to the physics, and obtained at the desired precision. A mesh has a better quality if it brings smaller errors than another mesh. These errors can be evaluated a priori, by controlling some mesh properties, or a posteriori, by controlling simulation results.

However by default a priori criteria generally used in meshing, see for example the review of Field [2000]. The goal of these criteria is to eliminate mesh element that (a priori) create difficulties for the numerical simulation of a process (that is supposed isotropic), particularly elements with small or large angles (figure 2.10), and elements
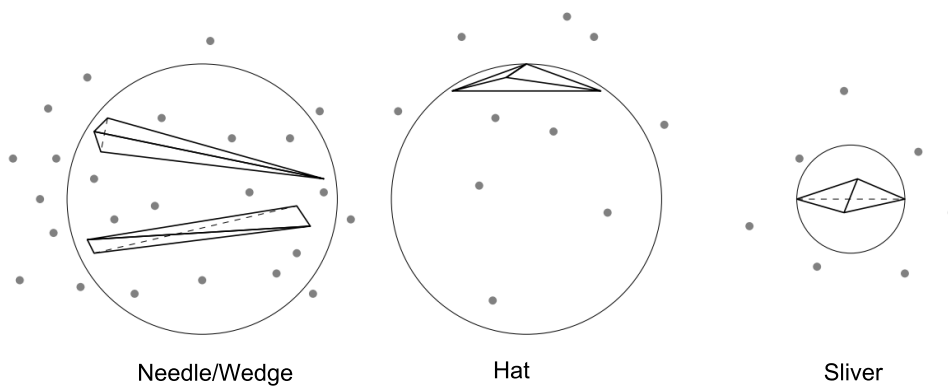
Figure 2.10: Tetrahedra with an a priori bad quality, from Shewchuk [2012].

with edge sizes outside given bounds.

To conclude, it is is pointless to define the quality of a mesh independently of any application. This application is related to partial differential equations and to a numerical scheme, and depending on these, some mesh characteristic might be desirable or harmful. For some codes the best element are equilateral ones, while other codes will behave better with anisotropic elements deformed in the preferential directions of this or that physical property.

2.2.2   Negative effects of model geometry

Thin model sections, highly curved ones, or the ones presenting surfaces intersecting at small angles are generally incompatibles with a priori mesh quality criteria. A model with a 16 degree angle between two surfaces must have at least an element in its mesh with a 16 degree angle (figure 4b).

Dey *et al.* [1997] define small model features as the model components, or model component parts, which size is inferior to the one that would permit to build a mesh satisfying given criteria. As these criteria depend on the application and are not always clearly defined, the identification of these small features may be complicated and is often done by the modelers and/or the engineers in charge of the model building or of simulations [Quadros et Owen, 2012]. To ease the generation of a good quality mesh, it is however necessary to detect them and take them into account before, during, or after meshing.

2.2.3   Managing model challenging features

In this section, we are interested in the methods identifying and managing the zones of a B-Rep model that complicate mesh generation independently of any model surface representation, any model objectives, or any meshing method. Challenging features specific to geological structural models will be described in chapter 3.

Pre-identification

The identification of small features of a B-Rep model can be performed using a measures evaluating surface proximity (distance to median surface), surface border proximity (distance to medial axis), surface curvature, surface border length, and

surface curvature [Quadros et Owen, 2012]. Model sharp features may also be challenging, they are generally already identified in the model, and if it is not the case, they can be recomputed, see Botsch *et al.* [2010].

Model complexity can also be evaluated locally based on a subdivision of the model. Andrle [1996] use varying radius circles to compute an angle measure at a given resolution and evaluate the complexity of geomorphic lines. Lindsay *et al.* [2013] propose to count in each of the cells of a structured grid the number of materials sampled by this cell and its neighbors. This subdivision principle is also the base of box-counting methods computing the fractal dimension of an object, see for example Kruhl [2013].

Model simplification

The most radical solution for complex zone management is undoubtedly to remove them before meshing, or at least to modify them so that they are less challenging. In geological modeling, model geometry simplification is often necessary, even if literature focuses on the crucial problem of rock properties upscaling, see the review of Durlofsky [2005], and is sparse on this subject, at the exception of research works on fracture networks [Bourbiaux *et al.*, 2002, Mustapha *et al.*, 2011]. There are a lot of methods in computer aided design to simplify models and suppress features impacting simulation robustness. Thakur *et al.* [2009] give a very good review of these methods. Three strategies seem relevant to structural model simplification, methods operating on model surfaces, method operating on model volumetric regions, and dimension reduction methods.

The firsts simplify the model or mesh with local modifications [Shephard *et al.*, 1998, Sheffer, 2001, Quadros et Owen, 2012]. The generalization of the edge contraction operation proposed by Garland et Heckbert [1997] allow the grouping of close vertices, and so some model topology modifications. This strategy was implemented by Mustapha *et al.* [2011] to modify the mesh of discrete fracture networks.

The volumetric method proposed by Andujar *et al.* [2002] use a model recursive subdivision recursive by an octree. Cells inside and outside the model are flagged, then the model is rebuilt from the remaining in-between cells. Different octree depths give different simplification levels. The advantage is that, because the complete model is considered, the relationships between its different components can be analyzed.

Model dimension reduction is a simplification technique used in computer aided design. It consists of replacing an object by one of lower dimension. For example, a cylindrical bar (3D) can be replaced by a line (1D) without a significant impact on the result of some simulations [Thakur *et al.*, 2009]. Resulting models may be constituted of elements which dimensions vary. Corresponding meshes must be mixed-dimensional, meaning that they contain elements of different dimensions (figure 1.5c), *e.g.* [Robinson *et al.*, 2011]. In geomodeling, faults are modeled with a similar approach. Indeed faults are volumetric zones where rocks are damaged, but they are most of the time modeled by surfaces to which are associated specific properties like transmissibility multipliers [Manzocchi *et al.*, 1999].

Mesh generation

To account for zones complicated to mesh, the most part of meshing methods rely on a mesh size function to obtain well shaped elements. This function generally depends on measures taken during a pre-identification step of the potentially challenging zones, curvature, normal deviation, distance to medial axis, see for example Frey et George [1999] and Quadros *et al.* [2004]. Besides adapting element size and increasing their number, it is also possible to modify their shape and their type to better capture model geometry and/or decrease numerical simulation errors. For a same number of elements, using anisotropic elements can permit to have a better approximation of a domain and to minimize the error of approximation of a given function on the mesh. A second possibility is to use elements of different types in different zones of the model, the third is to use higher degree (curved) elements. Their generation is however rather difficult, see for example Luo *et al.* [2004].

Post-processing

When complex zones are neither pre-processed, nor taken into account during meshing, they can be identified in a final step by evaluating fitting between the elements and the required quality criteria [Dey *et al.*, 1997]. The advantage is that all possible complications are detected, but the volumetric mesh must be generated. This mesh is then iteratively locally modified so that it respects quality criteria. This general approach is also used by mesh adaptation and optimization methods that modify the mesh until computational errors are below an admissible threshold [Frey et George, 1999, Loseille, 2008].

2.3   Volumetric meshing with tetrahedra

In the two last sections of this chapter, we review surface and volumetric simplicial mesh generation methods. We begin by describing the main approaches to generate tetrahedral meshes, because the fact that the dimension of the object to mesh is the same than the space dimension in which it is embedded (three) makes them easier to understand than surface remeshing.

After tetrahedral mesh generation methods, we detail meshing methods more particularly linked with our work: multi-material model meshing and tet-dominant mixed-element meshing. About the generation of other mesh type, the reader is referred to the reviews of Thompson *et al.* [1999], Frey et George [1999], Baker [2005] and Farmer [2005].

2.3.1   Tetrahedral meshes

There are many tetrahedral meshing methods, all related to one of the following three main approaches: octree based methods, advancing front methods, and Delaunay methods.

Space subdivision

The principle of octree based methods is to subdivide a bounding box of the model in cells of varying sizes, and build the mesh subdividing these cells (see for example

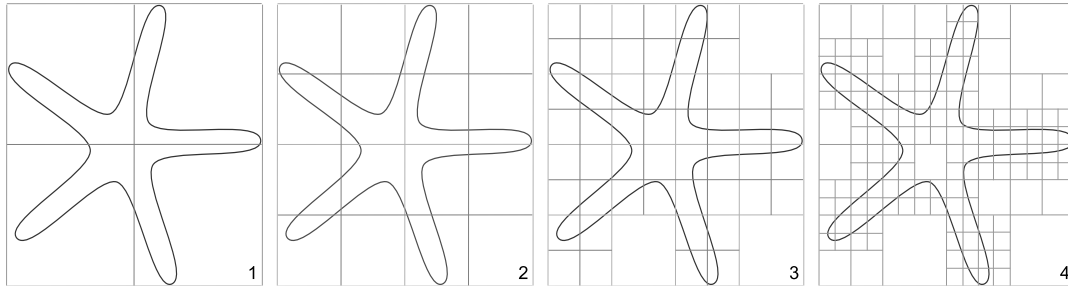Figure 2.11: Recursive subdivisions of a box containing the star.
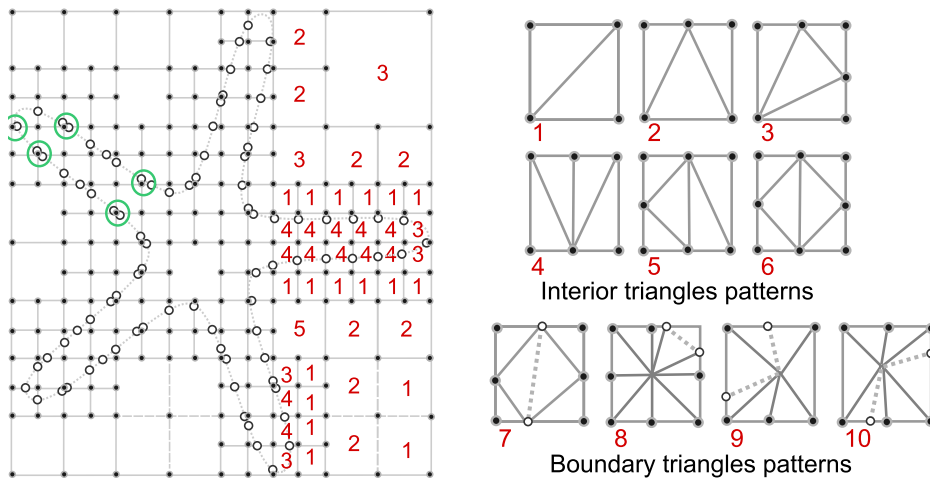

Figure 2.12: Patterns to build a mesh from a subdivision. The final mesh is built from the cell vertices (black dots) and intersection points between the star and the cells (white dots). To each cell correspond one of the ten triangle patterns. To avoid the creation of degenerated triangles, close vertices are merged (green circles).
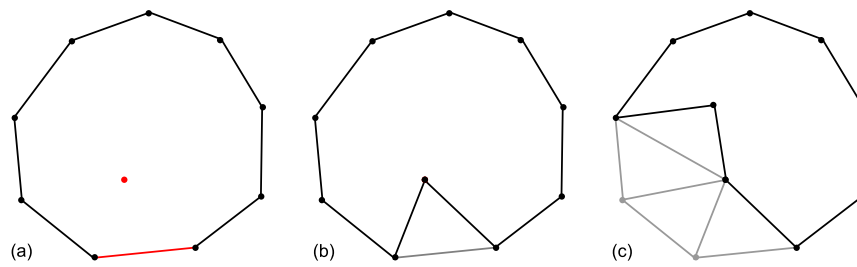
Figure 2.13: ADVANCING FRONT MESHING PRINCIPLE. (a) The initial front is a mesh of the domain boundary. A segment is chosen and the optimal point to built a triangle from it is determined. (b) Front update after triangle building. (c) Front after the building of three additional triangles.

[Shephard et Georges, 1991]). This subdivision uses a hierarchical tree structure. A model bounding box is subdivided into eight (four in 2D) cells, then each cell is recursively subdivided into eight (four) cells, until the stopping criteria is reached (figure 2.11). This stopping criteria depends on the desired element size and on a maximal number of intersections between model boundaries and cells. The intersection of each leaf of the tree with the model boundaries is often limited to have one connected component. To control cell size variations, depth differences between two adjacent cells are limited to two, see dotted line subdivisions added on figure 2.12. Final mesh tetrahedra vertices are the octree cells vertices to which are added the intersections between cells and model boundary and, if they exist, the initial boundary mesh vertices (figure 2.12). Final mesh tetrahedra (or triangles) are built by subdividing tree cells following predefined patterns. In two dimensions, there are ten patterns (figure 2.12); in three dimensions, there are a lot of configurations and more general strategies to subdivide the octants are implemented.

These methods are relatively robust and reliable [Frey et George, 1999]. They require to implement strategies to improve mesh element quality near boundaries, for example merge too close vertices. They do not require model boundary discretization, their mesh being a byproduct of volumetric meshing. If the boundaries are meshed, the final mesh will not be conformal to the input mesh. Recently, octree-type methods guarantying bounded dihedral tetrahedron angles were proposed [Labelle et Shewchuk, 2007, Wang et Yu, 2012].

Advancing front

The advancing front method strategy consists in building the mesh element per element advancing progressively inside the model to mesh from its boundary (figure 2.13) [Löhner et Parikh, 1988]. While the meshing front is not empty, an element is built from one segment of the front (2d) or one triangle (3D). These methods determine heuristically the points to create and the elements to build. This way mesh elements have the desired size and shape. Their very construction make them conformal to model boundaries, and, contrary to octree and Delaunay methods, mesh element quality is very good along model boundaries. Building one element require to (1) select an front element according to a specific criterion, (2) determine the optimal point to build an element which base is this front element, (3) check if an existing vertex can replace this optimal point, (4) build the element, (5) check its validity
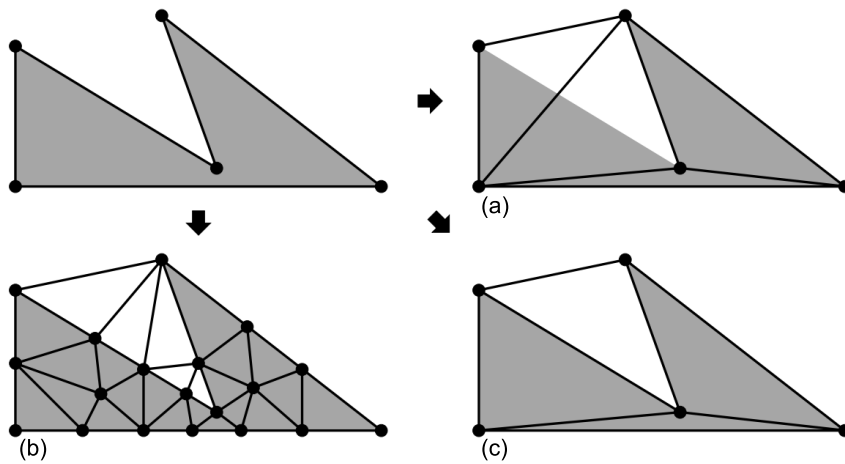
Figure 2.14: Constrained and refined Delaunay meshes, from Shewchuk [2012]. (a) The Delaunay triangulation of boundary vertices of the object does not contain one of the segments of the boundary. (b) The Delaunay triangulation obtained by inserting Steiner points. (c) The constrained Delaunay triangulation contains this segment.
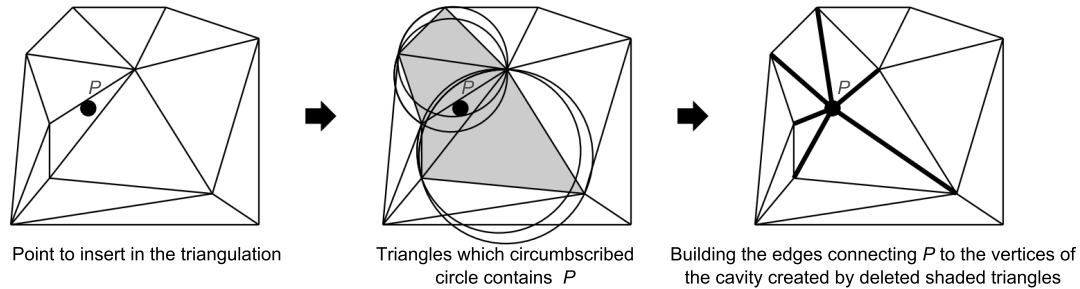
Figure 2.15: Insertion of one point in a Delaunay triangulation, Bowyer-Watson algorithm, modified from Shewchuk [2012].

and modify the optimal point if not, and finally, (6) update the front. Advancing front method convergence is not guaranteed in three dimensions, however efficient strategies can be implemented. For example, NetGen [4] is based on advancing front [Schöberl, 1997].

Delaunay

The third type of mesh generation methods is based on Delaunay triangulation (section 1.1.2). Their principle is to build the Delaunay triangulation of a set of points and to modify these points and/or this triangulation until the desired quality criteria are reached, see also George et Borouchaki [1997], Cheng [2013] and the lecture of Shewchuk [2012]. They are based on the point insertion procedure in a Delaunay triangulation that keeps it Delaunay (figure 2.15).

Constrained Delaunay methods aim at recovering model boundary discretization in the generated mesh (figure 2.14a). Model boundary vertices are inserted in the mesh of a model bounding-box. Then, the delicate step is to recover the bound-

---

[4]http://www.hpfem.jku.at/netgen/

| Random distribution of 200 points in a sphere | CVT optimization of point positions | Restricted Delaunay triangulation |

Figure 2.16: VORONOI-DELAUNAY OPTIMIZATION MESHING PRINCIPLE.

ary elements that are not in the Delaunay triangulation[5]. Additional vertices are then inserted until element shape and size criteria are reached [George *et al.*, 1991, Borouchaki *et al.*, 1997, Shewchuk, 2002a, Si et Gärtner, 2011, Si, 2010]. Softwares like Tetgen[6] and MG-Tetra [7] permit to obtained constrained tetrahedral meshes to model defined by conformal triangulated surfaces.

The principle of Delaunay refinement methods is to iteratively insert vertices at the center of circumscribed spheres to the tetrahedra that do not satisfy a given criteria [Chew, 1997, Shewchuk, 1998, Cheng *et al.*, 2005, Shewchuk, 2002b, Cohen-Steiner *et al.*, 2004, Rineau et Yvinec, 2007, Si, 2008]. This criteria is often a function of the ratio between the radius of the circumscribed sphere to the tetrahedron and the shortest edge length, since it is then proved that, under certain conditions, the algorithm terminates. These methods guarantee bounds on output tetrahedron dihedral angles. The main differences between the algorithms lie in the management of the object boundaries which discretization is generally modified. Gmsh [8], TetGen, NetGen and CGAL library [9] implement Delaunay refinement methods.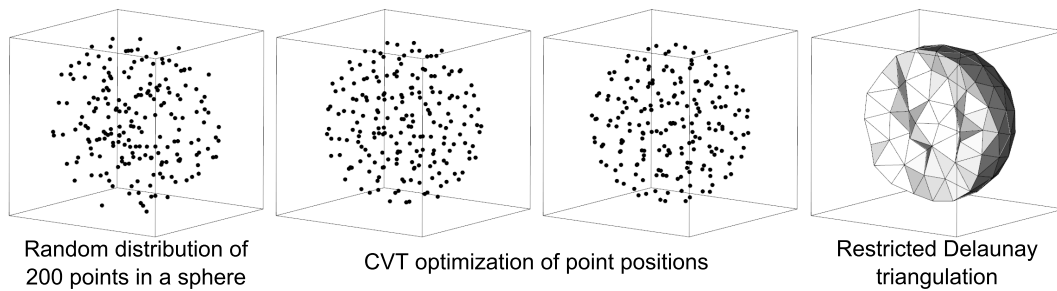 The quality of the obtained meshes is relatively good, however it is difficult to control the number of vertices added and the model boundaries are remeshed.

Voronoi-Delaunay optimization

A second strategy to generate Delaunay meshes consists in determining the positions of all final mesh vertices before building their Delaunay triangulation [Du et Wang, 2003, Alliez *et al.*, 2005a, Tournois *et al.*, 2009, Tournois, 2009, Dardenne *et al.*, 2009, Lévy et Liu, 2010]. First, a given number of points is distributed to sample the surface or volume to mesh, then the coordinates of these points are optimized to minimize an objective function, finally the restricted Delaunay triangulation of the points to the object is built and gives the new mesh (figure 2.16). This objective function is derived of the notion of centroidal Voronoi diagram (section 1.3.1) and/or of the notion of optimal Delaunay triangulation [Chen et Xu, 2004].

The two features distinguishing this approach from more classical meshing methods is that (1) the number of vertices is fixed and that (2) tetrahedra shape and

---

[5]This mesh is then not strictly speaking Delaunay.

[6]http://wias-berlin.de/software/tetgen/

[7]http://www.meshgems.com/volume-meshing-meshgems-tetra.html

[8]http://geuz.org/gmsh/

[9]http://www.cgal.org/
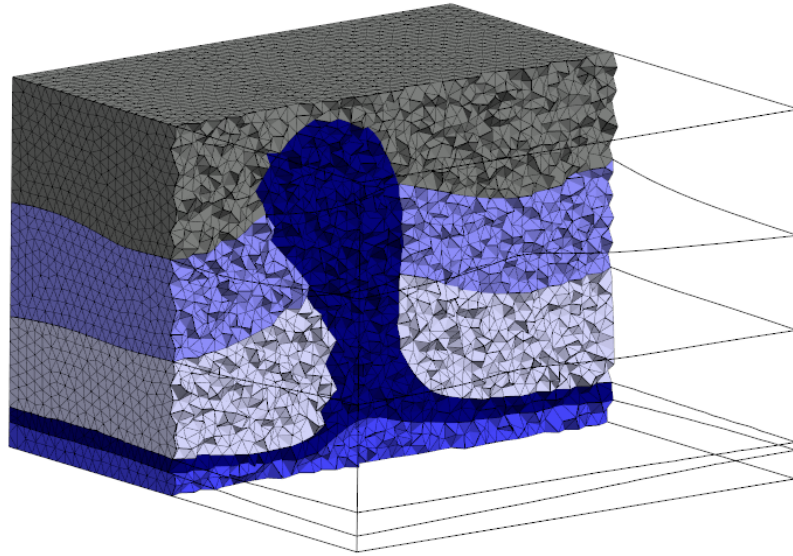
Figure 2.17: SOLID SLICE IN A TETRAHEDRAL MESH OF A DIAPIR MODEL. The mesh of each region is constrained to the mesh of the triangulated surfaces defining the model. The five regions were meshed independently with TetGen[10].

quality are globally controlled by the objective function. Their computational cost is bigger than the above described methods. Note that considering the Voronoi diagram, that is a subdivision of the space, bring similarities between these methods and octree methods. The pattern corresponding to the Voronoi diagram is given by the dual Voronoi-Delaunay relationship (section 1.1.2). Moreover, like octree methods, boundary surface mesh can be obtained at the same time than the volumetric mesh with the restricted Delaunay triangulation to the surfaces (section 1.2.3).

2.3.2 Multi-material model meshing

Geological model represent several rock units, so they are divided in several regions. The objective is to conformably mesh these regions, the surfaces delimiting them, and the lines of intersection between these surfaces, i.e. tetrahedra on both sides of a surface must share the same triangular facet, and triangles neighbors through a contact line must share the same segment.

With a constrained meshing method, that generates a mesh strictly conformal to the given discretization of the model boundaries, model regions can be meshed independently (figure 2.17). Methods that do not generate a constrained mesh are less robust. Lepage [2003], Prévost *et al.* [2005] propose to use a modified version of a Delaunay refinement method to mesh structural model surfaces. The result meshes are typical of this type of method, they are very refined near model corners.

Methods developed in computer graphics generally do not consider non-manifold surfaces or multi-material models. Some of them do it explicitly and are developed for medical applications. Their objective is to generate volumetric meshes from 3D digital pictures (CT scan, MRI) in order to simulate wave/heat propagation, *etc.* Input data is then not a B-Rep model. The method proposed by Sullivan *et al.* [1997] is based on a subdivision determined by a grid, the more recent works of Zhang *et al.* [2010], Mohamed et Davatzikos [2004] using a similar approach. Delaunay refinement
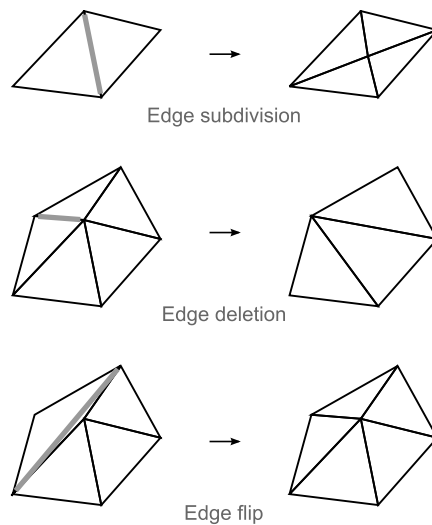
Figure 2.18: LOCAL SURFACE REMESHING OPERATIONS.

[Boltcheva *et al.*, 2009, Dey et Levine, 2009], and Voronoi optimization [Dardenne *et al.*, 2009, Dardenne, 2009] methods have also been proposed.

2.3.3   Tetrahedron-prism mixed-element meshing

In computational fluid dynamic, specific zones of interest, like the layers surrounding a plane, are meshed by thin layers of prisms or tetrahedra. The most part of the methods generating these boundary layer meshes use an advancing surface (or advancing facet) strategy and develop solutions to obtain a valid mesh when the input surface is locally non-convex or angular (see *e.g.* [Garimella et Shephard, 2000, Sahni *et al.*, 2008, Dyedov *et al.*, 2009, Ito *et al.*, 2011]). The volume to fill with prisms is determined from the boundary of the object and a generally pre-defined height for prisms. A notable exception is the work presented by Dyedov *et al.* [2009], where a face offsetting method [Jiao, 2007] is adapted to biological geometries. This method produces mixed-element (also called hybrid) meshes of very good quality in which prism thickness depends on a local feature size measure. Marchandise *et al.* [2013] exploit the tubular geometry of blood vessels. Loseille et Löhner [2013] propose to use local mesh modification strategies to generate prism layers.

To mesh the interior of objects, complementary approaches have been developed. Garimella et Shephard [1999] refine an isotropic tetrahedral mesh when the number of tetrahedra between two triangular facets on two opposite sides of the model is below a given threshold. Luo *et al.* [2010] evaluate the surface medial axis of the model boundary to identify its thin sections. Then, to build prisms they duplicate the triangles from one side of the model.

2.4   Triangular surface meshing

The various possible representations for surfaces (implicit, parametric, discretized) and the various applications using surfaces to represent objects explain the large number of surface remeshing methods. Meshing a surface means to generate a valid
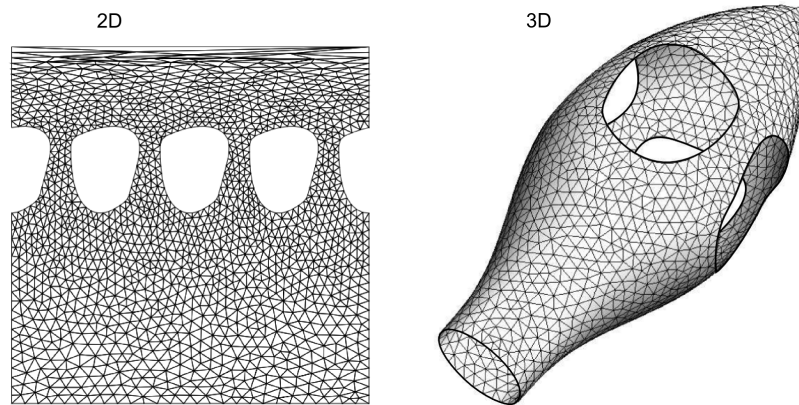
Figure 2.19: Surface remeshing in a parametric space, modified from Geuzaine et Remacle [2009]. Meshing is performed in the plane for a projection of the 3D surface.

mesh for this surface; remeshing a surface implies that this surface is already meshed and discretized. In that case, the initial mesh can be modified to obtain a second mesh that has the desired properties. This iterative modifications, vertex displacement or operations on the edges (figure 2.18), are done while given quality criteria are not reached (distance between mesh elements and the input surface, metric to enforce, *etc.*, see for example [Frey, 2000, Geuzaine et Remacle, 2009, Botsch *et al.*, 2010]).

3D surface meshing has the specificity to consider objects which dimension is inferior to space dimension. Parametric methods operate on a projection of the surface in a plane, while direct methods operates in the 3D space. When an adequate parameterization of a surface is available, parametric methods are undoubtedly the more robust, because in the plane, Delaunay and advancing front meshing methods are guaranteed to terminate. However the computation of this adequate projection can itself be an issue when the initial surface is discretized or not open. It is then possible to adapt 2D methods such as advancing front [Löhner, 1996, Sifri *et al.*, 2003, Peyré et Cohen, 2006, Aubry *et al.*, 2011] and Delaunay refinement methods (section 2.4.2) to 3D surfaces or to use dedicated methods.

2.4.1 Space subdivision

Octree methods

We saw in section 2.3.1 that tetrahedral meshing methods based on space subdivision, octree or Voronoi based methods generate a mesh of the model boundaries. The contour of the star (figure 2.12) and the one of the sphere (figure 2.16) are meshed at the same time than the interiors of these models. Whether it is to mesh surfaces or volumes, the octree subdivision is the same. Intersection points between the corners, edges, facets of the cells with the surface (plus some specific points) are then linked to create edges and loops (contour of the intersection of one cell with the surface) and to build the final mesh [Shephard et Georges, 1991].

Restricted centroidal Voronoi diagram

For surface meshing methods based on a centroidal Voronoi subdivision, it is the intersection between the surface and the Voronoi diagram that must be centroidal

(section 1.3.2). The optimization of the volumetric model subdivision is not necessary. The result mesh vertices are the optimized sites of the Voronoi diagram (equation 1.6).

These methods permit to generate meshes with an a priori good quality. Du et al. [2003] define the notion of constrained centroidal Voronoi diagram, where the sites are constrained to lie on the surface, and produce results of adaptive isotropic meshing for surfaces defined explicitly by a function $f(x, y, z)$. Alliez et al. [2005b] remesh triangulated surfaces in the plane using a global parameterization, Surazhsky et al. [2003] use a local parameterization. Yan et al. [2009], Liu et al. [2009] compute in the 3D space the intersection of the Voronoi diagram with the model surfaces and optimize the objective function given by equation 1.6. This approach is generalized in Lévy et Liu [2010] to manage model sharp features without requiring their previous identification and control spacing between the sites and the input surfaces, and in Lévy et Bonneel [2013] to generate anisotropic meshes. Valette et Chassery [2004], Valette et al. [2008] use a discrete version of Voronoi diagrams to decrease a mesh resolution and improve its quality.

The main difficulty of subdivision meshing methods is that, a priori, all possible configurations for the intersections between one subdivision cell and the model do occur. It is to avoid too complex configurations, that cells are generally subdivided while intersections do not have a unique connected component, this even permits for Voronoi based methods to verify the topological ball property (section 1.2.4).

2.4.2   Guaranteed surface meshing

Since their beginning, Delaunay refinement methods have been used to directly mesh 3D surfaces [Chew, 1993]. As for tetrahedral meshing, theoretical work, provide guarantees on the topology and/or the final element quality. One part of these methods consider separately the determination of the mesh vertices, that is nothing else than a sampling of the surface, and the building of the triangles. This links 3D mesh generation to surface reconstruction problems [Hoppe et al., 1992, Boissonnat et Cazals, 2000]. It is in this framework that the notion ϵ-sampling was introduced by Amenta et Bern [1999], which gives that, when the surface point sampling is dense enough compared to the distance to the surface medial axis, the points have the topological ball property for the surface (section 1.2.4). From the topological ball property are derived works aiming at relaxing the constraints to obtain a good sampling and at considering more general surfaces. Based on these works, were developed Delaunay remeshing algorithms with guarantees, see for example [Boissonnat et Oudot, 2005, Cheng et al., 2007]; more recent papers are particularly interested in implicit surface meshing [Cheng et al., 2009, Dey et Levine, 2009, Gelas et al., 2009, Dey et al., 2010]

2.5   Discussion

We saw that meshes have two main objectives in geomodeling: represent geological objects and run numerical simulations; all to understand the organization and the behavior of subsurface rocks. Meshes are used in a very wide range of domains, but their generation concerns a more restricted community. Mesh generation require knowledge about computer science, geometry, computational geometry and numerical simulation.
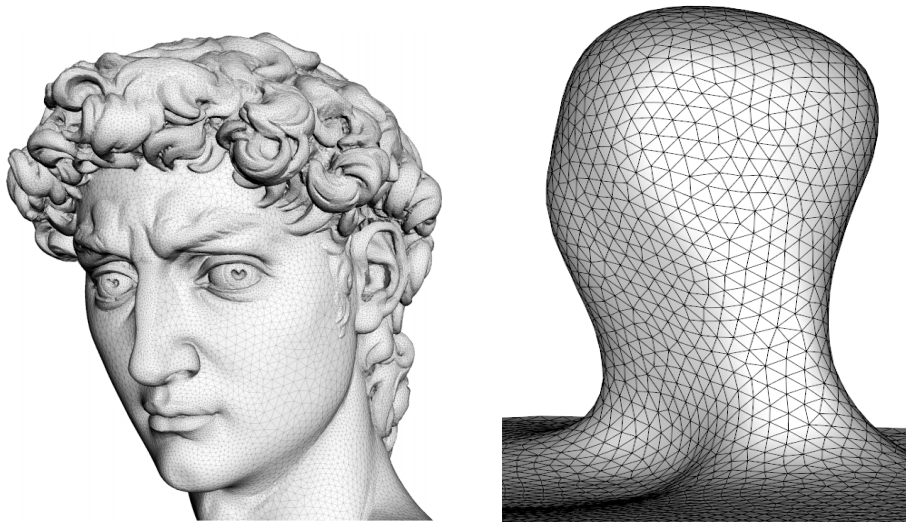
Figure 2.20: David model meshed by Valette *et al.* [2008] and a synthetic salt diapir model.

Methods developed by the computer graphic and computational geometry communities are generally to model surfaces. The objectives of meshing methods developed for numerical simulation are to obtain rapidly reliable, precise enough results. In geomodelling, if the first objective is to represent and model the interfaces between rock volumes, the second one cannot be ignored because the goal is to simulate the real behavior of these rocks. From a topological point of view, surfaces considered in computer graphics are more simple than geological structural models, they generally are manifold and do not have any boundary; they are however more complicated from a geometrical point of view, because they can be highly curved (figure 2.20). Similarities are more important with the models studied in computer aided design[11].

---

[11]CAD is indeed part of the geomodeling software Gocad.

Chapter 3

Contribution: Elements for measuring the complexity of structural models

A paper corresponding to this chapter is in preparation. Guillaume Caumon, Charline Julio, Pablo Mejia and Arnaud Botella collaborated to this research.

Abstract

In this chapter, we propose to analyze geometrical sources of complexity in structural models at a given level of detail. We do not define an absolute complexity criterion, but describe systematically the elements that contribute to the complexity of a structural model using connectivity and geometry measures of the model components (regions, surfaces, lines, and corners). The proposed metrics are computed for a set of 9 synthetic models.

3.1   Motivations

The terms structurally complex, are often mentioned to qualify models built or analyzed with this or that method. However the notion of complexity, as something that is difficult to understand, difficult to realize, or simply unusual, is highly subjective. It depends on the person that says so, on her education, on her experience, on her means, and, above all, on the problem to solve. Depending on the application domain, the point of view on structural model complexity varies a lot. A structural geologist could consider complex the inverse reactivation of normal faults [Sassi *et al.*, 1993], while this would be less important to a reservoir engineer who would consider complex reservoirs where fault networks and fractures have a preponderating control on hydrocarbon trapping and production [Jolley *et al.*, 2007].

This subjectivity of complexity makes difficult the comparison of structural models, making more difficult the comparison of methods developed in geomodeling, comparisons that are nonetheless crucial in research. In this chapter, we restrict our point of view to the structural model complexity from a meshing perspective (a step common to the most part of geomodeling applications) and we try to give elements evaluating the relative complexity of two models, estimate the minimal mesh
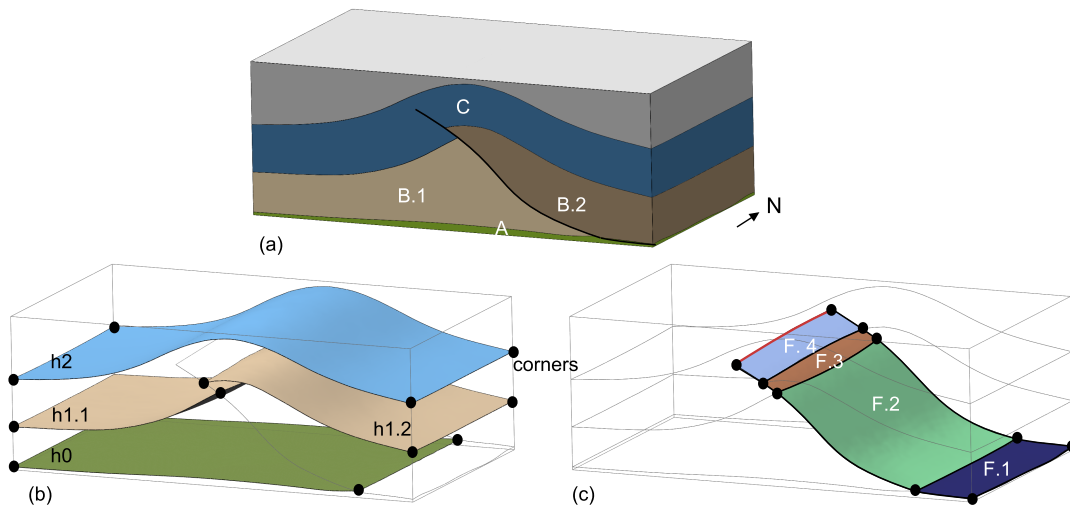
Figure 3.1: Structural model elements. The model has 4 layers A, B, C, D) delimited by 3 horizons (h0, h1, h2) and cut by one fault F. (a) Layer B is split in 2 regions B.1 and B.2. (b) Horizon h1 has two surface connected components, that we call surfaces. (c) The fault has 4 surfaces numbered 1 to 4. Each surface is delimited by 4 lines, themselves delimited by corners. The red line is on the border of one surface only, that is F4.

size for a model, and identify problematic zones of the model for a given resolution. Complexity is then linked to the geometry and to the model level of detail on which depends the feasibility of a mesh with locally or globally defined element sizes.

We saw several measures developed to characterize model complex zones for various applications in section 2.2.3. Some authors even propose geometrical complexity computation [Quadros *et al.*, 2004] or hex-mesh generation complexity evaluation [White *et al.*, 2005]. After analyzing the geometrical complexity sources in geological models (section 3.2), we propose global and local measures of this complexity (section 3.3) and evaluate them on synthetic models (sections 3.4 and 3.5).

3.2   Sources of complexity

Before giving sources of complexity in a model, we define the vocabulary used in this thesis. We consider independently the connected components of all the model components: regions, surfaces, lines, and corners. Each volumetric region is completely defined by the set of surfaces constituting its boundary (figure 3.1). These surfaces are themselves defined by their boundary, lines that are either at the intersection of several surfaces, or that are on the boundary of only one surface. Open lines are delimited by two points that we call corners. Each region, surface, line, or corner corresponds to a unique geological entity, while one geological entity can be divided into several regions, surfaces, lines, or corners (figure 3.1). To have a valid model, its elements[1] must intersect only along their boundaries and the elements that have the same dimension must have the same geometry on these boundaries (their meshes must be conformal) .

---

[1] Also called components in this thesis.
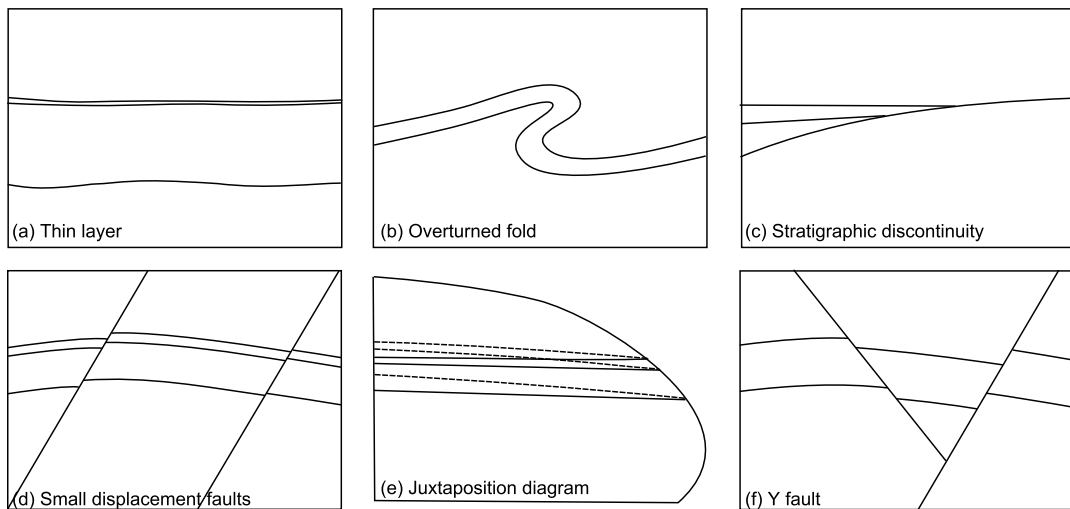
Figure 3.2: Some sources of complexity in structural models. The juxtaposion diagram (f) is a view on the fault surface of the traces of the horizons cut by this fault.

3.2.1 Number of geological features

The complexity of a model mainly depends on the number of continuous layers it contains and on the number of discontinuities affecting these layers. During model building, the consistency of each one of these features must be checked, having a direct impact on modeling time. The number of volumetric regions (one per layer and per fault block) also often determines the number of stationary regions to be used in petrophysical models, hence the effort needed for geostatistical inference and modeling. Because each feature may correspond to localized petrophysical contrasts and induce a compartmentalization of the domain, it often has a first-order impact on flow and geophysical processes.

3.2.2 Interactions between features

The distribution inside the model of geological features, that is their the density, has a direct impact on the modeling, gridding and simulation steps. This density is linked to the geometry of the features but also to the intersections between the model layers, faults and unconformities. Simpler elements have only a few interactions with the other model elements, they can more easily be removed or be modified than those like discontinuities that potentially intersect a lot of elements.

Conformable layers

Conformable layers[2] may be challenging if one of them locally has a very small thickness. Indeed, in that case, the layer validity, i.e. non-crossing top and bottom horizons, is generally more difficult to check (figure 3.2a). Moreover deformations affecting layers may modify their thickness and horizon curvatures. Structures such as overturned folds (figure 3.2b) are more difficult to model than simple folds since

---

[2]Layers resulting of continuous sediment deposits

they cannot be represented as single value height fields, which can be problematic for some applications [Farmer, 2005].

Stratigraphic unconformities

The vertical relationships between layers are controlled by unconformities (erosions, onlaps) which are very common in stratigraphic reservoirs but are difficult to characterize from the data and require more complex modeling steps than continuous sequences (figure 3.2c). The determination of their exact position is often not well known [Caumon, 2003, Lallier, 2012]. as we saw in chapter 2. Their geometries often imply very thin objects and very small contact angles that are particularly challenging for meshing methods.

Faults

Faults are discontinuities inducing a displacement of the layers localized along a surface (figure 3.2d). They are often difficult to characterize from subsurface data and introduce significant complexity due to their connectivity, shape and specific properties [Jolley *et al.*, 2007]. In all faulted configurations, the presence of possibly noisy data calls for a quality control step to validate the fault slip, for instance by analyzing the fault cutoff lines through an Allan (or juxtaposition) diagram (Fig. 3.2e) [Groshong, 2008, Caumon *et al.*, 2009]. Juxtaposition of rocks having different flow properties is also very important for flow purposes because it leads to strong nonlinearities of the flow response to small geometric perturbations [Jolley *et al.*, 2007, Tavassoli *et al.*, 2005]. Intersections at small angles of fault-horizons contact lines may introduce difficulties for layer juxtaposition mapping and gridding, and can affect fault transmissibility. Blind faults raise similar challenges because they stop in the model and displacement is nil at their tips (figure 3.2e). Unlike surfaces cutting through the model, they do not separate two regions making some algorithms unusable as they are.

When considering a fault network, the total complexity is not only a combination of the individual fault complexities. The more different the average orientations and dips of the faults are, the more complex the model is. The number of intersections between the faults and the angles between at these intersections have a major impact on the approximations required for griding. Horizontal branch lines between faults (Y-shaped configurations) (figure 3.2f) or strong variations of the orientations and dip of faults can prevent the easy representation of the model by the extrusion of a cross-section, or pillar gridding (section 2.1.3) [Farmer, 2005].

3.3   General measures

Two types of measures can be used to evaluate the complexity of 3D structural model components: connectivity[3] measures and geometrical measures. The firsts characterize the relationships between model components and are independant of the geometry, the seconds characterize the size and shape of each element.

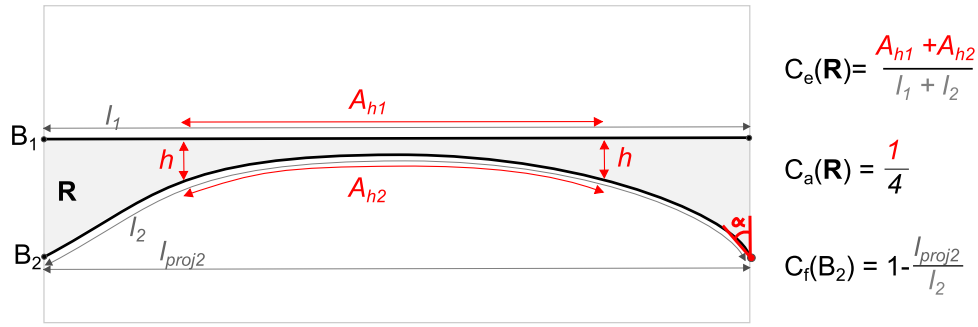[3]Interactions between the model components, also called topology.

Figure 3.3: Geometrical measure computations in the plane. Thickness measure C_e and angle measure C_a for a region **R** and shape measure C_f for one of its boundaries B$_2$.

3.3.1   Global complexity measures

We propose three measures to globally compute the complexity of one model. The first count the number of model elements (regions, surfaces, lines, and corners) excluding those defining the volume of interest. This measure gives the same weight to each component.

To take into account the importance of potential problems due to a given element, the second measure considers geometrical properties of the elements. This permits the comparison or two elements from the same model of from two models. Corners are not taken into account in this measure, however they do have an impact on the values obtained for the lines and surfaces. We compute each element geometrical complexity as the sum of four measures characterizing (1) its size C_t; (2) its shape C_f; (3) its thickness C_e; and (4) its angles C_a. These measures are chosen so that they have values between 0 and 1. Size and thickness measures of a component e of dimension d are defined relatively to a given characteristic size h:

$$C_t(e) = \begin{cases} 0 & \text{if } size(e) > h^d \\ 1 & \text{else} \end{cases}$$

$$C_e(e) = \begin{cases} 0 & \text{for lines} \\ \frac{A_h}{size(B_e)} & \text{for regions and surfaces} \end{cases}$$

where B_e is the set of elements on the boundary of e, A_h the size of the zone where the component thickness is inferior to h (figure 3.3). The shape measure C_f globally evaluates the line and surface deformation. It is taken equal to 1 minus the size of the projection of e on its middle line or surface divided by $size(e)$ (figure 3.3). For regions it is taken at 0.

The angle measure C_a is defined for regions (respectively surfaces) relatively to a given angle α, its evaluates the percentage of the line length (respectively corner number) where the angle between two surfaces (respectively two lines) is inferior to α (figure 3.3).

With the third measure we propose to evaluate the complexity of the elements of a given type as a statistic on their sizes. We chose the variation coefficient[4] that characterizes the relative distribution of element sizes and evaluates scale changes for one element type.

---

[4]Mean over standard deviation.

3.3.2   Neighborhood measures

Computing connectivity measures in the neighborhoods of points sampling the model permits to capture locally model components and to identify more precisely the zones introducing complexity on the global scale. We saw in section 2.2.3 strategies proposed to analyze model complexity by taking measures in the neighborhoods of points sampling the model. Such methods require to compute efficiently and robustly the intersection between the model and the chosen neighborhoods.

To capture spatial relationships between the different elements defining a model, we propose to locally count the corners, line connected components, surface connected components, and regions in the neighborhood of points sampling the model. Basic statistics: mean, variation coefficient, maximum and 90th percentile of these values evaluate the complexity. Obtained measure values depend on the the sampling resolution, on the position of the points, and on the shape of the chosen neighborhoods.

3.4   Models

We propose a suite of relatively simple models numbered A2 to A6 that are all derived from **model A1**, a simple cylindrical anticline composed of three slightly folded horizons (figure 3.4).

In **model A2**, two regional normal faults affect the anticline (figure 3.4). These faults are planar, parallel one to another, cut the whole volume of interest, and have dips close to 60 degrees toward the East. Moreover, they have a constant total slip, corresponding to parallel horizon cutoff lines.

In **model A3**, the regional faults are restricted to an ellipsoid shape and terminate in the model (figure 3.4). These faults do not compartmentalize the domain and fault slips vary from a maximum near fault centers to zero at fault tips.

In **model A4**, one fault is regional while the western fault dies out to the South (figure 3.4). Fault displacements increase to the North. As a result, horizon cutoff lines intersect with small angles.

The faults of **model A5** intersect along a branch line, resulting in a Y configuration (figure 3.4). Fault slips are regular and the model can be restored to model A1 by rigid block motion. However, the slip on the east fault is close to the thickness of the top layer, which generates thin features in the Allan diagram.

Model A6 is obtained by cutting model A4 with a topography surface (erosion). This results in several very small isolated regions and in very small angle contact between the erosion surface and the eroded layers (figure 3.4).

The three other models illustrate challenges arising in other contexts. **Model B** corresponds to a compressive fault-propagation fold (figure 3.5). In the lower part, the fault has a low dip and branches onto a horizontal décollement level. The thrust dip changes to a medium angle (ramp) in the upper part and stops in the upper layer in which the shortening is accommodated by internal layer deformation. **Model C** is built from the folded basal horizon of model A1 overlaid by onlapping horizontal layers deposited at a low angle above it (figure 3.5). The diapiric dome of **model D** intrudes and cuts three layers. Except in the intrusion influence area, the horizons are only slightly deformed (figure 3.5).

Model A1: Slightly folded layers
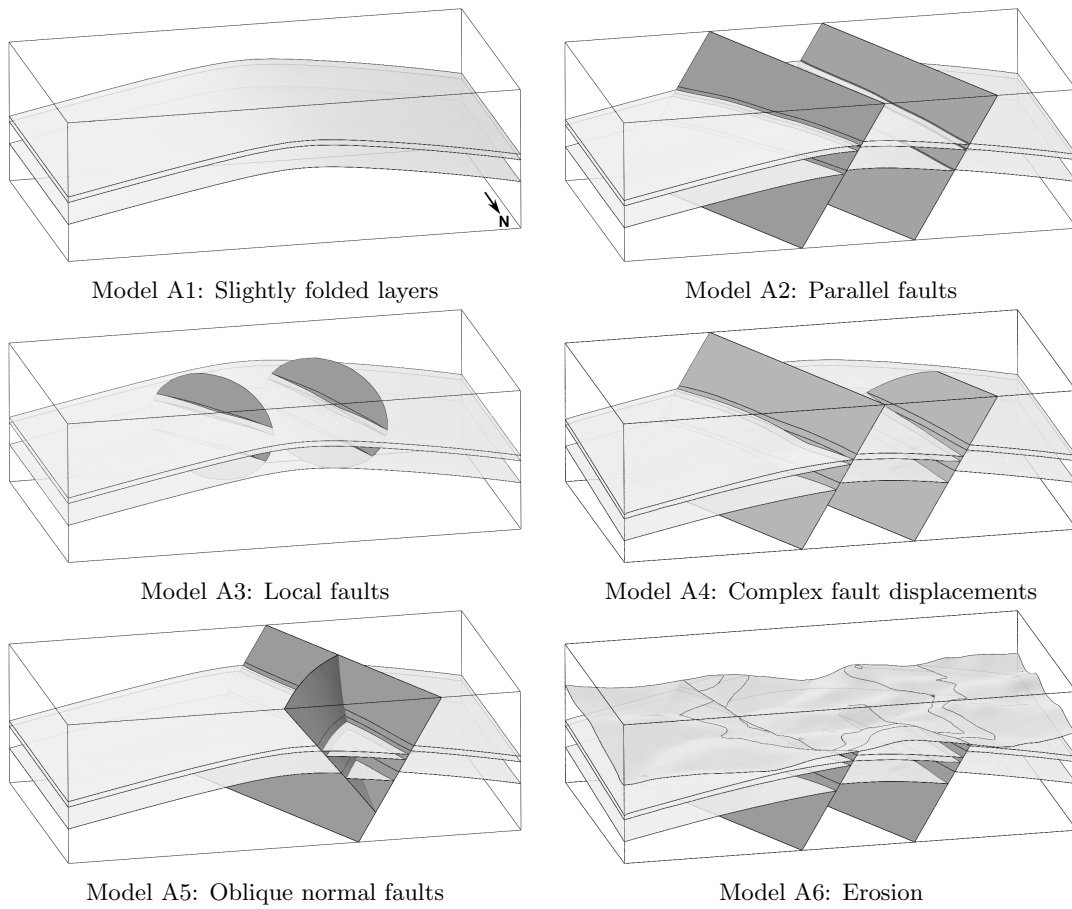
Model A2: Parallel faults

Model A3: Local faults

Model A4: Complex fault displacements

Model A5: Oblique normal faults

Model A6: Erosion

Figure 3.4: Suite of models built from model A1. Dimensions : $1600m \times 930m \times 500m$.

Model B: Thrust fault ($1590m \times 915m \times 578m$)

Model C: Stratigraphic onlap ($1600m \times 930m \times 500m$)

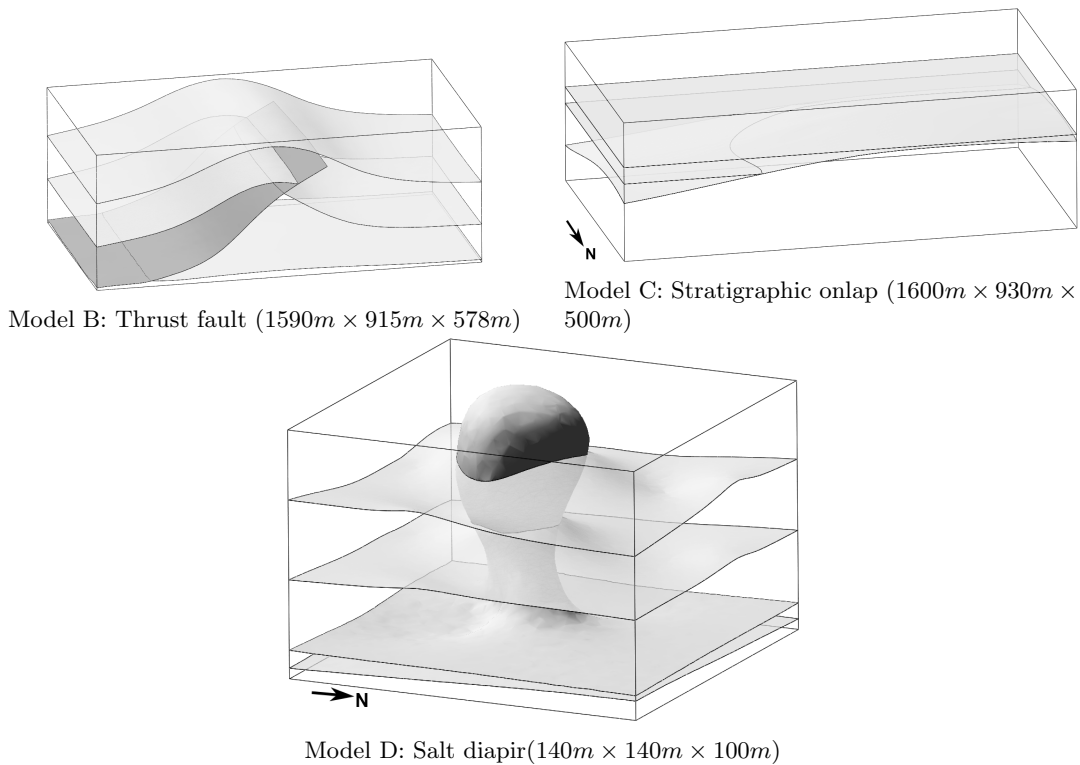Model D: Salt diapir($140m \times 140m \times 100m$)

Figure 3.5: MODELS LEADING TO POTENTIALLY PROBLEMATIC CONFIGURATIONS.

3.5 Results

We compute the measure proposed in section 3.3 for the nine models presented above. The components defining the volume of interest (box) are not taken into account, permitting to characterize the intrinsic model complexity.

3.5.1 Global measures

The first measure that counts the number of elements in the model gives a first classification of the models, in increasing order: A1, C, D, B, A2, A3, A4, A5, A6 (table 3.1). This classification reflects the number of discontinuities affecting the models and on their connectivity. Three groups of models can be distinguished: those with one or no discontinuity (A1, B, C, and D), those with two discontinuities (A2, A3, and A4) and those with two or three intersecting discontinuities (A6 and A5). Because the elements on the boundaries are not taken into account, this simple measure differentiates faults that ends in the model from regional faults that cuts the whole model.

To compute the second measure we choose a reference resolution of 100m and an angle α at 20 degrees (table 3.2). The obtained classification A1, C, B, A2, D, A4, A3, A5 and A6 is slightly different of the first one but extremities are left unchanged. A1 is extremely simple and A6 and A5 are the most complex. The increased complexity of D is due to the fact that the scale of this model is significantly smaller, and its bottom region is almost completely subscale. Model A3 is the third most complex model because of the high complexity introduced by the faults ending in the model.

	A1	A2	A3	A4	A5	A6	B	C	D
Regions	4	12	4	8	12	14	5	4	5
Surfaces	3	23	16	23	31	42	8	4	6
Lines	0	13	24	22	30	44	4	1	2
Corners	0	0	12	6	10	15	0	0	0
Total	7	48	56	59	83	115	17	9	13

Table 3.1: NUMBER OF ELEMENTS.

	A1	A2	A3	A4	A5	A6	B	C	D
Regions	0.13	0.59	0.22	0.34	1.19	6.58	0.35	0.55	2.97
Surfaces	0.03	3.21	12.01	7.41	9.30	12.58	0.25	0.00	1.20
Lines	0.00	0.01	0.56	0.10	4.01	2.92	0.00	0.00	1.62
Total	0.16	3.81	12.79	7.85	14.50	22.07	0.60	0.55	5.79

Table 3.2: SUM OF THE GEOMETRICAL COMPLEXITY MEASURES $(C_t + C_f + C_e + C_\alpha)$.

The fault cutoff lines intersect at angles inferior to 10 degrees.

The third measure (table 3.3) gives a third classification: A1, D, B, C, A2, A4, A3, A5, A6 which is similar to the previous ones. Its meaning is however different since it identifies complexity sources due to scale variations in the models.

3.5.2 Local measures

Method

To determine the neighborhoods in which measures will be computed, we use the cells of the centroidal Voronoi diagram of a given number of sites (sections 1.1.1 and 1.3.1). The cells define a model subdivision relatively isotropic and less sensitive to a certain orientation like Cartesian grids.

Local connectivity measures

These measures were computed for three numbers of cells: 1 000; 10 000, and so at three resolutions, the resolution being the cubic root of the volume of the model divided by the number of points. For A, B and C models these resolutions are respectively 1980m, 919m, and 427m; model D is smaller and the corresponding resolutions are 265m, 123m, and 57m.

	A1	A2	A3	A4	A5	A6	B	C	D
Regions	0.74	0.76	0.74	0.84	1.08	1.67	0.57	0.94	0.54
Surfaces	0.00	0.93	1.97	1.41	1.74	1.62	0.79	0.71	0.56
Lines		0.01	0.63	0.67	0.82	1.06	0.00		0.13
Total	0.74	1.71	3.35	2.92	3.64	4.35	1.37	1.65	1.23

Table 3.3: VARIATION COEFFICIENTS OF ELEMENT SIZES TYPE BY TYPE.

		A1	A2	A3	A4	A5	A6	B	C	D
	Q10	1	1	1	1	1	2	3	1	3
	Q50	5	5	5	5	5	7	5	5	5
	Q90	7	11	10	11	11	12	7	8	6
100	Max	7	15	15	16	30	22	8	8	9
	Mean	4.300	5.950	5.210	5.630	5.510	6.710	4.290	4.040	4.060
	Var.Coeff.	0.547	0.630	0.658	0.665	0.775	0.696	0.390	0.593	0.390
	Q10	1	1	1	1	1	1	1	1	1
	Q50	1	3	1	3	3	3	3	1	3
	Q90	5	7	5	7	6	7	5	5	5
1000	Max	7	15	13	14	22	19	6	8	6
	Mean	2.500	3.137	2.710	2.960	2.950	3.170	2.630	2.360	2.569
	Var.Coeff.	0.751	0.814	0.808	0.804	0.858	0.871	0.523	0.813	0.581
	Q10	1	1	1	1	1	1	1	1	1
	Q50	1	1	1	1	1	1	1	1	1
	Q90	3	3	3	3	3	3	3	3	3
10000	Max	5	11	11	12	19	15	6	6	6
	Mean	1.688	1.910	1.746	1.850	1.840	1.920	1.770	1.570	1.760
	Var.Coeff.	0.728	0.788	0.755	0.778	0.795	0.827	0.609	0.721	0.676

Table 3.4: Statistics of the number of elements per cell.

Results

The statistics of the number of elements per cell are given in table 3.4. The mean, maximum, coefficient of variation and the 90th percentile are drawn in a radar chart (figure 3.6). For a given statistic, the relative classification of the models at the different resolutions slightly varies specially for the simpler models. However the separation of the models into two groups is clear for almost all statistics and resolutions: the simplest models (A1, B, C and D) that have none or one discontinuity and those with at least two (A2, A3, A4, A5, and A6).

An expected observation is that, when resolution increases, the local complexity and the differences between models decrease[5]. The mean is strongly impacted by this decrease, for example the mean in A5 diminish from 5.51 (100 cells) to 1.84 (10000 cells) that is a loss of 66.6%, the maximum only decrease from 30 to 19 (36.6%). The maximum characterizes the most complex zone of the model, that is the element which is contained in the greatest number of elements (typically a corner or a contact line). According to this criteria obtained classification is: B, D, A1, C, A3, A2, A4, A6, A5. The 90th percentile is the same for all the models at the highest resolution (the value 3 corresponds to a cell intersecting a surface part and two regions), but it may permit to classify the models at lower resolutions. The variation coefficient evaluates the dispersion of the measures and can also be used as a complexity measure.

The main advantage of these local measures is the possibility to understand the spatial organization of the complexity and estimate the extension of the zones where a given method may fail using the number of elements found in a cell. As we can see on figure 3.7, these cells are those nearest to thin features of the models, thin layers (model A6), small fault displacement (model A2), small contact angle on a fault (model A5), contact lines and corners figure 3.7).

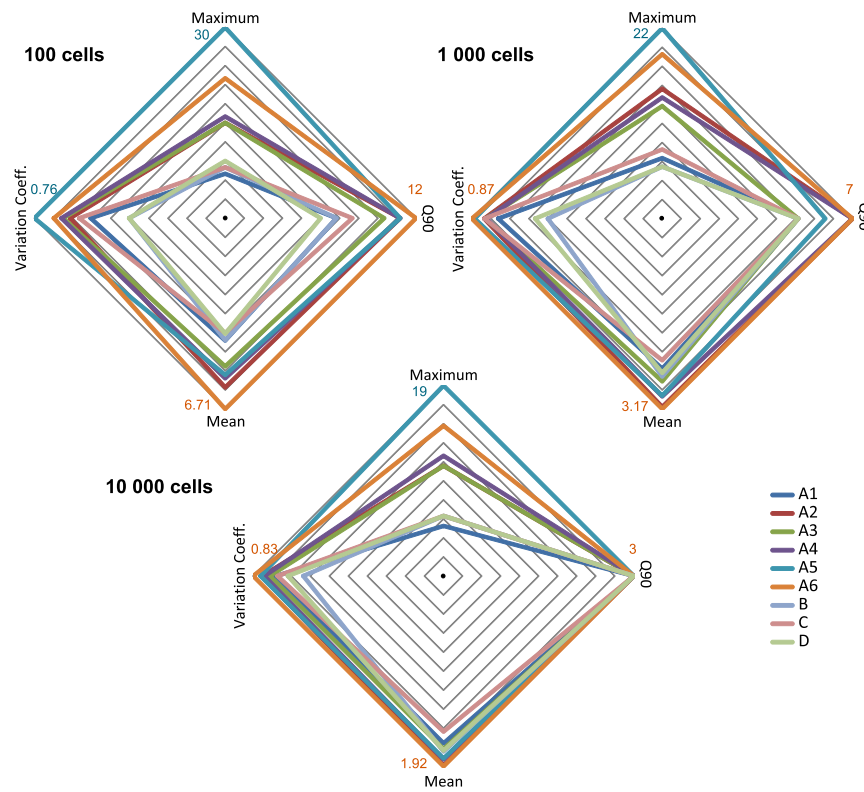[5]This effect is similar to the support effect in geostatistics [Journel, 2003].

Figure 3.6: Normalized statistics on the numbers of elements counted in 100; 1 000; and 10 000 Voronoi cells.
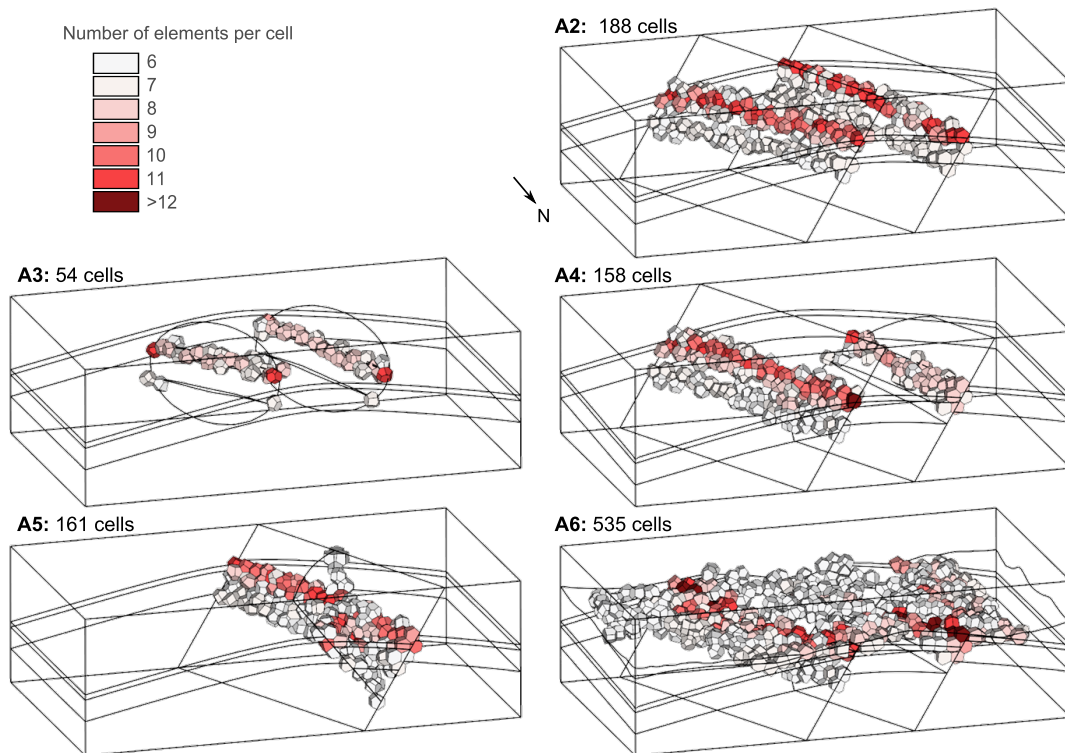

Figure 3.7: Complex zones in models A. Cells containing more than six elements are localized near discontinuities.

3.6   Discussion

3.6.1   Contributions

In this chapter, we proposed to use general measures to evaluate the complexity of structural models in order to compare more objectively several models. The metrics derived from these measures and the proposed benchmark models are important tools to quantify our perception of a model complexity, that is the configurations that we find difficult to understand and that challenge the software we use and develop. These measures are simple, some of them are computed for a given resolution. They help understanding the complexity induced by each element of a model independently of its type and to compare several models of the same area at different resolutions.

3.6.2   Perspectives

There are a lot of perspectives for this work. The measures could be used to determine the necessary resolution to mesh a model [Quadros *et al.*, 2004]. They also could be combined to evaluate the complexity of a given modeling task. This requires to perfectly understand the involved methods and algorithms, to consider the representation of the model (mesh size and quality), and to realize sensibility analysis. These three facts make difficult the determination of such measures evaluating, for example, if a given meshing method will permit to reach the desired quality, resolution, and number of elements for a model.

Additional results on real models and on more synthetic benchmark models created to evaluate the impact of a upscaling or a downscaling of the geometry, or the addition of a geological entity, would permit to refine our measures and to confirm the impact of identified configurations. Type specific complexity measures could also give supplementary information. For example, for fault surfaces, the number of cut layers, displacement distribution, angles between the fault and the horizons, induced layer contacts, are crucial in geomodeling. To compute the complexity of a fault network, the connections between the different faults and the variations of orientations are important. For the layers, the number of fault blocks, deformation intensity, and thickness variations could be considered.

Geometry computations could also be performed in Voronoi cells. This would permit to locally characterize the complexity independently of the model representation, basically its mesh quality and resolution, unlike the measures that we compute that depend on the input model mesh. We could also consider other cells like voxels or spheres to compute these local measures.

Chapter 4

Contribution : Structural model surface remeshing at a given resolution

A paper corresponding to this chapter was published in *Computers & Geosciences* [Pellerin *et al.*, 2014], a preliminary version having been presented at the IAMG annual meeting [Pellerin *et al.*, 2011].

Abstract

In this chapter, we propose a method to remesh the surfaces of structural models with triangles as equilateral as possible. We use a centroidal Voronoi diagram optimization method to place the vertices of the remeshed surfaces. We introduce an energy to improve site placement along surface boundaries. The mesh is built by analyzing the intersections between the model and the Voronoi cells. Where the Voronoi cells restricted to the model surfaces, lines, and corners have a unique connected component, we build the restricted Delaunay triangulation of the sites to the model. Where they do not, we build a mesh dual of these connected components. So, if the final resolution is sufficient, input lines and corners are also lines and corners of the final model. However, in models where contacts are complex, resolution is often not sufficient, and instead of a mesh refinement strategy, we propose to simplify model features. The method is applied to twelve structural models.

4.1   Motivations

The various strategies used to build structural models lead to surfaces that are, most of the time, defined by triangles [Caumon *et al.*, 2009]. Depending on the modeler's choices and on the algorithms used to build the model, mesh quality and resolution vary significantly. Triangle quality may be very poor[1], especially when implicit horizons are extracted with a marching tetrahedra method. The mesh must then be adapted to efficiently visualize and modify the model, as well as run simulations, like restoration [e.g., Dunbar et Cook, 2003], and above all to generate an adequate volumetric mesh.

---

[1]Our goal is to have equilateral triangles.

As we saw in section 3.2, many configurations are challenging when meshing a model with an acceptable number of elements of good quality. In this chapter, we choose to authorize simplifications of the model in order to adapt its resolution and to give priority to the number and the quality of the remeshed surface triangles. There are two objectives: remesh the surfaces defining the model and adapt the model resolution.

The most part of the many surface (re)meshing methods do not allow input model modifications (section 2.4). Constrained Delaunay or advancing front methods remesh one by one the surfaces while ignoring the whole model. Methods giving theoretical guarantees on the final mesh topology and quality do not give any control on resolution and on the final mesh number of elements (section 2.4.2). When the input triangle quality is very poor, computing a parametrization to project surface triangles in a 2D space may be an issue. Octree surface remeshing methods exploit a voxel subdivision of the model. This 3D subdivision is also used by simplification methods operating on volumetric model components that locally analyze the relationships between the model components and the subdivision cells (section 2.2.3). We propose a similar approach combined with a Voronoi diagram optimization remeshing method and exploit the fact that sites not verifying the topological ball property have a restricted Delaunay triangulation that is a simplified version of the initial object (section 1.2.3 and figure 1.5).

4.2 Goals

Input The input of the surface remeshing method we propose is a valid triangulated B-Rep model. Surface meshes must be conformal.

Result A global remeshing of the model surfaces with triangles as equilateral as possible. Contact lines between surfaces are remeshed and the surfaces remain conformal along these lines. The model is modified when contact lines or corners are too close (figure 4.1). This functionality allow the automatic adaptation of the model resolution. The method was applied on twelve geological structural models (section 4.5).

Principle We use a centroidal restricted Voronoi diagram to adequately place the final mesh vertices near input surfaces and contact lines (section 4.3). A topological control allow then the determination of the triangle vertices from the intersections between the site Voronoi diagram and the model components (section 4.4).

4.3 Model sampling optimization

4.3.1 CVT optimization

First, a fixed number of sites are placed so that they are a good sampling of the geological model. Each site samples the model in the sense that it represents the part of the model closest to it than to any other site: its restricted Voronoi cell (section 1.2.1). The input number of sites then determines the resolution at which the model will be remeshed, it may be computed from the square root of the model area divided by the target edge length. We saw in section 1.3.2 that when the
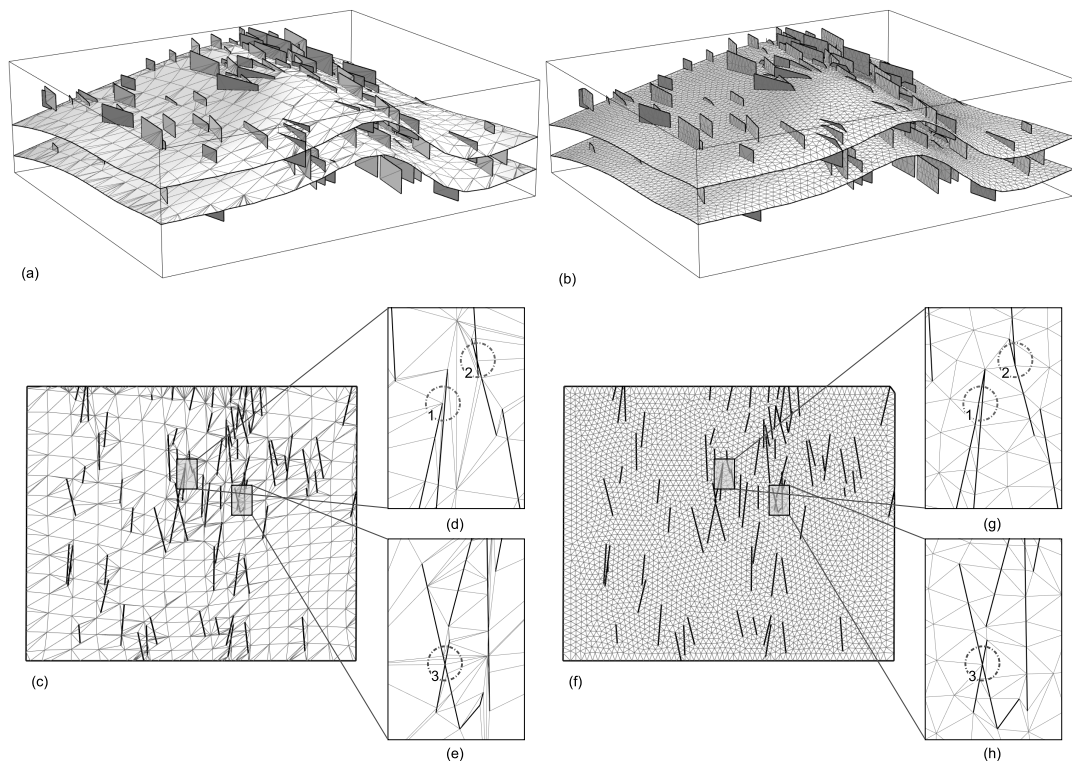
Figure 4.1: Remeshing a model cut by 200 fractures. Quality of the remeshed surfaces is improved, three types of challenging intersections (1) slightly crossing fractures (2) almost intersecting fractures (3) small angle crossing, are remeshed and modified according to the desired resolution.

restricted Voronoi diagram is centroidal its restricted Voronoi cells are compact and that the restricted Delaunay triangulation remesh the model surfaces with almost equilateral triangles.

4.3.2 Optimization of sites near boundaries

When computing a restricted centroidal Voronoi diagram to a surface that has a boundary, optimized sites are not on the boundary because the centroid of a cell intersecting a boundary line is not on this line. To modify this stable position, a border energy term can be added to the objective function for sites whose Voronoi cell (V_p) intersects the boundary (B):

$$F_B(S) = \sum_{p \in S} \left[\int_{V_p \cap B} ||y - p|| dy \right]^2 \tag{4.1}$$

To evaluate this function and its gradient we decompose the restriction of each Voronoi cell to the boundary $(V_p \cap B)$ into segments (figure 4.2). For each segment, $E = C_1 C_2$, we denote $\overrightarrow{N} = \overrightarrow{C_2 \, p}.\overrightarrow{C_2 \, C_1}$ and we have $F_B^E = 1/2\,||\overrightarrow{N}||^2$, that is the square area of the triangle $p\, C_1\, C_2$ (figure 4.2). The corresponding gradient is:

$$\frac{dF_B}{dS}(p, C_1, C_2) = \frac{dF_B}{dp} + \frac{dF_B}{dC_1}\frac{dC_1}{dS} + \frac{dF_B}{dC_2}\frac{dC_2}{dS} \tag{4.2}$$

where $dF_B/dp = \overrightarrow{N} \times \overrightarrow{C_1 \, C_2}$, the terms dF_B/dC_1 and dF_B/dC_2 are evaluated similarly. The term dC/dS depends on point C configuration. Either C is a vertex of the initial mesh and the gradient is a null vector, or C is at the intersection of the bisector between sites p_0 and p_1 with an edge of an initial triangle and is computed as:

$$\frac{dC}{dS} = \begin{pmatrix} [p_1 - p_0]^t \\ [N_1]^t \\ [N_2]^t \end{pmatrix}^{-1} \begin{pmatrix} [C - p_0]^t & [p_1 - C]^t \\ [C - p_0]^t & 0 \\ 0 & 0 \end{pmatrix} \tag{4.3}$$

where N_1 and N_2 are the normals to two planes built so that they intersect along a line containing the segment $C_1 C_2$. The proof is given in Lévy et Liu [2010]. To improve the placement of the sites near boundaries and contact lines we minimize the objective function $F = (1 - \alpha)F_{CVT} + \alpha F_B$ where α is the ratio between the boundary energy and CVT energy gradient norms.

4.3.3 Implementation

Algorithm 4.1 summarizes the steps to perform the optimization of a given number of sites over a model Ω. (1) The initial random placement of the sites on the model surfaces is done using the algorithm given by Lévy et Bonneel [2013]. (2) The computation of the restricted Voronoi diagram is done using the fast parallelized method also described by Lévy et Bonneel [2013]. (3) The contributions of each cell of the restricted Voronoi diagram to the objective function and to its gradient is computed following Yan *et al.* [2009] for the CVT energy and the above for the boundary term. The minimization of the objective function F is done with a L-BFGS algorithm [Nocedal, 1980]. The optimization can be stopped when the norm of the gradient is
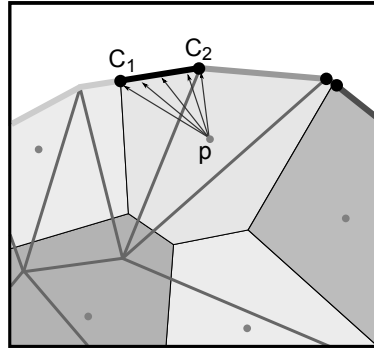
Figure 4.2: INTEGRATION SEGMENTS FOR THE COMPUTATION OF THE BORDER ENERGY.

ALGORITHM 4.1 - OPTIMIZATION OF THE SITES.

Data: a model Ω, the desired number of points n
Result: an isotropic sampling **S** of Ω
(1) **S** $\leftarrow$ initial random sampling of Ω [Lévy et Bonneel, 2013] ;
while *minimum not reached* **do**
    (2) Compute the restricted Voronoi diagram of **S** to Ω [Lévy et Bonneel, 2013] ;
    (3) Compute $F(\mathbf{S})$ and $dF/d\mathbf{S}$ [Liu *et al.*, 2009] ;
    Determine the search direction $\mathbf{\Delta S}$ [Liu *et al.*, 2009] ;
    $\mathbf{S} \leftarrow \mathbf{S} + \mathbf{\Delta S}$;
end

---

inferior to a given value. From our experience, convergence is very fast, and in practice we stop the optimization process after 100 iterations, the input mesh resolution does not impact the convergence while increased feature density slightly decreases the convergence. Specific convergence rates are discussed by Liu *et al.* [2009].

4.4 Mesh building

Once the sites have been optimally distributed, we compute their restricted Voronoi diagram to the structural model surfaces to determine the vertices and triangles of the output mesh.

4.4.1 Surface component remeshing

Let's first consider a (non-geological) model in which the different surface parts do not intersect and have no boundary: two nested spheres (figure 4.3). The two surface parts are sampled by 100 sites which optimized positions are between the spheres (figure 4.4a). To recover the input surface parts, each site is replaced by two vertices, one for each connected component of the restricted Voronoi cell (figure 4.4b). There is then one triangle to build for each point shared by three restricted Voronoi cells (figure 4.3c and 4.4c). The obtained mesh is a dual of the connected components of the restricted centroidal Voronoi diagram, it is closer to the input mesh than the restricted Delaunay triangulation (one sphere in this case) where the topological ball property is not true - section 1.2.4). The multi-nerve theorem gives that, if all restricted Voronoi cell connected components are contractile, the restricted Delaunay
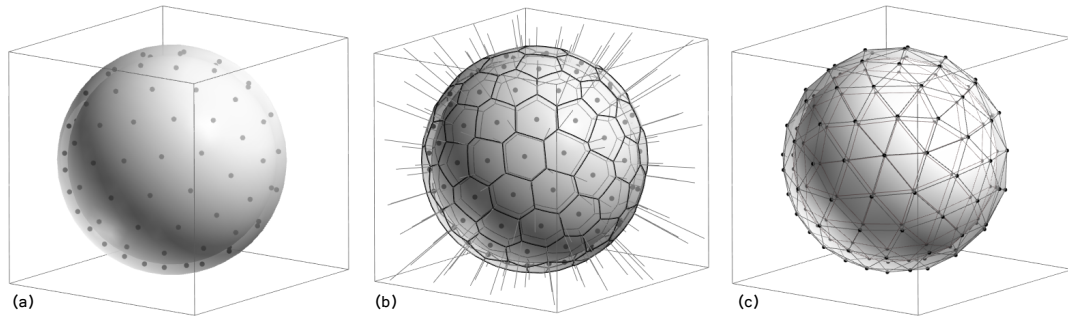
Figure 4.3: NESTED SPHERES REMESHING. (a) 100 optimized sites are sandwiched between two spheres (b) Each restricted Voronoi cell has 2 connected components (c) Dual of the connected components of the restricted Voronoi diagram (see figure 4.4).
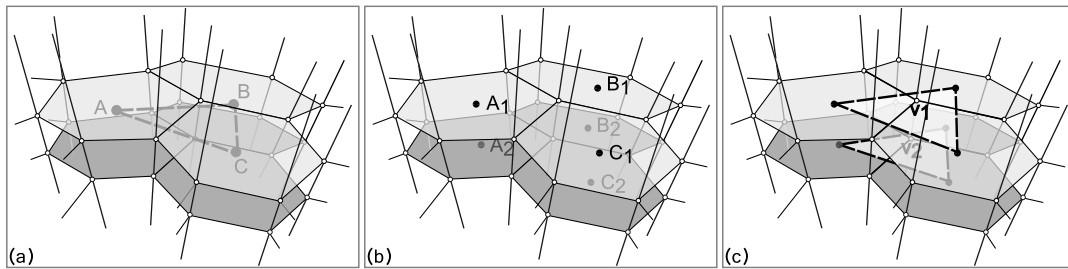

Figure 4.4: REMESHING TWO CLOSE SURFACES. (a) 3 sites (A, B and C) are sandwiched between two close surfaces. Their restricted Voronoi cells have two connected components. The restricted Delaunay triangulation has one triangle ABC. (b) Each site is replaced by two points. (c) Triangles $A_1B_1C_1$ and $A_2B_2C_2$ correspond to points v_1 and v_2 that are shared by three restricted cell connected components.

triangulation it is homotopy equivalent to the input model [Colin de Verdière *et al.*, 2012].

4.4.2   Line remeshing

Let's consider now a surface that has a boundary. Similarly to what happens for surface components, this boundary may not be correctly remeshed when the number of sites is too small, i.e. when the topological ball property is not true. To remesh the boundary adequately as many points as there are connected components for the intersection between its restricted Voronoi cell to the boundary are associated to each site (figure 4.5). These additional points must be taken into account when building final triangles. But, because one restricted Voronoi cell may then correspond to several points, the dual of the Voronoi point is not always a triangles. Polygons that are dual of Voronoi edges intersecting twice the boundary are to build (figures 4.5c & d).

The more intersections between a restricted Voronoi cell and model lines, the more vertices in the final mesh corresponding to this cell. This may lead to configurations where the polygons to build intersect (figure 4.6a). We propose to merge the points corresponding to one cell connected component if there are more than two. This makes our method more robust, but at the cost of modifications of the surface
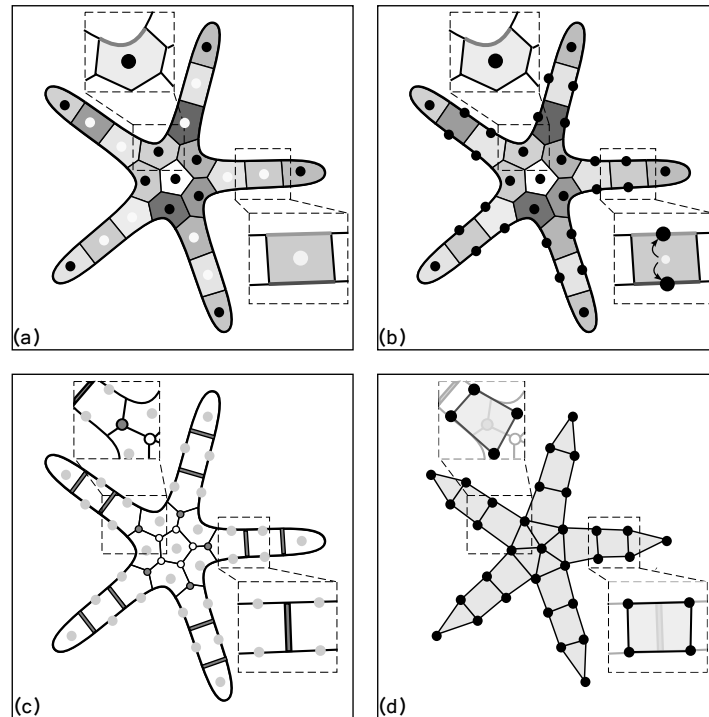
Figure 4.5: REMESHING A SURFACE WITH A BOUNDARY. (a) 21 sites sample the star; Voronoi cells of the white sites intersect twice the boundary, those of the black sites intersect it once or not at all. (b) Each white site is replaced by two points, one per intersection of the cell with the boundary (d) Final mesh polygons correspond to restricted Voronoi points shared by at least one restricted Voronoi cell that corresponds to two points (gray), or to Voronoi segments intersecting twice the boundary (c).

connections that are questionable from a geological point of view and depend highly on the optimized site positions. Moreover these modifications depend on the exact positions of the sites, and a tiny modification of one site coordinates might sufficient to locally change the performed modifications. It is but these modifications that allow a control on model resolution in our meshing method.

4.4.3   Corner meshing

The last elements to take into account for geological model remeshing are triple points, i.e. points defining boundary lines connected components. To recover all the triple points of the input model, there is no other option than to put one point for each triple point present in the restricted Voronoi cell. So, to fully reconstruct the input model, we need to have for each restricted Voronoi cell, one point per triple point, one point per line connected component, and one point per surface connected component (algorithm 4.2).

When there are more than one triple point on a connected component of a restricted Voronoi cell to the boundary, i.e. the final resolution is not sufficient, we choose to not recover all the triple points of the input model and we merge them (figure 4.6b). When this merging operation is done, the previously described merging is also performed. This way, each restricted Voronoi cell connected component has 1 or 2 points and the quads or triangles to build with these points do no intersect.
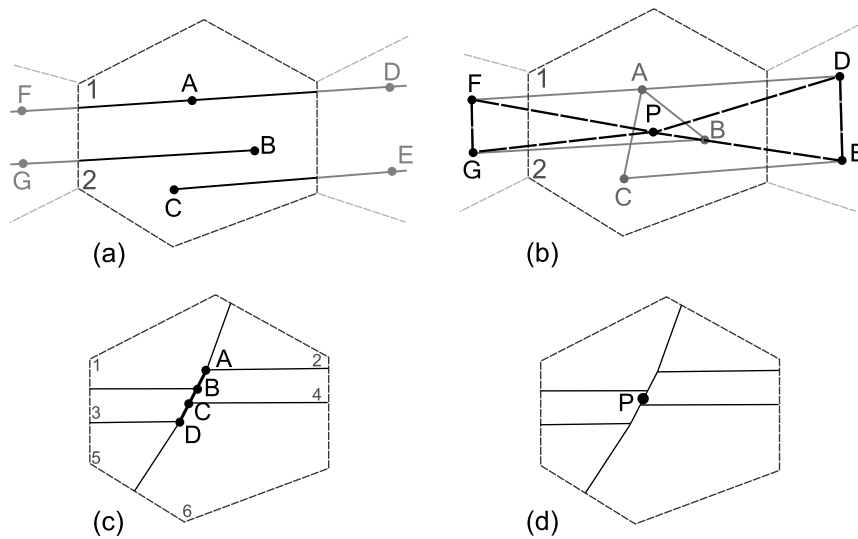
Figure 4.6: CONFIGURATIONS LEADING TO MODIFICATIONS OF THE MODEL. (a) The centralrestricted Voronoi cell corresponds to 3 points (A, B, C) (b) Polygons to build with these points ABGF and ADEC intersect. The three points are merged in P. (c) Contact lines (black) cut the cell into 6 connected components. (d) 4 corners (A, B C, and D) are merged in P because they are connected through boundary segments.

The last modification is the merging of the vertices that correspond to close features, close meaning that the distance between them is inferior to a specified input value (figure 4.6c & d). This is a way to make the model easier to mesh and simplify very small features by removing small fault throws and joining fault tips close to another fault (figure 4.7).

4.4.4   Implementation

Algorithm 4.3 summarizes the implementation of the mesh building steps. The input of the method is a restricted Voronoi diagram, a polygonal surface in which each facet is associated to the triangle and the site from which it was obtained First, each restricted Voronoi cell and its connected components are determined, then the vertices to put for each one of them are computed (algorithm 4.2). The last step is to build the polygons linking these vertices (figure 4.5).

4.4.5   Mesh improvements

The quality of the triangles of the final mesh is completely dependent on the shape of the connected components of the restricted Voronoi cell. When they are close to regular hexagons the dual triangles are close to being equilateral, but relatively small triangular facets might appear on the restricted Voronoi diagram when a Voronoi point or edge is close to one of the input surface. When such a facet is in the interior of the surface part it results in a valence three vertex that can be easily removed (figure 4.8a). When it is on a free boundary, the corresponding triangle is degenerated and is simply removed (figure 4.8b). When this facet is along a contact (figure 4.9a), the dual is also a degenerated triangle but a specific processing is necessary to remove it while maintaining the contact sealed. The procedure is described in algorithm 4.4
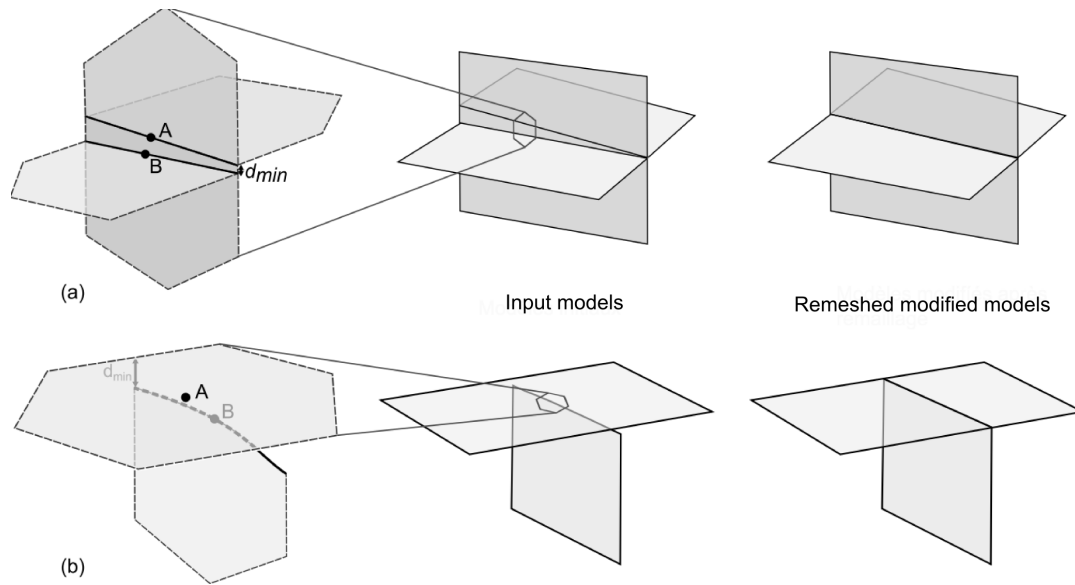
Figure 4.7: Model resolution control. If the surfaces sampled by one cell are close compared to a given threshold $d_{resolution}$, corresponding points are merged. (a) The minimal displacement on the fault d_{min} is below $d_{resolution}$ and points A and B are merged. Vertical displacement is canceled in the final model. (b) The minimum distance between the two surfaces is below $d_{resolution}$ and they are connected in the remeshed model.

Algorithm 4.2 - Output mesh vertex computation.

Data: the restricted Voronoi cell of site i, distance $d_{resolution}$
Result: set of points remeshing the cell
foreach *Connected component CC* **do**
    if *CC intersects boundary lines* **then**
        foreach *Boundary connected component BC* **do**
            if *BC contains corners* **then**
                Add one point per corner ;
            else
                Add a point on the boundary part BC ;
            end
        end
    else
        Add a point at the centroid of the connected component CC ;
    end
end
(2) Cluster and merge points sampling triple points connected by a boundary line (figure 4.6b) ;
(3) **foreach** *Connected component CC* **do**
    if *number of points > 2 (figure 4.6a)* **then**
        Merge the points ;
    end
end
(4) Cluster and merge the points whose corresponding model parts are close ($d_{min} < d_{resolution}$) (figure 4.6c & d) ;

ALGORITHM 4.3 - OUTPUT MESH BUILDING STEPS.

Data: the restricted Voronoi diagram of optimized sites **S** to model Ω
Result: a triangular remesh of the model Ω
foreach $i \in$ **S do**
  (1) Compute the connected components of the restricted Voronoi cell ;
  (2) Compute the points remeshing the cell ;
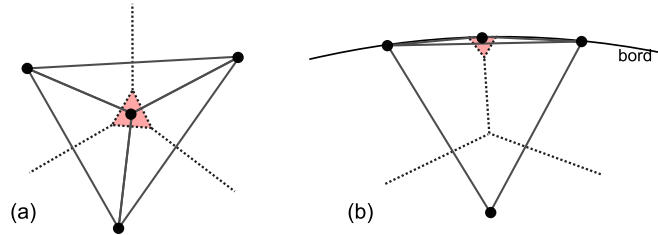**end**
(3) Build triangles ;

Figure 4.8: SMALL VORONOI CELL DUAL OF DEGENERATED TRIANGLES. (a) A triangular restricted Voronoi cell connected component in the interior of a surface correspond to a valence 3 vertex. (b) If it is on a free boundary line, the dual triangle is degenerated.

and on figure 4.9

Removing these needle-shaped triangles corresponds to ignoring a small intersection of the Voronoi diagram with the input surface and can be seen as the result of the remeshing if the input surface and/or the contacts lines were slightly moved so that the small facet on the restricted Voronoi diagram disappears.

As we use the Euclidean distance to approximate the geodesic distance (the length of the shortest path on the surface between two points) when sampling the surfaces and making some simplifications, triangles of the output mesh might intersect. They must be identified and the intersections must be resolved by vertex displacements or edge flipping.

ALGORITHM 4.4 - POST-PROCESSING OF DEGENERATED TRIANGLES ALONG CONTACT LINES.

Data: Set of triangles T along contact lines
Result: T has no degenerated triangles
foreach *triangle* **do**
  Compute the sum of its vertex configurations (figure 4.9b) ;
end
while T *modified* **do**
  foreach *chaque triangle* **do**
    if *configuration == 6* **then**
      Remove one degenerated triangle edge that is on the contact (figure 4.9d) ;
    end
    if *configuration totale == 9* **then**
      Remove the triangle edge linking the two configuration 4 vertices
      (figure 4.9c) ;
    end
    Update triangle configurations ;
  end
end

(a) Problematic site positions

(b) Triangles and point configurations

(c) Triangle ABC processing
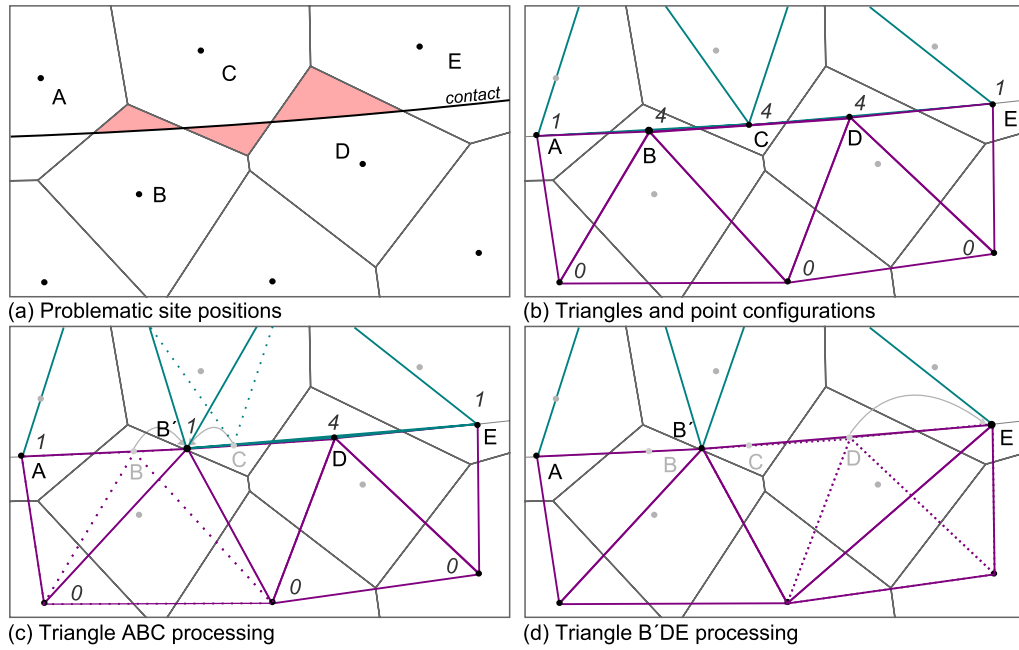
(d) Triangle B´DE processing

Figure 4.9: IDENTIFICATION AND PROCESSING OF DEGENERATED TRIANGLES. (a) Triangular restricted Voronoi cell connected components adjacent to a contact line (red) correspond to degenerated triangles ABC, BCD and CDE (b) The value associated to each vertex identify its configuration: 4 for the vertices dual of a red cell, 1 for the vertices on the contact, 0 for the others. (c) Triangle ABC, configuration $9 = 4 + 4 + 1$, is removed by merging points B and C, at their centroid B'. (d) Triangle B'DE, configuration $6 = 4 + 1 + 1$, is removed by deleting edge DE.

4.5   Results for 12 structural models

We have applied our surface remeshing method on twelve structural models described in table 4.1 and illustrated on figures 4.10 to 4.18. The models are presented in an increasing meshing difficulty order. This order is subjective, the work on complexity presented in chapter 3 being posterior to this one. The difficulty to remesh fractured or faulted models depends on four factors: the number of faults, the number of intersections between faults, the number of faults terminating in the model, and throw sizes.

Input mesh sizes vary from several thousand triangles to almost one million triangles. Computation times to optimize the site positions (100 iterations) and build the final mesh range between 13s and 150s on a 8-core laptop (frequency 1.73GHz). They depend mainly on the size of the input mesh, on the number of sites (algorithmic complexity) and on the number of degenerated cases to process (model complexity). The input and final triangle quality are compared using three criteria: the smallest angle, the percentage of angles under 30 degrees, and the average triangle quality. The quality of a triangle is taken as $Q = 6\,S/(\sqrt{3}\,h_{max}\,p)$ where S is the area of the triangle, h_{max} the length of its longest edge, and p its half perimeter [Frey et Borouchaki, 1999]. Note that the output quality of the triangles is neither fixed beforehand, nor does it depend on the quality of the input mesh. The Hausdorff distance between the output and input model is computed with the code of Aspert et al. [2002] and is given in percentage of the boundary box diagonal.

Dataset	Horizons	Faults	Main challenges	Credentials	Figures
Coal veins	29	0	Thin layers	Courtesy of Gocad	figure 4.10
10.2km × 1.3km × 280m				consortium	
Forward	7	0	Thin layers,	Laurent [2013]	figure 4.11
110m × 65m × 40m			onlaps		
Detachment	8	1	Thin layers	Courtesy of Chevron	figure 4.12
22km × 14km × 7.7km				Guzofski *et al.* [2009]	
Leipzig	2	9	Fault network	Courtesy of Total	figure 4.12
1.2km × 1.2km × 0.4km					
Lambda	2	13	Low angle faults	Courtesy of Gocad	figure 4.12
6km × 4.5km × 1.9km			fault throws	consortium	
DFN	2	200	Fracture relations	Courtesy of Gocad	figure 4.13
13km × 11km × 4km				consortium	and 4.1
HC	7	2	Thin layers,	Courtesy of	figure 4.13
18km × 10km × 10.2km			Inverse fault	Harvard-Chevron	
Cloudspin	3	10	Low angle faults,	Courtesy of PDGM	figure 4.14
14.7km × 12km × 2km			fault throws	and Schlumberger	
Clyde	4	22	Fault intersections,	Confidential	figure 4.15
12km × 10.3km × 1.7km			fault throws		and 4.17
Nancy	7	26	Complex faults,	Courtesy of Total	figure 4.16
11km × 3km × 1.4km			fault throws		
Annot	9	3	Thin layers, onlap,	Salles *et al.* [2011]	figure 4.18
11km × 5.5km × 2.8km			fault throws		
Sandbox	8	33	Fault throws	Courtesy of IFPEN	figure 4.18
3.5km × 3km × 0.5km				Colletta *et al.* [1991]	

Table 4.1: Main features and challenges of the 12 remeshed models. Main features and challenges of the 12 remeshed models
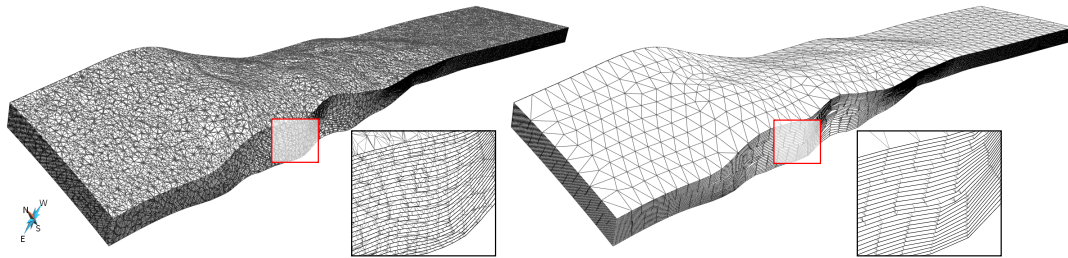
Figure 4.10: Coal veins remeshing. 29 sub-vertical surfaces delimit thin coal veins. 1000 sites are sufficient to remesh the model decreasing the number of triangles from nearly one million to 35 thousand (see tables 4.1 and 4.2 for details).

In the remeshed models, the most important elements (the biggest) are kept, but the numbers of surface connected components, line connected components, and corners do change because of the performed model modifications. Detailed statistics on the input and output meshes are given in table 4.2.
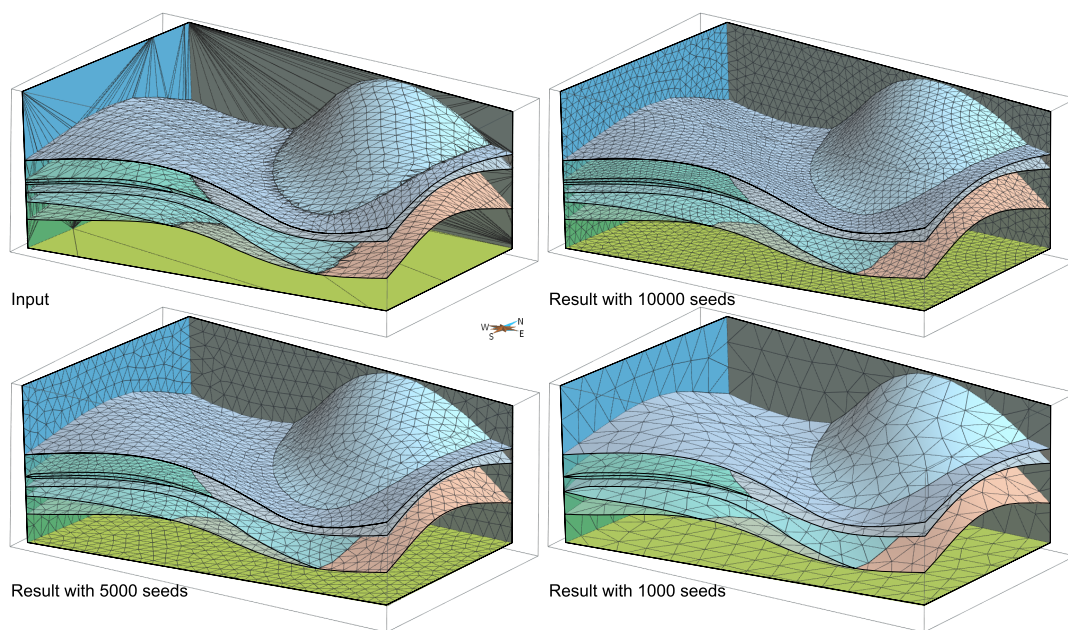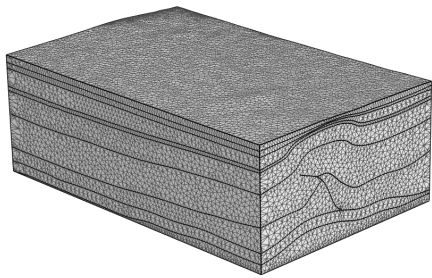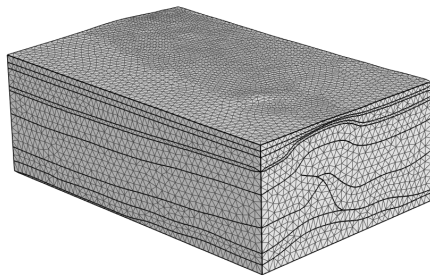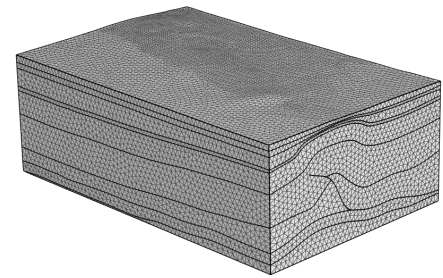
Figure 4.11: FORWARD MODEL REMESHING WITH VARYING RESOLUTIONS. Input model shows 3 three challenges for remeshing, very thin layers, major layer thickness variations and low-angle contacts between horizons due to onlapping geometries (see tables 4.1 and 4.2 for details).
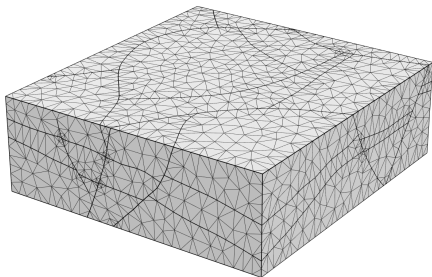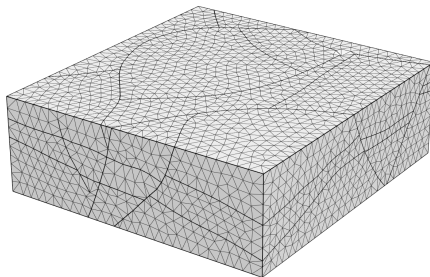
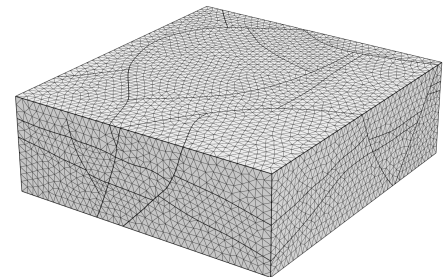Detachment (22km×14km×7.7 km)

Detachment remeshing (15 000 sites)

Detachment remeshing (30 000 sites)

Leipzig (1.2km×1.2km×0.4km)

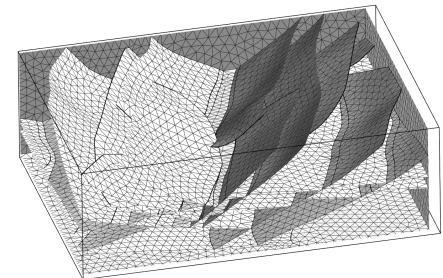Leipzig remeshing (5 000 sites)

Leipzig remeshing (10 000 sites)
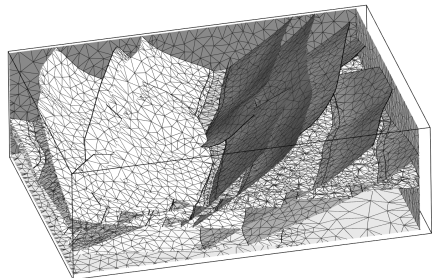
Lambda (6km×4.5km×1.9km)
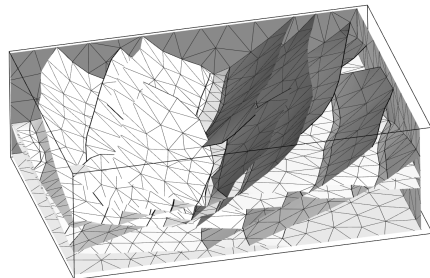
Lambda remeshing (1 000 sites)

Lambda remeshing (10 000 sites)

Figure 4.12: REMESHING RESULTS FOR MODELS DETACHMENT, LEIPZIG, AND LAMBDA. (see tables 4.1 and 4.2 for details).

DFN   DFN remeshing (30 000 sites)

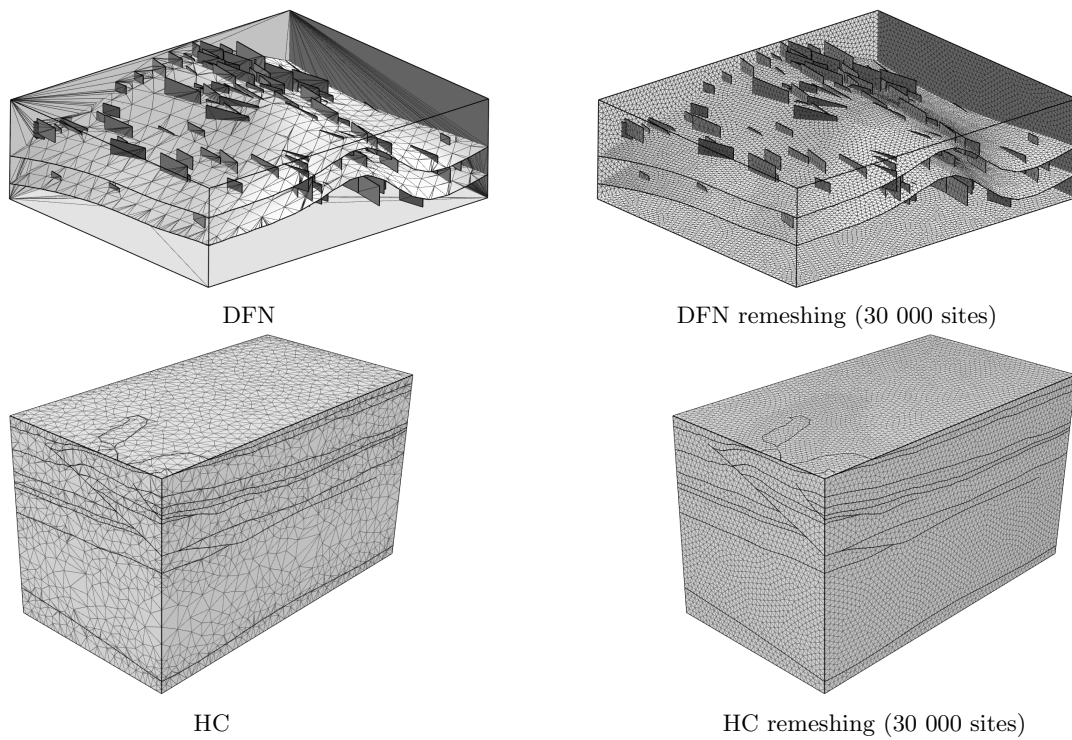HC   HC remeshing (30 000 sites)

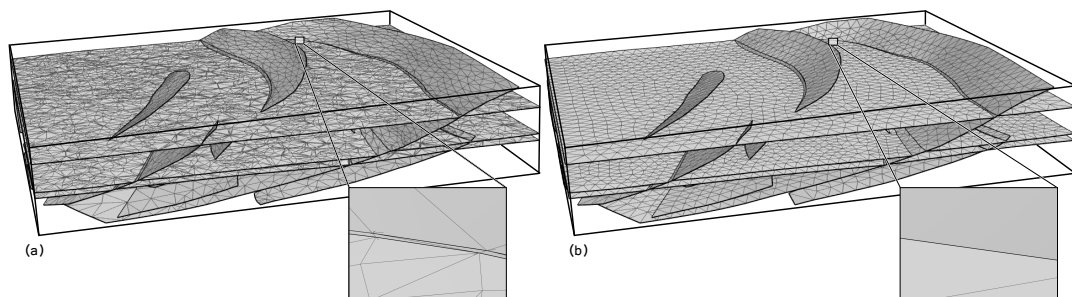Figure 4.13: Remeshing of models DFN and HC. (see tables 4.1 and 4.2 for details).

Figure 4.14: Cloudspin model remeshing. (a) Input model with very small throw near fault ends. (b) Output surfaces, remeshing was done with 5000 sites, contact lines are locally merged (see tables 4.1 and 4.2 for details).
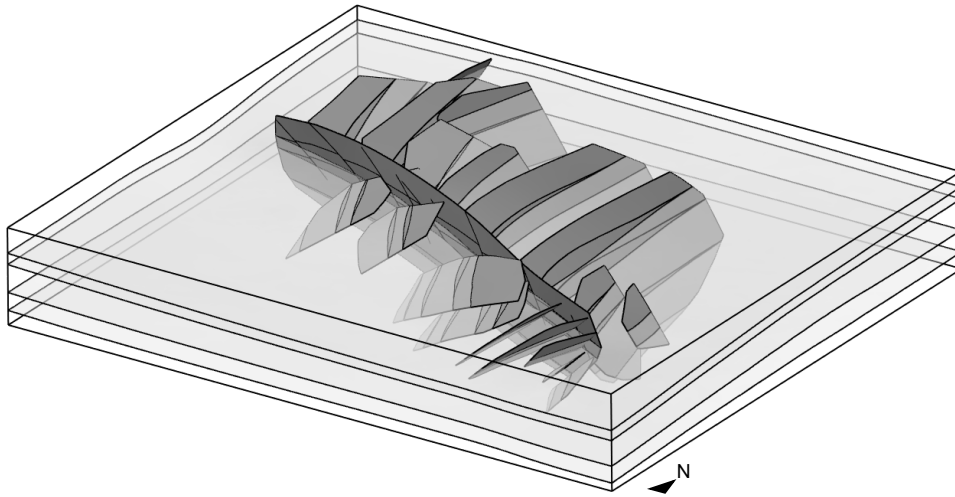
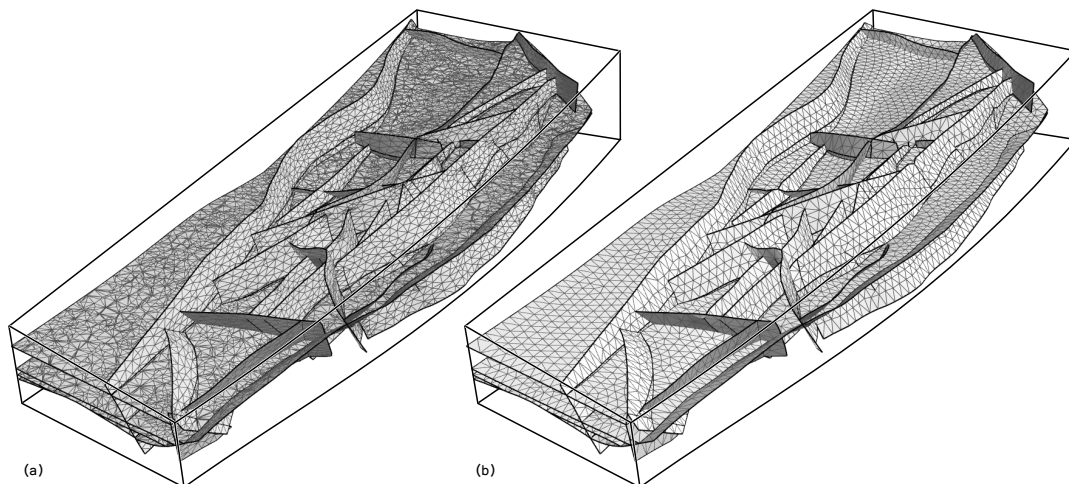Figure 4.15: CLYDE. This model presents complex fault intersections.

Figure 4.16: NANCY MODEL REMESHING. (a) Input model (b) Model remeshed with 10000 sites (see tables 4.1 and 4.2 for details).
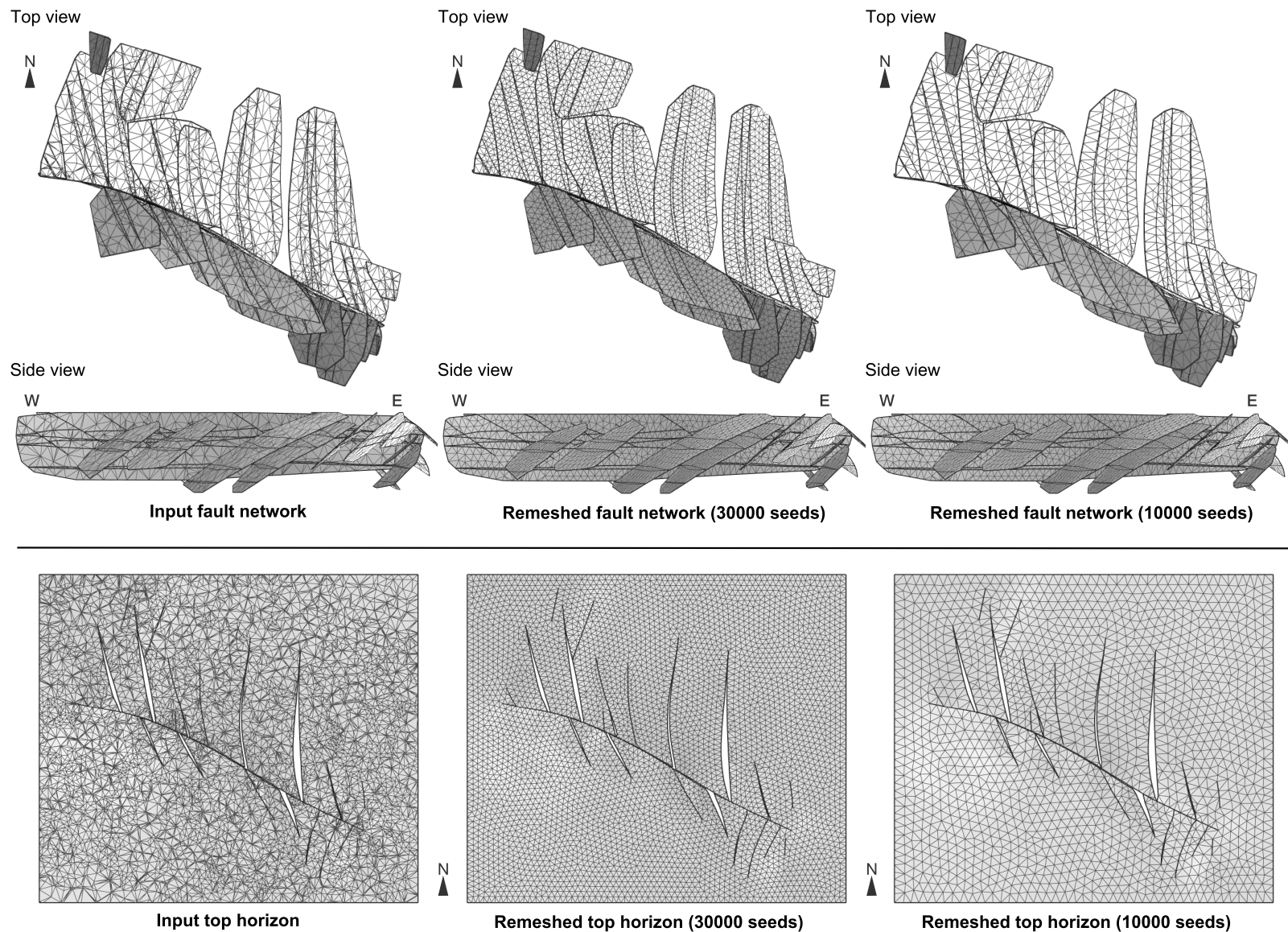
Figure 4.17: CLYDE REMESHING WITH 30 000 AND 10 000 SITES. (see also figure 4.15) and tables 4.1 and 4.2 for details).
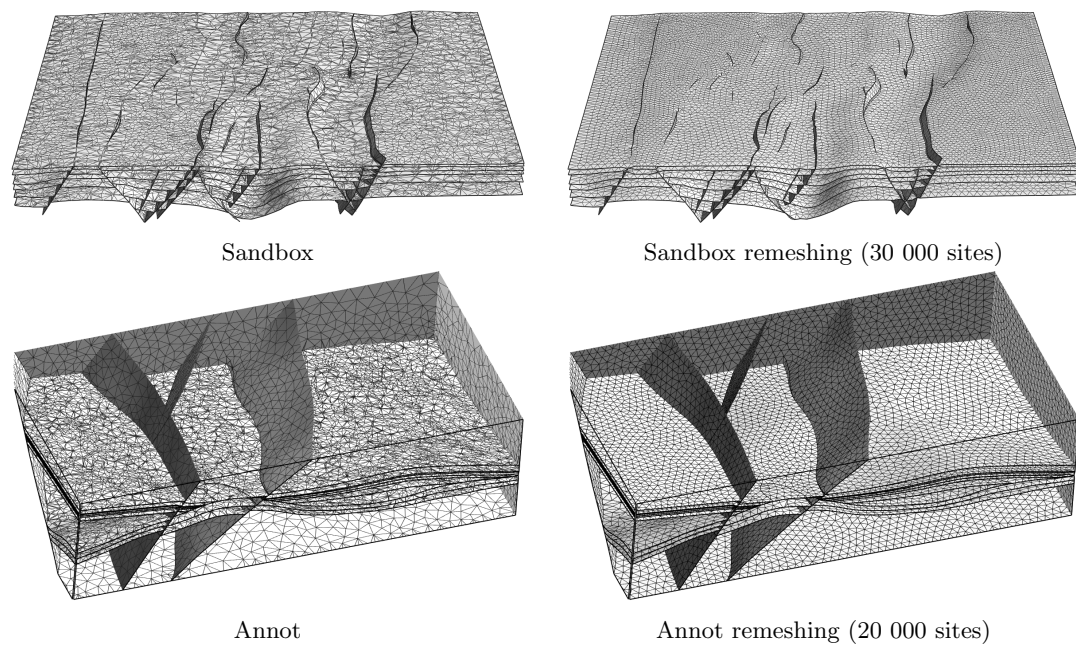
Sandbox

Sandbox remeshing (30 000 sites)

Annot

Annot remeshing (20 000 sites)

Figure 4.18: CHALLENGING MODEL REMESHING: SANDBOX AND ANNOT. (see tables 4.1 and 4.2 for details.)

Input top horizon with density property

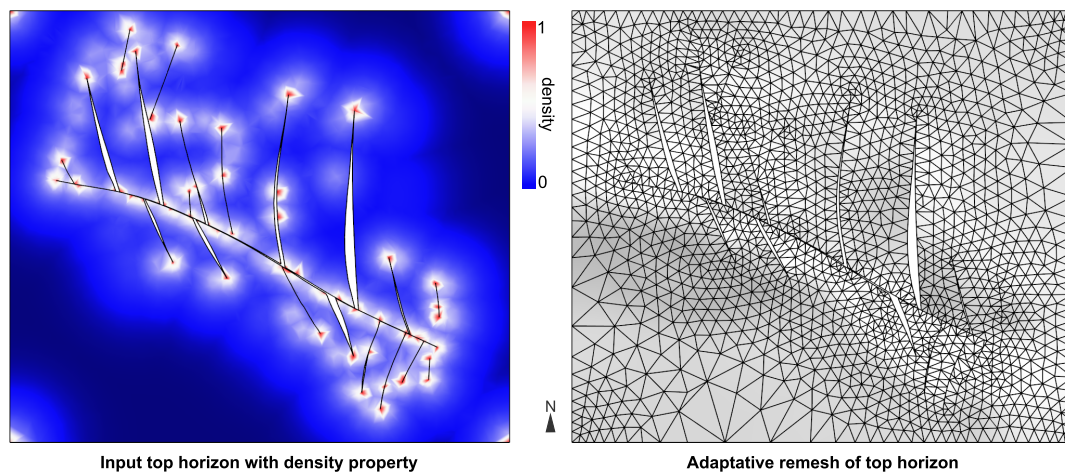**Adaptative remesh of top horizon**

Figure 4.19: ADAPTIVE REMESHING OF TOP HORIZON IN CLYDE MODEL. A density property computed from the distance to the triple points of the model $\rho(y) = (1 - d(y)/d_{max})^4$ was used to obtain an adaptive remesh of the Clyde model with 10000 sites. Unlike uniform remeshing, the result depends on the input mesh quality because density is interpolated on it.

Dataset	#Sites	#V	#T	#Surf.	#Lines	#Corners	Angles (deg)		Avg qual.	Area (m²)	Time (s)		Haus.dist.	Bbox diag.
							Min	< 30 (%)			Sampling	Mesh	(% bbox diag.)	(m)
Veins	**Input**	**471337**	**923286**	**29**	**0**	**0**	**0.01**	**22.07**	**0.55**	**5.20E+08**				11069
	1000	19928	35484	29	0	0	1.04	3.46	0.81	5.16E+08	153	33	0.44	11069
Forward	**Input**	**10151**	**13588**	**46**	**76**	**40**	**0.01**	**20.21**	**0.53**	**6.63E+04**				152.847
	1000	2457	3400	47	71	35	0.56	3.25	0.82	6.61E+04	12	1	1.45	152.847
	5000	7961	12849	46	74	36	1.85	1.00	0.88	6.62E+04	28	1	0.25	152.847
	10000	14096	23845	46	77	41	1.30	0.58	0.89	6.62E+04	46	2	0.18	152.847
Detachment	**Input**	**61480**	**109098**	**50**	**84**	**46**	**7.86**	**2.19**	**0.79**	**3.98E+09**				36816.7
	15000	25165	44599	50	79	41	2.60	0.50	0.90	3.98E+09	61	3	0.31	36814.9
	30000	42219	76514	50	82	44	3.85	0.24	0.91	3.98E+09	85	3	0.12	36814.8
Leipzig	**Input**	**9286**	**11344**	**188**	**320**	**166**	**0.98**	**7.54**	**0.73**	**1.00E+07**				1724.07
	5000	8578	11694	186	287	135	4.05	1.61	0.84	1.00E+07	13	1	0.51	1724.07
	10000	14911	22281	186	295	143	6.08	0.96	0.86	1.00E+07	23	2	0.79	1724.07
Lambda	**Input**	**24528**	**37553**	**132**	**256**	**177**	**0.09**	**15.52**	**0.62**	**2.57E+08**				7814.07
	1000	3416	3711	144	236	147	0.98	8.35	0.73	2.57E+08	20	2	1.17	7814.07
	10000	16113	24223	134	242	155	0.57	1.46	0.86	2.57E+08	33	3	0.374	7814.07
DFN	**Input**	**7876**	**7723**	**435**	**307**	**481**	**0.00**	**40.70**	**0.33**	**1.03E+09**				18282.6
	30000	38081	62070	435	300	480	1.00	0.88	0.88	1.03E+09	48	3	1.2	18279.6
HC	**Input**	**39919**	**70684**	**80**	**140**	**80**	**0.12**	**19.54**	**0.60**	**2.39E+09**				23083.6
	30000	37255	65198	80	141	81	0.78	0.25	0.91	2.39E+09	72	5	0.327	23083.6
Cloudspin	**Input**	**18313**	**30049**	**97**	**124**	**112**	**0.00**	**25.59**	**0.52**	**8.93E+08**				19339.8
	5000	10778	16494	91	117	103	0.45	3.52	0.82	8.92E+08	21	3	0.77	19339.7
	10000	17725	28725	94	134	124	0.30	2.25	0.85	8.92E+08	29	3	0.6	19339.5
Clyde	**Input**	**41355**	**69343**	**227**	**387**	**303**	**0.01**	**20.39**	**0.56**	**9.05E+08**				15883.8
	10000	15551	23367	206	318	244	0.72	2.51	0.85	9.04E+08	38	4	0.79	15883.8
	30000	38884	64850	220	354	282	0.15	1.30	0.88	9.05E+08	66	9	0.74	15883.8
Nancy	**Input**	**59115**	**85775**	**753**	**1307**	**774**	**0.00**	**25.98**	**0.50**	**1.83E+08**				13502.4
	10000	24840	30445	719	1096	626	0.13	6.88	0.75	1.83E+08	43	21	0.83	13500.9
	50000	79087	119309	741	1259	774	0.05	2.53	0.84	1.83E+08	106	49	0.27	13502.3
Annot	**Input**	**76204**	**130403**	**332**	**590**	**300**	**0.00**	**20.61**	**0.56**	**7.42E+08**				12650.5
	3000	12737	18253	301	455	212	0.51	5.69	0.77	7.42E+08	40	7	1.02	12650.5
	20000	41761	68240	311	522	264	0.55	2.31	0.85	7.42E+08	80	10	0.26	12650.5
Sandbox	**Input**	**72927**	**109267**	**500**	**688**	**713**	**0.00**	**21.98**	**0.53**	**7.60E+07**				4641.93
	30000	52498	77688	503	890	897	0.00	1.11	0.85	7.59E+07	93	28	0.64	4641.93

Table 4.2: Remeshing result statistics. For each model, input model and produced results are compared in terms of mesh sizes, numbers of components (surfaces, lines, and triple points), and quality (minimum triangle angle, percentage of triangles with an angle inferior to 30 degrees, average quality); the distance between them is measured with the Hausdorff distance.

4.6   Discussion

4.6.1   Contributions

In this chapter we proposed an automatic remeshing method for the surfaces of structural models. All surfaces are simultaneously remeshed with triangles as equilateral as possible. The method operate both locally and globally on the input model, which surfaces, lines, and corners are remeshed at the same time according to a given resolution. The counterpart of this automatism is that it is not possible to precisely control the performed model modifications. The method do no give any formal guarantee neither on triangle quality, nor on the final model topology. Results are obtained in less than several minutes on typical structural models. A quality check of the disappearing and appearing elements is necessary for a better evaluation of the results.

Global optimization and local analysis both have clear limitations. Indeed, since site density is not adapted to the local number of corners or contact lines, very important modifications may occur in some Voronoi cells. These modifications are questionable because they depend on the positions of a few sites and may imply the disappearance of important model elements from a geological point of view.

4.6.2   Perspectives

A first improvement of the method would be to avoid modifications such as the merging of two corners aligned on a contact line (figure 4.6b). The second would be to modify the minimized objective function, either by adapting site density to a distance to the corners and other model elements, or by adding a term to the function to prevent problematic configurations. Varying site density is already possible, since the objective CVT function (equation 1.6) includes a density and the method can be used to generate adaptive meshes such as the one figure 4.19. However, it is difficult to add terms to the function, the one we propose to drag site closer to line is not completely satisfactory. We also tried to add a term influencing the distance between Voronoi vertices and the surfaces, but it failed.

The volumetric subdivision defined by the Voronoi sites is undoubtedly the key to obtain results with better mesh quality, a better control on mesh size and on the modifications. There are several common points between our method and the *octree* meshing methods, and maybe strategies that they use could be adapted in the cases where cell intersections with model boundaries are problematic. Instead of a globally defined density, a local analysis of the complexity of the intersections between the model and the cells could be used to add or remove sites and locally re-optimize their positions.

Chapter 5

Contribution: Toward a mixed-element meshing based on Voronoi diagrams

This research has been presented as a research note at the IMR [Pellerin *et al.*, 2012].

Abstract

In this chapter we propose a method to generate a mixed-element finite element mesh, that is made of tetrahedra, triangular prisms, and square pyramids, for a structural model. This method is the extension in three dimensions of the surface remeshing method presented in chapter 4. The vertices, edges, facets, and cells of the final volumetric mesh are determined from the intersections between the Voronoi diagram cell and the surfaces defining the model. Inside the volumetric regions, the Delaunay tetrahedra, dual of the Voronoi diagram of sites sampling the model are built. Where the intersection of the Voronoi cells with the model surfaces has a unique connected component, the elements built are also tetrahedra. Where these intersections are more complicated, we introduce a correspondence between the elements of the Voronoi diagram and the element of the mixed-element mesh and build a volumetric mesh. The meshes obtained are not valid in the general case and post-processing is necessary.

5.1 Motivations

Finite element volumetric meshing is a prerequisite to compute the restoration of geological layers [Durand-Riard *et al.*, 2011, Vidal-Royo *et al.*, 2012], wave propagation [Lelievre *et al.*, 2012], heat diffusion [Liu *et al.*, 2012], or stratigraphy in the deposit space [Mallet, 2004]. The mesh must then capture the model components that have an impact on the modeled process. We saw in chapter 3 that the resolution of these components can be smaller than the desired mesh size making its generation pretty complicated.

In the general case, the finite element meshes used in geological modeling are tetrahedral meshes generated with one of the methods that we presented in section 2.3. The most robust methods are probably those generating a mesh constrained to a triangulation of the model boundaries. These methods then require a good mesh quality

of the boundaries. Methods developed for medical applications (section 2.3.2) generate simultaneously a mesh of the boundaries and the volumetric mesh. This is also possible with octree type meshing methods (section 2.3).

We propose an Voronoi optimization method (section 2.3.1) that meshes at the same time the corners, the lines, the surfaces, and the regions of a geological structural model represented by its boundary surfaces conformably triangulated. The surfaces are remeshed with triangles as equilateral as possible. Regions are meshed with cells conformal to the surface remeshes. The thin sections of the models, which definition depends on the resolution of the mesh to generate, are filled with prisms, pyramids, and tetrahedra, the others are meshed with tetrahedra only. Using different types of elements permit to generate less elements of, a priori, better quality.

5.2   Principle

We describe shortly in this section the main steps of the proposed method and the differences with the surface remeshing method.

Sampling optimization   We use a centroidal Voronoi diagram to place sites sampling adequately the model and its surfaces. The positions of the sites are first optimized to obtain a volumetric centroidal Voronoi diagram (section 1.3.1) then, the sites sampling the models surfaces are optimized so that their restricted Voronoi diagram to the model surfaces is centroidal (section 1.3.2). The final mesh resolution and the zones that are determined thin by the method directly depend on the number of sites.

Surface remeshing   Models surface are meshed with the method described in section 4.4. The difference is that here we associate each connected component of each restricted Voronoi cell to a unique point, this corresponds to an additional simplification of the model. Moreover, the triangular restricted Voronoi diagram facet or buttonhole like facets with only two neighbors, are filtered and not considered when building triangles. When remeshing surfaces, this triangles were deleted during the post-processing step (section 4.4.5). This would prevent to keep the conformity between the volumetric mesh and the surface remesh. Once the surfaces are remeshed, the vertices of the final mixed element meshed are known and will not be modified anymore.

Correspondence Voronoi diagram - mixed-element mesh   We propose to put in correspondence the cells, facets, edges, and vertices of the Voronoi diagram cut into several parts by the model surfaces (figure 5.1) with the cells, facets, edges, and vertices of a mixed element mesh (table 5.1). We consider that the maximum number of intersection between a Voronoi cell part and the model surfaces is two. This is not always the case, and it is possible to identify this Voronoi cells and apply simplifications strategies similar to those proposed to determine the vertices of remeshed surfaces (section 4.4), so that the number of points in each part of a Voronoi cell is one or two.
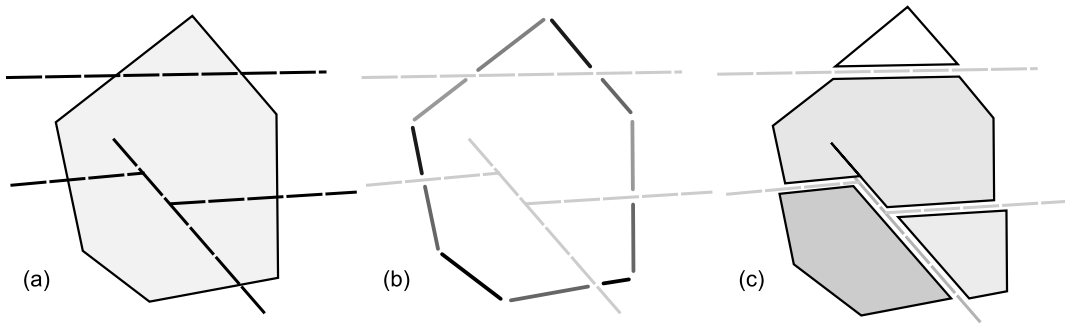
Figure 5.1: Voronoi cell cut by model boundaries. (a) Model boundaries in a Voronoi cell. (b) Cut edges. (c) Voronoi cell parts.

Voronoi diag. elts	Intersections connected components	Mixed-elt mesh
Cell part	0	1 interior vertex
	1	1 boundary vertex
	2	2 boundary vertices & 1 interior edge
Facet part	0	1 interior edge
	1	1 boundary edge
	2	2 boundary edges & 1 interior facet
Edge part	0	1 interior facet
	1	1 boundary facet
	2	2 boundary facets & 1 cell
Vertex	0	1 cell

Table 5.1: Relationship between the mixed element mesh and the model restricted Voronoi diagram elements.
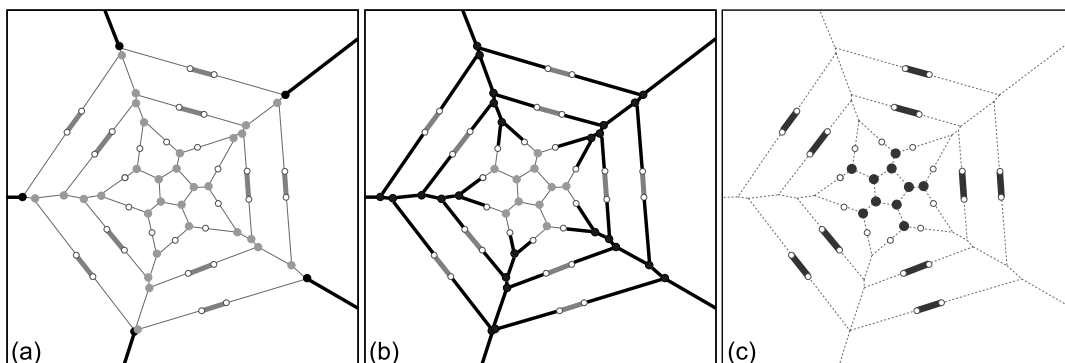
Figure 5.2: Determination of the Voronoi vertices and edges inside a star. (a) The 5 Voronoi vertices at the extremity of an infinite edge not intersecting the boundary are outside the star. (b) Propagation along Voronoi edges gives all Voronoi segments and vertices outside the star. (c) Voronoi vertices and segments inside the star are kept.

Algorithm 5.1 - Definition of the Voronoi vertices and segments inside the model.

Data: Voronoi diagram vertices S
Result: Flagged Voronoi vertices and edges as inside or outside the model Ω
(1) All vertices are inside;
(2) Get all Voronoi vertices S_E at the extremity of an infinite Voronoi edge not intersecting Ω, and flag them as outside (figure 5.2a) ;
(3) Build stack $P \leftarrow S_E$;
(4) **while** P *non empty* **do**

    $v \leftarrow$ top P ;
    foreach *neighbor n of v* **do**

        if *n is not outside* **then**

            $nb \leftarrow$ # of intersections between the edge vn and Ω ;
            if $nb == 0$ **then**

                Flag n outside;
                Push n ;
            else if *nb is even* **then**

                Flag n outside;
                Push n ;
                Flag alternatively inside and outside segments between two intersections ;
            else

                Flag alternatively inside and outside segments between two intersections ;

        end
    end
end
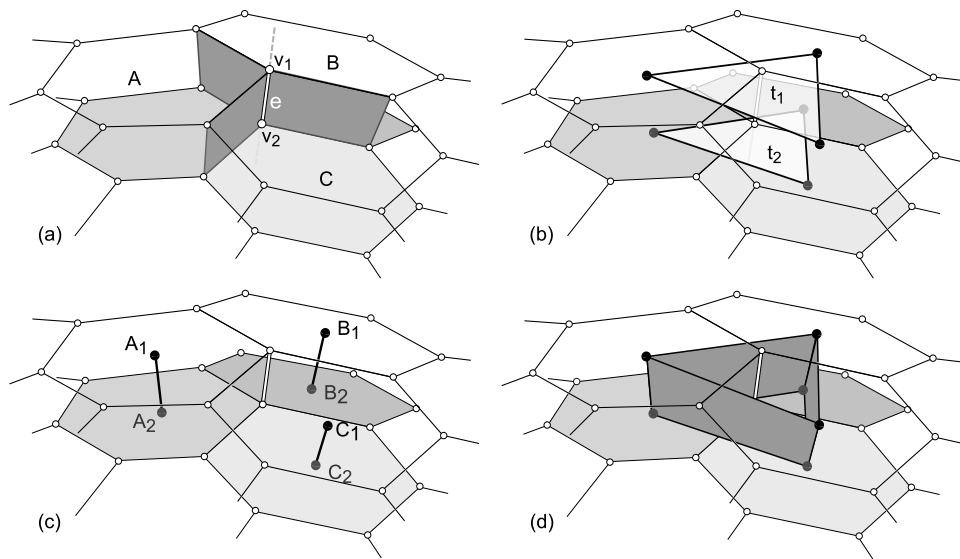
Figure 5.3: PRISM DUAL OF A VORONOI SEGMENT. (a) Three restricted Voronoi cells, A, B and C to a layer share segment e that is delimited by intersections with the surfaces v_1 and v_2. (b) Triangles t_1 and t_2 duals of v_1 and v_2 determine the six vertices of the prism. (c) One edge links each pair of vertices corresponding to the same cell. (d) One quad facet corresponds to each Voronoi facet part containing segment e.

5.3 Volumetric cells building

There are two main steps to build the mixed element mesh. First, the cells to build are counted (section 5.3.1), then they are build one by one by adding successively their vertices, edges, and facets (sections 5.3.2 and 5.3.3).

5.3.1 Determining the cells to build

According to the relationship established in table 5.1, there are two types of cells to build: the ones duals of Voronoi vertices and the ones dual of segments of a Voronoi edge (portion of the edge between two intersections with the model surfaces). The first step is to determine the elements of the Voronoi diagram skeleton that are outside the model, so that the ones inside the model can be found (algorithm 5.1 and figure 5.2).

5.3.2 Segment dual cells

The first cells to build are those dual of a Voronoi segment e, i.e. a portion of a Voronoi edge delimited by two restricted Voronoi vertices v_1 and v_2 (figure 5.3a). These two vertices correspond to two triangles, t_1 and t_2, that remesh the model surfaces, and are two facets of the cell to build (figure 5.3b). Segments linking vertices corresponding to the same Voronoi cells are added to these triangles (figure 5.3c) and the facets linking these edges and the triangles (figure 5.3d). Depending on the total vertex number the cell to build is either a tetrahedra, or a pyramid, or a prism. Degenerated cells with only three vertices are ignored. All the other segment dual cells are valid.
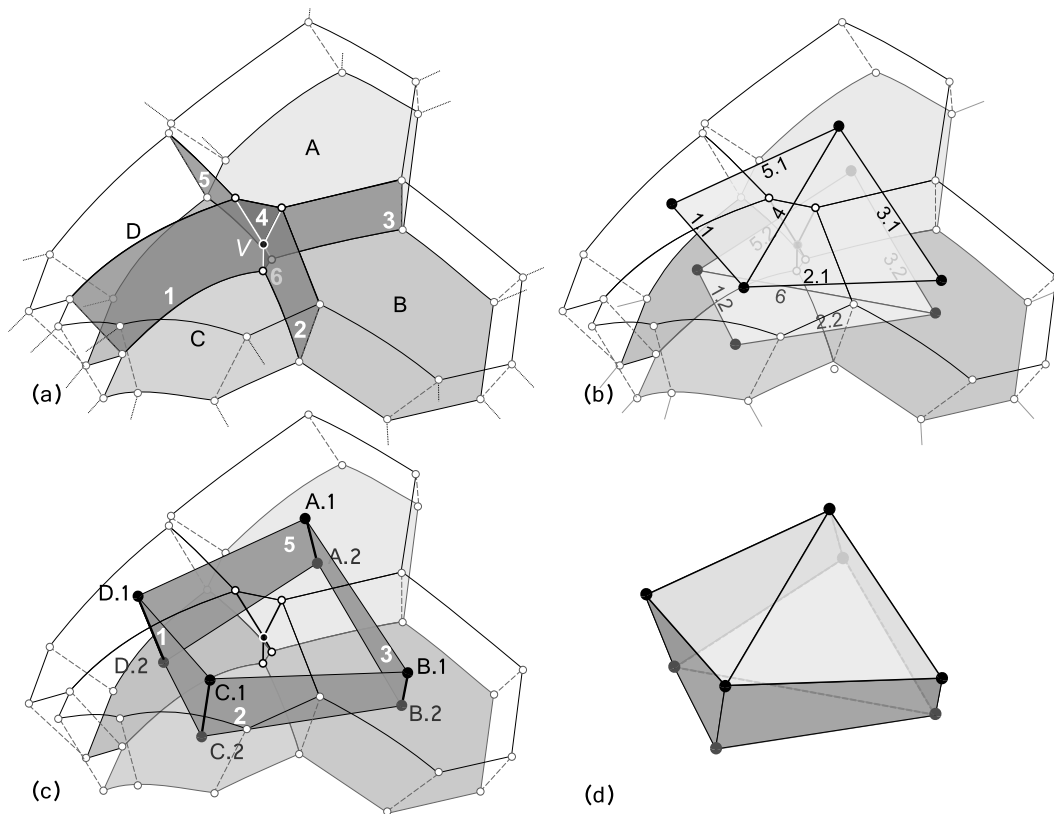
Figure 5.4: VORONOI VERTEX DUAL CELL WITH 8 VERTICES BUILDING. (a) Vertex v is shared by four parts of four Voronoi cells (A, B, C, D), four edge parts, and six facet parts. (b) To each edge part corresponds on triangle. (c) For each Voronoi facet part that intersect twice the model surfaces there is one facet (numbers 1, 2, 3, 5). (d) The final cell has eight vertices, four triangular facets, and four quad facets.

5.3.3 Vertex dual cells

The remaining volumetric cells to build correspond o the Voronoi vertices. As we saw in section 1.1.1, each Voronoi vertex is shared by four Voronoi cells, six Voronoi facets, and four Voronoi edges (figure 1.4a). Their dual according to the classical Voronoi-Delaunay relationship, is a tetrahedra linking the sites of these four cells (figure 1.4c). When the Voronoi cells intersect the model surfaces we analyze the polyhedra resulting of the cutting of the Voronoi cells by the surfaces (figure 5.1) to build the different volumetric elements [1] (table 5.1).

Adding vertices

For each of the four Voronoi cell pieces containing the Voronoi vertex, there is one or two points to add to the cell. For example, each Voronoi cell piece figure 5.4a that contains v intersect twice the model surfaces and corresponds to two points (figure 5.4c). The next step is to choose what are the points to add to this specific cell,

---

[1]Because the computation of these polyhedra is difficult and not robust, cells are built from Voronoi diagram and the restricted Voronoi diagram to the model surfaces.
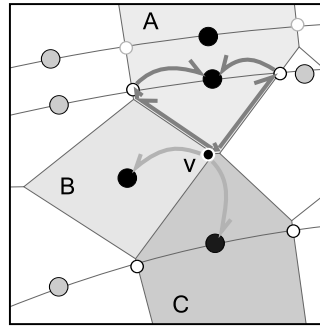
Figure 5.5: VERTEX DEFINITION OF A VORONOI VERTEX DUAL CELL.

as there might be more than two. All the points corresponding to each (complete) Voronoi cell were determined at the surface remeshing step. We determine the ones that can be reached by propagating along Voronoi edges from vertex v (cell A, figure 5.5). This is unnecessary when a unique point is associated to the Voronoi cell, either because the intersection between the cells and the surface is empty (cell B, figure 5.5), or because it has only one connected component (cell C, figure 5.5).

Adding edges

There are two types of edges to add, those linking points corresponding to the same Voronoi cells bold edges on figure 5.4c, and those corresponding to Voronoi facets containing v. Facets 1, 2, 3 and 5 on figure 5.4a correspond to two edges numbered 1.1, 1.2 on figure 5.4b; facets number 4 and 6 intersect but once the model surfaces and correspond to a unique edge in the cell to build. Edges are not always correctly determined: typically when the Voronoi facet does not intersect at all the models surfaces and when one of its two neighboring cell correspond two several points. It is not possible to determine from which points the edge should be built (figure 5.6). This edge is flagged undefined.

Adding facets

The facet to add first are those corresponding to edges containing v. Either they are triangles remeshing model surfaces (figure 5.4b), or they are polygons built from the edges corresponding to the facets that contains the Voronoi edges. The other facets to add correspond to Voronoi facets containing v and intersecting twice the model surfaces, for example facets 1, 2, 3 and 5 on figure 5.4c correspond to Voronoi facet with the same number on figure 5.4a. They are determined from the edges corresponding to those facets, figure 5.4b. One facet may have up to six vertices, and six edges. If one edge is undefined, the faced is flagged undefined too.

5.4 Invalid cell processing

Once all vertices, edges, and facets have been added to the cell, its type is determined from the number of these elements. Theoretically, one cell may have four to eight vertices, six to sixteen edges, four to ten facets, each facet having up to six vertices.
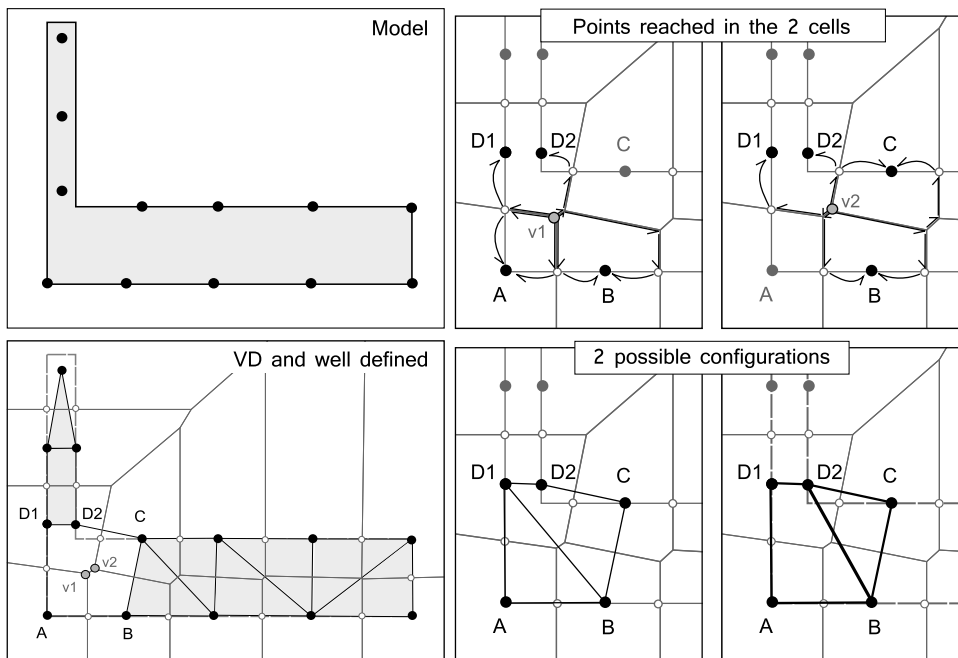
Figure 5.6: Configuration leading to an undefined edge in 2D. Potential vertices for the cell dual of v_1 are: A, B, D1 and D2, and for the cell dual of v_2: B, C, D1, and D2. Because the Voronoi edge (resp. facet) that separates cells B and D do not intersect model boundaries, the edge linking reliant D and B is undefined.

Really most of the cells are tetrahedron, prisms, or pyramids. The other cells are processed following the procedures described in the following.

They are first sorted into four categories: (1) the cells to subdivided (cells with 7 or 8 vertices defining a valid volume, for example the one figure 5.4d), (2) undefined cells (with at least one undefined cell), (3) invalid cells (in which at least one edge is a diagonal of a facet, or in which two quad facets share more than two vertices, for example 5-point cells, figure 5.7a, that are quite abundant) and (4) the cells that belong to non of the above categories. Cells to subdivide are subdivided by adding a vertex at their centroid and building pyramids and tetrahedra with their facets. Undefined cells are defined by choosing among the possible edges the one that damage less mesh quality (angles). This choice made for each edge is propagated to facets containing it. This strategy may not work when a facet or a cell has several undefined edges. To compute tetrahedra, pyramids, and prisms from invalid cells, two steps are necessary. First, all the facets of a cell so that there is an edge, in the same cell, that is one of it diagonal, are cut in two along this edge. Then the validity of cell facets must be ensured. Facets with more than four vertices are triangulated and quad facets that share three vertices with another facet are split (figure 5.7b). This processing permits to reduce the number of invalid cells, but is not sufficient to obtain a final valid mesh in all cases.

5.5 Results

We applied this mixed element meshing method to geological and non geological models. Computational time (between several seconds and several minutes) depends
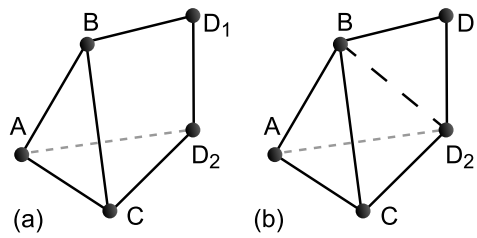
Figure 5.7: INVALID CELLS WITH 5 VERTICES. (a) Vertices D correspond to the same Voronoi cell. Facets ABD_1D_2 and BCD_1D_2 share three vertices. (b) Cutting these facets with BD_2 results in a tetrahedron plus a triangular facet.

on the number of sites, on the input model number of triangles, on the number of invalid cells to process. The meshes obtained for models in which layer thicknesses do no vary significantly and that have smooth boundaries reproduce boundary layer meshes (figures 5.8 and 5.9). Results for geological model are promising (5.10), thin layers of the model are meshed with prisms. These zones depend on the resolution of the subdivision of the model induced by the Voronoi diagram, and so on the number of sites sampling the model (figure 5.9).

5.6   Discussion

5.6.1   Contributions

In this chapter we propose a method to generate a mixed element mesh (tetrahedra, prisms, pyramids) that should be adequate for finite element simulation from a Voronoi diagram and its intersections with a the surfaces defining the model. This automatic method is relatively fast. It permits to build a mesh in which the type of the element built depends on the local thickness of the region considered. No previous identification of the thin section of the model is required, they are determined from the subdivision of the model by the Voronoi cells.

    Cell building in thin sections works very well, and Delaunay tetrahedra away of the model surfaces building does not poses any problem. However, in transition zones where numerous invalid cells are created, the current version of the post-processing is not yet sufficient to obtain a valid mesh. On the other hand, because the tetrahedra built near the surfaces do not link the initial sites but vertices remeshing the model surfaces, some tetrahedra are inversed and intersect their neighbors. Another problem is that the volumetric mesh depends on the surface remeshing result and robustness, that still could be perfected, even if it work already quite well. The potentially necessary mesh fixes by hand cannot be integrated in the volumetric mesh. Finally the implemented post-processing for surface remeshing along the border lines would be difficult to extend in three dimensions.

5.6.2   Perspectives

The current implementation does not account for surfaces that stops inside the model (typically faults). If it is possible to ensure, for example with a point merging strategy, that there is no more that two points for one Voronoi cell piece, they could be taken
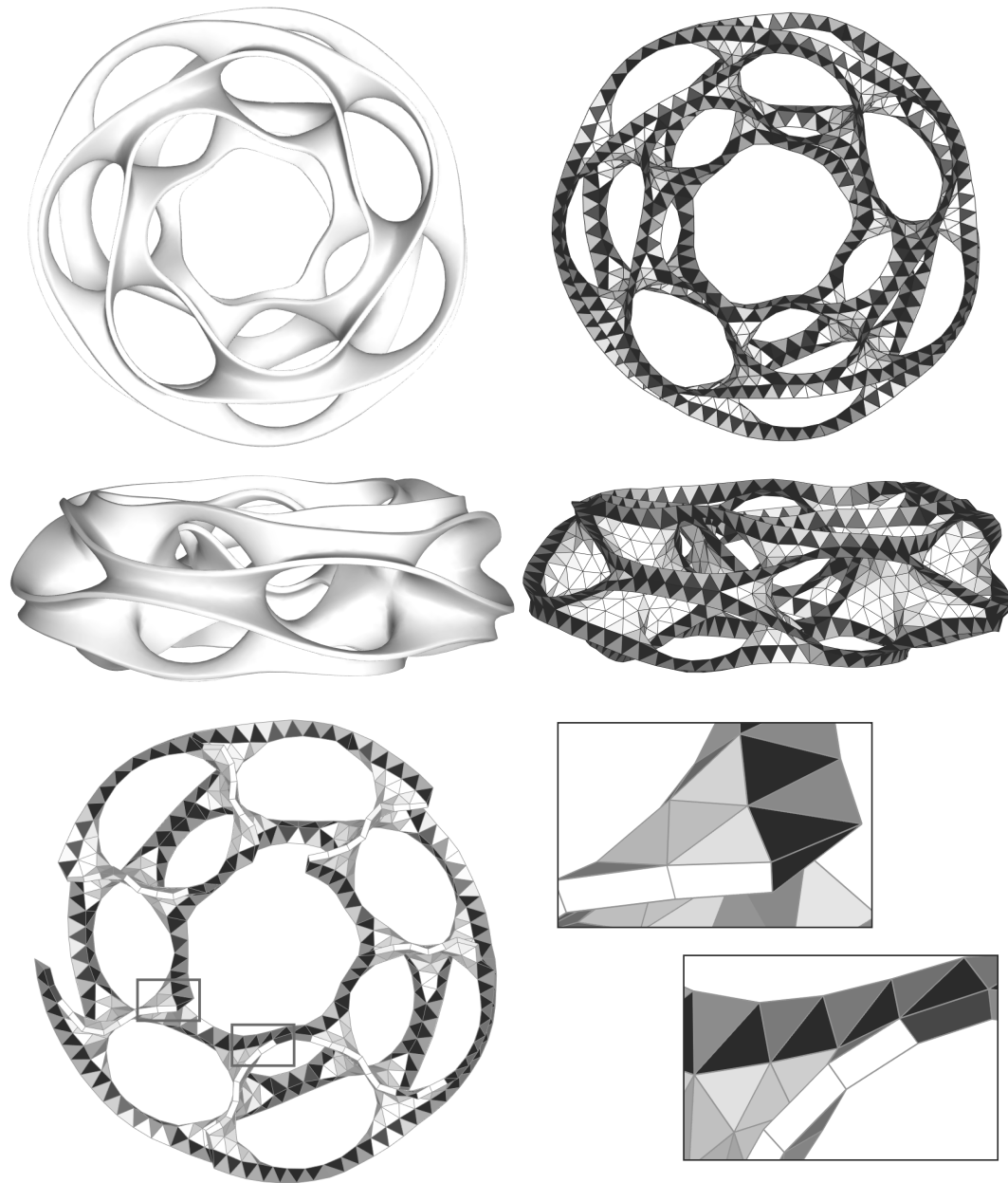
Figure 5.8: Mixed element mesh inside a smooth surface. 1 010 sites are optimized to sample the surface (8 seconds). The final mesh (3 seconds) has 516 tetrahedra (gray), 665 prisms (white) and 507 pyramids (black).
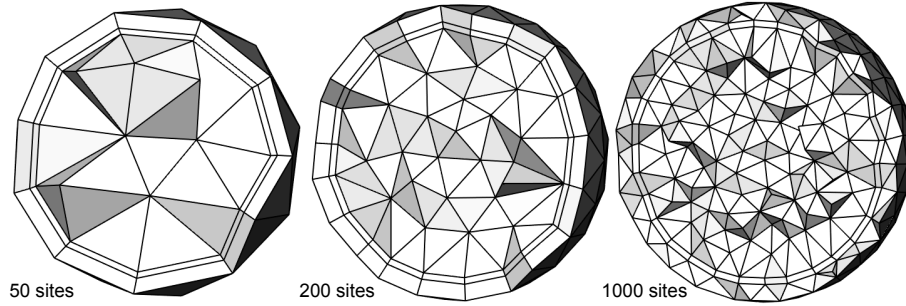
Figure 5.9: THREE NESTED SPHERES MESHING AT THREE RESOLUTIONS. The total number of sites impacts which layer are thin and meshes with prisms.
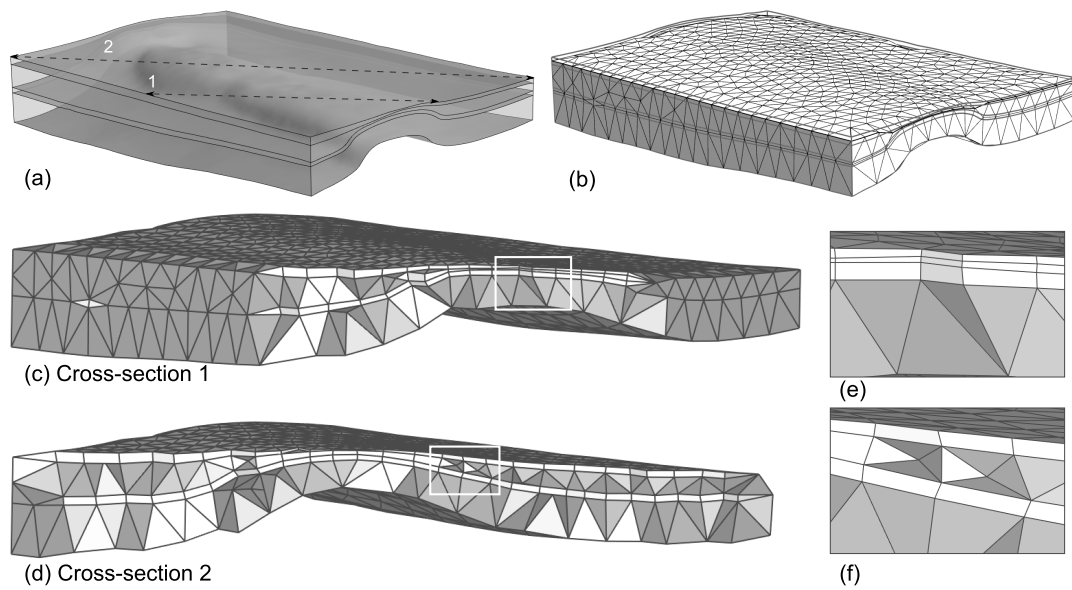

Figure 5.10: MESH OF LAYERS WITH VARYING THICKNESSES. (a) Input model (b) Mixed element mesh generated from 1,000 sites (4,674 tetrahedra, 1,754 prisms, and 335 pyramids). (c&d) Cross-sections in the mesh: tet (gray), prisms and pyramids (white). (e) Prism layer meshing the thin sections. (f) Elements obtained from dividing a 8-vertex cell.
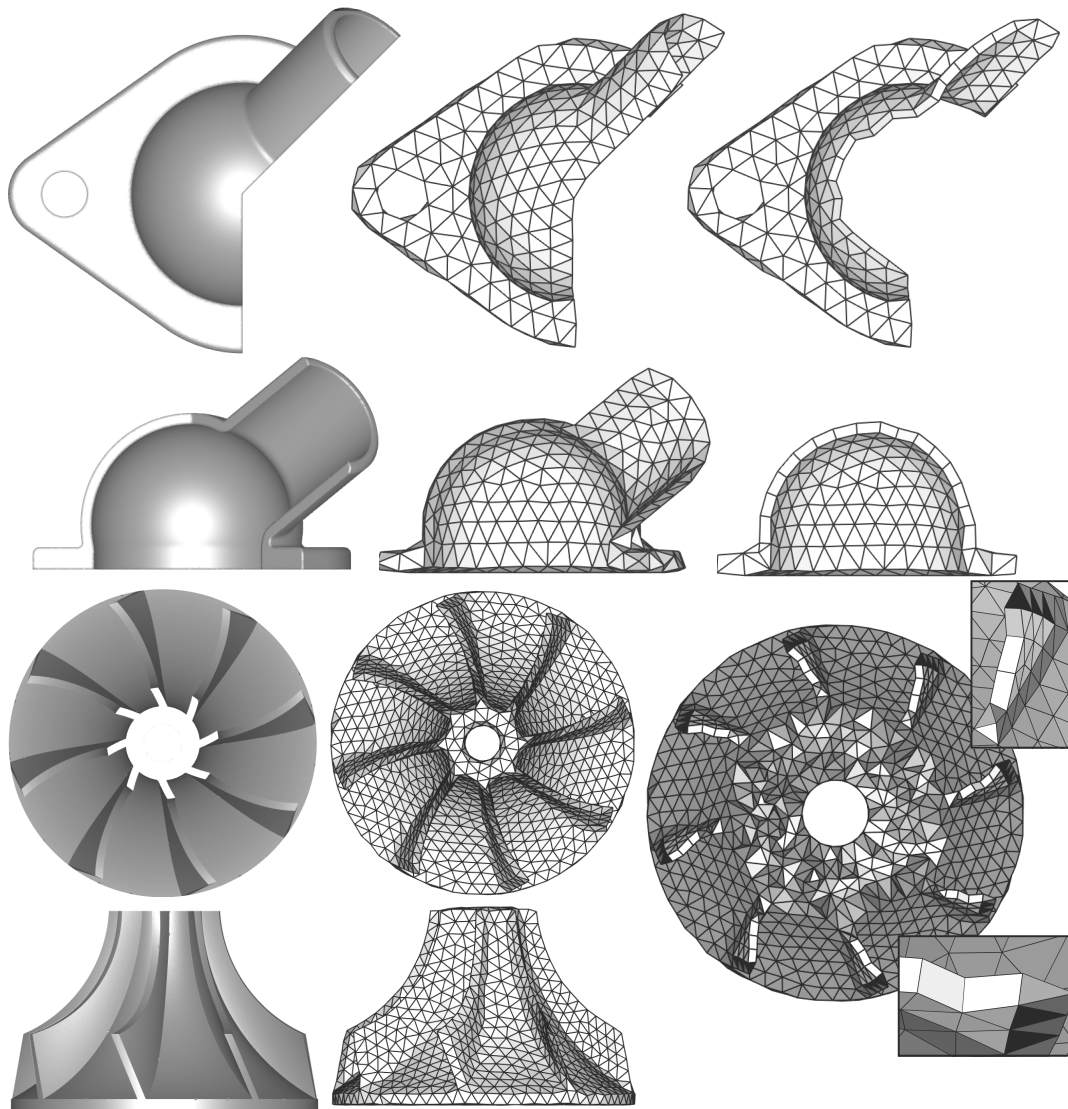
Figure 5.11: MIXED ELEMENTS MESH OF TWO MODELS WITH SHARP FEATURES. Thin sections are mainly filled with prisms. The top model ('bracket') mesh is constituted of 593 tets, 215 prisms, 47 pyramids; the bottom one ('impeller') is constituted of 13, 845 tetrahedra, 195 prisms, 237 pyramids. The meshes are not completely valid.

into account or simplified. Border lines and corners should also be considered when remeshing the surfaces, as it is not the case at this moment (section 5.2).

The use of a global subdivision of the model by a Voronoi diagram is beneficial because all elements built are of rather good quality, and problematic because partly random. Mesh building in the zones where intersections with the models surfaces are not those expected is very complicated. For this method to be applicable to real structural models, it should be possible to evaluate the quality of a given sampling (and of its corresponding subdivision) for a given B-Rep model and define strategies to improve it.

Several ideas could be developed to improve the method and generate a valid mesh. The first is to analyze the model elements intersected in each Voronoi cell to correctly determine the final mesh vertices and implement merging strategies of points similar to those proposed for surface remeshing. A second idea is to build all the easiest cells to build of the mesh, and then to extract cavities around problematic zones (transition, post-processed contact lines) so that they can be meshed with a constrained tetrahedralization. The third is to completely change the cell building strategy, and instead of building a mesh from scratch, to progressively modify the Delaunay triangulation of the sites by local operations that would permit to obtain the desired conformal mixed element mesh. This would imply identifying non-conformity issues to solve and to implement operations to solve these. In all cases, similarly to surface remeshing, one of the keys of the improvement of the results is the improvement of the spatial distribution of the sites and an adapted adjustment of their resolution.

Conclusion

Contributions

In this thesis we proposed strategies to automatically remesh and simplify 3D geological structural models. Our strategy is based on a space subdivision determined by the Voronoi diagram of a set of points sampling the model. These points are placed so that their Voronoi diagram or their restricted Voronoi diagram to the model surfaces are centroidal. The main contributions of the thesis are summarized below.

Measures to identify the small geometrical characteristics of geological models The measures of structural model geometry and connectivity we proposed will help the future definition of tools permitting a more objective comparison of geological models at a given resolution. Courting the model components in the cells of a centroidal Voronoi diagram allow a precise identification of the more complex zones. The metrics we proposed are computed for a set of 9 synthetic models. This research work is presented in chapter 3 and a paper is in preparation.

A method to build a surface remesh from a restricted Voronoi diagram The method permits to conformably and simultaneously remesh the triangulated conformable surfaces defining a B-Rep model. We propose to authorize input model modifications to remesh the model whatever the topology and the geometry of the restricted Voronoi cells. We use a centroidal Voronoi diagram optimization to place the Voronoi diagram sites which permit to obtain triangles as equilateral as possible independently of the input mesh quality. This methods is presented in chapter 4 and has been published in Pellerin *et al.* [2014], a first version having been proposed in Pellerin *et al.* [2011].

A method to build prisms, pyramids and tetrahedra from the skeleton of a Voronoi diagram and a restricted Voronoi diagram This method is the 3D extension of the surface remeshing method defining a structural model. The model volumetric regions are meshed simultaneously by elements conformal to that remesh of the surfaces. Thin model section, that are identified analyzing the intersections between the Voronoi cells and the model surfaces, are filled with prisms, pyramids and tetrahedra, the others are meshes with tetrahedra. We propose post-processing procedure to improve the final meshes that are generally not valid. A short version of this project was presented as a research note at the IMR [Pellerin *et al.*, 2012].

This measures and methods were implemented in C++ in two plugins of the modeler Graphite (`http://alice.loria.fr/index.php/software.html`). The code is

available to the members of the Gocad consortium (`http://www.gocad.org/w4/index.php/consortium/consortium`) that funded this thesis.

Publications

J. Pellerin, B. Lévy et G. Caumon : Topological control for isotropic remeshing of nonmanifold surfaces with varying resolution: application to 3D structural models. *In Proc. IAMG*. cogeo@oeaw-giscience, sept. 2011.

J. Pellerin, B. Lévy et G. Caumon : A Voronoi-based hybrid meshing method. *In International Meshing Roundtable, Research Notes*, oct. 2012.

J. Pellerin, B. Lévy, G. Caumon et A. Botella : Automatic surface remeshing of 3D structural models at specified resolution: A method based on Voronoi diagrams. *Computers & Geosciences*, 62(0):103 – 116, 2014.

Perspectives

Beyond the technical improvements perspectives described in the conclusions of the thesis chapters, we see three main perspectives.

The first is to validate, and possibly adapt, the automatic model simplification on reference models. This require to evaluate the results obtained for the same model represented and meshed at different resolutions for a given numerical simulation. This validation is necessary to define an automatic simplification method of geological models for all the possible applications (mechanical restoration, fluid flows in fractured media, wave propagation, *etc*).

We already underlined that the key to improve our meshing methods is to improve the model sampling. This requires to determine what is a good sampling of a model, this probably includes the identification of the zones that have a high geometrical complexity. Then strategies should be developed to really improve this sampling. A centroidal Voronoi diagram optimization takes into account a site density, but it is difficult to add terms to the objective function. Instead of a Voronoi cell subdivision, other subdivisions like *octree* could be used to build the surface and volumetric meshes, models simplifications staying the same.

Finally, the meshing methods we proposed could be adapted to other problems like the generation of mixed-dimensional meshes that are necessary when the dimension of certain model components is reduced [Robinson *et al.*, 2011].

Bibliography

K. Aki et P. G. Richards : *Quantitative seismology.* University Science Books, Sausalito, CA, 2009. (Cited page 23.)

G. Allaire : *Analyse numérique et optimisation : Une introduction à la modélisation mathématique et à la simulation numérique.* Mathematiques appliquees. Ecole polytechnique, Palaiseau, 2005. (Cited page 23.)

P. Alliez, D. Cohen-Steiner, M. Yvinec et M. Desbrun : Variational tetrahedral meshing. *ACM Transactions on Graphics*, 24(3):617–625, juil. 2005a. (Cited page 33.)

P. Alliez, E. Colin de Verdiere, O. Devillers et M. Isenburg : Centroidal voronoi diagrams for isotropic surface remeshing. *Graphical Models*, 67(3):204–231, 2005b. (Cited page 37.)

N. Amenta et M. Bern : Surface reconstruction by voronoi filtering. *Discrete and Computational Geometry*, 22(4):481–504, 1999. (Cited pages 14 and 37.)

R. Andrle : Complexity and scale in geomorphology: Statistical self-similarity vs. characteristic scales. *Mathematical Geology*, 28(3):275–293, avr. 1996. (Cited page 28.)

C. Andujar, P. Brunet et D. Ayala : Topology-reducing surface simplification using a discrete solid representation. *ACM Transactions on Graphics*, 21(2):88–105, 2002. (Cited page 28.)

N. Aspert, D. Santa-Cruz et T. Ebrahimi : Mesh: Measuring errors between surfaces using the hausdorff distance. *In Proceedings IEEE International Conference on Multimedia and Expo*, vol. 1, p. 705–708. IEEE, 2002. (Cited page 61.)

D. Attali, J.-D. Boissonnat et H. Edelsbrunner : Stability and computation of medial axes - a state-of-the-art report. *In* T. Möller, B. Hamann et R. Russell, éds : *Mathematical Foundations of Scientific Visualization, Computer Graphics, and Massive Data Exploration*, Mathematics and Visualization, p. 109–125. Springer Berlin Heidelberg, 2009. (Cited page 14.)

R. Aubry, G. Houzeaux et M. Vazquez : A surface remeshing approach. *International Journal for Numerical Methods in Engineering*, 85(12):1475–1498, 2011. (Cited page 36.)

F. AURENHAMMER : Voronoi diagrams—a survey of a fundamental geometric data structure. *ACM Computing Surveys (CSUR)*, 23(3):345–405, 1991. (Cited pages 7 and 8.)

T. J. BAKER : Mesh generation: Art or science? *Progress in Aerospace Sciences*, 41 (1):29–63, jan. 2005. (Cited pages 23 and 29.)

M. BERZINS : Mesh quality: A function of geometry, error estimates or both? *Engineering with Computers*, 15(3):236–247, sept. 1999. (Cited page 26.)

J.-D. BOISSONNAT et M. YVINEC : *Geometrie algorithmique*. Ediscience international, Paris, 1995. (Cited page 10.)

J.-D. BOISSONNAT et F. CAZALS : Smooth surface reconstruction via natural neighbour interpolation of distance functions. *In Proceedings of the sixteenth annual symposium on Computational geometry*, p. 223–232. ACM Press, 2000. (Cited page 37.)

J.-D. BOISSONNAT et S. OUDOT : Provably good sampling and meshing of surfaces. *Graphical Models*, 67(5):405 – 451, 2005. (Cited page 37.)

D. BOLTCHEVA, D. CANINO, S. M. ACEITUNO, J.-C. LÉON, L. D. FLORIANI et F. HÉTROY : An iterative algorithm for homology computation on simplicial shapes. *Computer-Aided Design*, 43(11):1457 – 1467, 2011. (Cited page 26.)

D. BOLTCHEVA, M. YVINEC et J.-D. BOISSONNAT : Feature preserving delaunay mesh generation from 3D multi-material images. *Computer Graphics Forum*, 28 (5):1455–1464, juil. 2009. (Cited page 35.)

H. BOROUCHAKI, P. L. GEORGE, F. HECHT, P. LAUG et E. SALTEL : Delaunay mesh generation governed by metric specifications. part I. Algorithms. *Finite elements in analysis and design*, 25(1):61–83, 1997. (Cited page 33.)

M. BOTSCH, L. KOBBELT, M. PAULY, P. ALLIEZ et B. LÉVY : *Polygon Mesh Processing*. AK Peters, 2010. (Cited pages 28 and 36.)

B. BOURBIAUX, R. BASQUET, M.-C. CACAS, J.-M. DANIEL et S. SARDA : An integrated workflow to account for multi-scale fractures in reservoir simulation models: Implementation and benefits. Society of Petroleum Engineers, oct. 2002. (Cited page 28.)

H. CAO : *Development of techniques for general purpose simulators*. Thèse de doctorat, Stanford University, 2002. (Cited page 24.)

G. CAUMON : *Représentation, visualisation et modification de modèles volumiques pour les géosciences*. Thèse, INPL, Nancy, France, mars 2003. (Cited page 42.)

G. CAUMON, P. COLLON-DROUAILLET, C. Le Carlier de VESLUD, J. SAUSSE et S. VISEUR : Surface-based 3D modeling of geological structures. *Mathematical Geosciences*, 41(9):927–945, 2009. (Cited pages 21, 42, and 51.)

L. CHEN et J. XU : Optimal delaunay triangulations. *Journal of Computational Mathematics*, 22(2):299–308, mars 2004. (Cited page 33.)

S. CHENG, T. DEY, E. RAMOS et T. RAY : Sampling and meshing a surface with guaranteed topology and geometry. *SIAM Journal on Computing*, 37(4):1199–1227, 2007. (Cited page 37.)

S.-W. CHENG : *Delaunay mesh generation.* Chapman & Hall/CRC computer and information science series. CRC Press, Boca Raton, 2013. (Cited page 32.)

S.-W. CHENG, T. K. DEY et E. A. RAMOS : Delaunay refinement for piecewise smooth complexes. *Discrete and Computational Geometry*, 43(1):121–166, jan. 2009. (Cited page 37.)

S.-W. CHENG, T. K. DEY, E. A. RAMOS et T. RAY : Quality meshing of polyhedra with samll angles. *International Journal of Computational Geometry & Applications*, 15(04):421–461, août 2005. (Cited page 33.)

L. P. CHEW : Guaranteed-quality mesh generation for curved surfaces. *In Proceedings of the ninth annual symposium on Computational geometry*, p. 274–280. ACM Press, 1993. (Cited page 37.)

L. P. CHEW : Guaranteed-quality delaunay meshing in 3D (short version). *In Proceedings of the thirteenth annual symposium on Computational geometry*, p. 391–393. ACM Press, 1997. (Cited page 33.)

D. COHEN-STEINER, E. Colin de VERDIERE et M. YVINEC : Conforming delaunay triangulations in 3D. *Computational Geometry*, 28(2–3):217 – 233, 2004. (Cited page 33.)

E. Colin de VERDIÈRE, G. GINOT et X. GOAOC : Multinerves and helly numbers of acyclic families. *In Proceedings of the 2012 symposuim on Computational Geometry*, p. 209–218. ACM, 2012. (Cited page 56.)

B. COLLETTA, J. LETOUZEY, R. PINEDO, J. F. BALLARD et P. BALÉ : Computerized x-ray tomography analysis of sandbox models: Examples of thin-skinned thrust systems. *Geology*, 19(11):1063–1067, 1991. (Cited page 62.)

J. DARDENNE, S. VALETTE, N. SIAUVE, N. BURAIS et R. PROST : Variational tetrahedral mesh generation from discrete volume data. *The Visual Computer*, 25 (5-7):401–410, mars 2009. (Cited pages 33 and 35.)

J. DARDENNE : *Maillage 3D de structures anatomiques pour la simulation électro-magnétique et thermique.* Thèse, INSA de Lyon, nov. 2009. (Cited page 35.)

D. DEBAUN, T. BYER, P. CHILDS, J. CHEN, F. SAAF, M. WELLS, J. LIU, H. CAO, L. PIANELO, V. TILAKRAJ, P. CRUMPTON, D. WALSH, H. YARDUMIAN, R. ZORZYNSKI, K.-T. LIM, M. SCHRADER, V. ZAPATA, J. NOLEN et H. TCHELEPI : An extensible architecture for next generation scalable parallel reservoir simulation. *In SPE Reservoir Simulation Symposium.* Society of Petroleum Engineers, jan. 2005. (Cited page 24.)

B. DELAUNAY : Sur la sphere vide. *Izv. Akad. Nauk SSSR, Otdelenie Matematicheskii i Estestvennyka Nauk*, 7(793-800):1–2, 1934. (Cited pages 8 and 10.)

S. Dey, M. S. Shephard et M. K. Georges : Elimination of the adverse effects of small model features by the local modification of automatically generated meshes. *Engineering with Computers*, 13(3):134–152, sept. 1997. (Cited pages 27 and 29.)

T. K. Dey, J. A. Levine et A. Slatton : Localized delaunay refinement for sampling and meshing. *Computer Graphics Forum*, 29(5):1723–1732, sept. 2010. (Cited page 37.)

T. K. Dey et J. A. Levine : Delaunay meshing of piecewise smooth complexes without expensive predicates. *Algorithms*, 2(4):1327–1349, 2009. (Cited pages 35 and 37.)

Q. Du, V. Faber et M. Gunzburger : Centroidal voronoi tesselations: Applications and algorithms. *SIAM Review*, 41(4):637–676, 1999. (Cited page 15.)

Q. Du, M. Gunzburger et L. Ju : Constrained centroidal voronoi tessellations for surfaces. *SIAM Journal on Scientific Computing*, 24(5):1488–1506, 2003. (Cited pages 16 and 37.)

Q. Du et D. Wang : Tetrahedral mesh generation and optimization based on centroidal voronoi tessellations. *International Journal for Numerical Methods in Engineering*, 56(9):1355–1373, mars 2003. (Cited page 33.)

J. A. Dunbar et R. W. Cook : Palinspastic reconstruction of structure maps: an automated finite element approach with heterogeneous strain. *Journal of Structural Geology*, 25(7):1021–1036, juil. 2003. (Cited page 51.)

P. Durand-Riard : *Gestion de la complexité géologique en restauration géomécanique 3D.* Thèse de doctorat, INPL, 2010. (Cited pages 24 and 99.)

P. Durand-Riard, L. Salles, M. Ford, G. Caumon et J. Pellerin : Understanding the evolution of syn-depositional folds: Coupling decompaction and 3D sequential restoration. *Marine and Petroleum Geology*, 28(8):1530–1539, août 2011. (Cited pages 25 and 71.)

L. J. Durlofsky : Upscaling and gridding of fine scale geological models for flow simulation. *In 8th International Forum on Reservoir Simulation Iles Borromees, Stresa, Italy*, p. 20–24, 2005. (Cited page 28.)

V. Dyedov, D. R. Einstein, X. Jiao, A. P. Kuprat, J. P. Carson et F. del Pin : Variational generation of prismatic boundary-layer meshes for biomedical computing. *International Journal for Numerical Methods in Engineering*, 79(8): 907–945, août 2009. (Cited page 35.)

H. Edelsbrunner et N. Shah : Triangulating topological spaces. *International Journal of Computational Geometry & Applications*, 7(4):365–378, 1997. (Cited pages 11, 13, and 14.)

H. Edelsbrunner et E. P. Mücke : Simulation of simplicity: a technique to cope with degenerate cases in geometric algorithms. *ACM Transactions on Graphics*, 9 (1):66–104, jan. 1990. (Cited page 7.)

R. EYMARD, C. GUICHARD, R. HERBIN et R. MASSON : Vertex-centred discretization of multiphase compositional darcy flows on general meshes. *Computational Geosciences*, 16(4):987–1005, juin 2012. (Cited page 24.)

C. L. FARMER : Geological modelling and reservoir simulation. *In* A. ISKE et T. RANDEN, éds : *Mathematical Methods and Modelling in Hydrocarbon Exploration and Production*, vol. 7, p. 119–212. Springer-Verlag, Berlin/Heidelberg, 2005. (Cited pages 23, 24, 29, and 42.)

D. A. FIELD : Qualitative measures for initial meshes. *International Journal for Numerical Methods in Engineering*, 47(4):887–906, fév. 2000. (Cited page 26.)

N. FLANDRIN, H. BOROUCHAKI et C. BENNIS : 3D hybrid mesh generation for reservoir simulation. *International Journal for Numerical Methods in Engineering*, 65(10):1639–1672, mars 2006. (Cited page 24.)

S. FORTUNE : Voronoi diagrams and delaunay triangulations. *Computing in Euclidean geometry*, 1:193–233, 1992. (Cited page 10.)

P. J. FREY : About surface remeshing. *In Proceedings of 9th International Meshing Roundtable*, p. 123–136, 2000. (Cited page 36.)

P. J. FREY et H. BOROUCHAKI : Surface mesh quality evaluation. *International Journal for Numerical Methods in Engineering*, 45(1):101–118, mai 1999. (Cited page 61.)

P. J. FREY et P.-L. GEORGE : *Maillages : applications aux éléments finis.* Hermès Science, Paris, 1999. (Cited pages 20, 26, 29, and 31.)

R. V. GARIMELLA et M. S. SHEPHARD : Generation of tetrahedral meshes with multiple elements through thin sections. *Engineering with Computers*, 15(2):181–197, avr. 1999. (Cited page 35.)

R. V. GARIMELLA et M. S. SHEPHARD : Boundary layer mesh generation for viscous flow simulations. *International Journal for Numerical Methods in Engineering*, 49(1-2):193–218, sept. 2000. (Cited page 35.)

M. GARLAND et P. S. HECKBERT : Surface simplification using quadric error metrics. *In Proceedings of the 24th annual conference on Computer graphics and interactive techniques*, p. 209–216. ACM Press, 1997. (Cited page 28.)

A. GELAS, S. VALETTE, R. PROST et W. L. NOWINSKI : Variational implicit surface meshing. *Computers & Graphics*, 33(3):312 – 320, 2009. (Cited page 37.)

P. L. GEORGE et H. BOROUCHAKI : *Triangulation de Delaunay et maillage: applications aux elements finis.* Hermes, Paris, 1997. (Cited page 32.)

P. L. GEORGE, F. HECHT et E. SALTEL : Automatic mesh generator with specified boundary. *Computer methods in applied mechanics and engineering*, 92(3):269–288, 1991. (Cited page 33.)

C. Geuzaine et J.-F. Remacle : Gmsh: A 3-D finite element mesh generator with built-in pre-and post-processing facilities. *International Journal for Numerical Methods in Engineering*, 79(11):1309–1331, 2009. (Cited pages 36 and 100.)

R. H. J. Groshong : *3-D structural geology: a practical guide to quantitative surface and subsurface map interpretation.* Springer, New York, 2 édn, 2008. (Cited page 42.)

C. A. Guzofski, J. P. Mueller, J. H. Shaw, P. Muron, D. A. Medwedeff, F. Bilotti et C. Rivero : Insights into the mechanisms of fault-related folding provided by volumetric structural restorations using spatially varying mechanical constraints. *AAPG Bulletin*, 93(4):479–502, avr. 2009. (Cited page 62.)

H. Hoppe, T. DeRose, T. Duchamp, J. McDonald et W. Stuetzle : Surface reconstruction from unorganized points. *In Proceedings of the 19th annual conference on Computer graphics and interactive techniques*, p. 71–78. ACM Press, 1992. (Cited page 37.)

Y. Ito, A. M. Shih et B. K. Soni : Hybrid mesh generation with embedded surfaces using a multiple marching direction approach. *International Journal for Numerical Methods in Fluids*, 67(1):1–7, sept. 2011. (Cited page 35.)

X. Jiao : Face offsetting: A unified approach for explicit moving interfaces. *Journal of Computational Physics*, 220(2):612–625, jan. 2007. (Cited page 35.)

S. J. Jolley, D. Barr, J. J. Walsh et R. J. Knipe : Structurally complex reservoirs: an introduction. *Geological Society, London, Special Publications*, 292(1):1–24, jan. 2007. (Cited pages 39 and 42.)

A. G. Journel : *Mining geostatistics.* Blackburn Press, Caldwell, N.J, 2003. (Cited page 48.)

P. M. Knupp : Remarks on mesh quality. *In 45th AIAA Aerospace Sciences Meeting and Exhibit*, p. 7–10, 2007. (Cited page 26.)

J. H. Kruhl : Fractal-geometry techniques in the quantification of complex rock structures: A special view on scaling regimes, inhomogeneity and anisotropy. *Journal of Structural Geology*, 46(0):2–21, jan. 2013. (Cited page 28.)

F. Labelle et J. R. Shewchuk : Isosurface stuffing. *ACM Transactions on Graphics*, 26(3):57, juil. 2007. (Cited page 31.)

F. Lallier : *Corrélation stratigraphique stochastique de puits.* Thèse, Université de Lorraine, mars 2012. (Cited page 42.)

T. J. Lasseter et S. A. Jackson : Improving integrated interpretation accuracy and efficiency using a single consistent reservoir model from seismic to simulation. *The Leading Edge*, 23(11):1118–1121, nov. 2004. (Cited page 24.)

G. Laurent : *Prise en compte de l'histoire géologique des structures dans la création de modèles numériques 3D compatibles.* Thèse, Université de Lorraine, 2013. (Cited page 62.)

P. G. LELIEVRE, C. G. FARQUHARSON et C. A. HURICH : Joint inversion of seismic traveltimes and gravity data on unstructured grids with application to mineral exploration. *Geophysics*, 77(1):K1–K15, fév. 2012. (Cited pages 25 and 71.)

F. LEPAGE : *Génération de maillages tridimensionnels pour la simulation des phénomènes physiques en géosciences.* Thèse, INPL, Nancy, France, 2003. (Cited pages 24 and 34.)

R. LÖHNER : Regridding surface triangulations. *Journal of Computational Physics*, 126(1):1 – 10, 1996. (Cited page 36.)

R. LÖHNER et P. PARIKH : Generation of three-dimensional unstructured grids by the advancing-front method. *International Journal for Numerical Methods in Fluids*, 8(10):1135–1149, oct. 1988. (Cited page 31.)

M. D. LINDSAY, M. W. JESSELL, L. AILLERES, S. PERROUTY, E. d. KEMP et P. G. BETTS : Geodiversity: Exploration of 3D geological model space. *Tectonophysics*, 594(0):27–37, 2013. (Cited page 28.)

L. LIU, Y. ZHAO et T. SUN : 3D computational shape- and cooling process-modeling of magmatic intrusion and its implication for genesis and exploration of intrusion-related ore deposits: An example from the yueshan intrusion in anqing, china. *Tectonophysics*, 526–529(0):110–123, mars 2012. (Cited pages 25 and 71.)

Y. LIU, W. WANG, B. LÉVY, F. SUN et D.-M. YAN : On centroidal voronoi tessellation - energy smoothness and fast computation. *In ACM Transactions Graphics*, p. 1–17, 2009. (Cited pages 16, 17, 37, and 55.)

S. LLOYD : Least squares quantization in PCM. *Information Theory, IEEE Transactions on*, 28(2):129–137, mars 1982. (Cited page 16.)

A. LOSEILLE : *Adaptation de maillage anisotrope 3D multi-échelles et ciblée à une fonctionnelle pour la mécanique des fluides. Application à la prédiction haute-fidélité du bang sonique.* Thèse, Université Pierre et Marie Curie-Paris VI, 2008. (Cited page 29.)

A. LOSEILLE et R. LÖHNER : Robust boundary layer mesh generation. *In Proceedings of the 21st International Meshing Roundtable*, p. 493–511. Springer, 2013. (Cited page 35.)

X.-J. LUO, M. S. SHEPHARD, R. M. O'BARA, R. NASTASIA et M. W. BEALL : Automatic p-version mesh generation for curved domains. *Engineering with Computers*, 20(3):273–285, juil. 2004. (Cited page 29.)

X.-J. LUO, M. S. SHEPHARD, L.-Z. YIN, R. M. O'BARA, R. NASTASI et M. W. BEALL : Construction of near optimal meshes for 3D curved domains with thin sections and singularities for p-version method. *Engineering with Computers*, 26 (3):215–229, jan. 2010. (Cited page 35.)

B. LÉVY et N. BONNEEL : Variational anisotropic surface meshing with voronoi parallel linear enumeration. *In X. JIAO et J.-C. WEILL, éds : Proceedings of the 21st International Meshing Roundtable*, p. 349–366. Springer Berlin Heidelberg, Berlin, Heidelberg, 2013. (Cited pages 37, 54, and 55.)

B. Lévy et Y. Liu : L_p centroidal voronoi tessellation and its applications. *ACM Transactions on Graphics*, 29(4):1, juil. 2010. (Cited pages 12, 17, 33, 37, and 54.)

J.-L. Mallet : Space–Time mathematical framework for sedimentary geology. *Mathematical Geology*, 36(1):1–32, jan. 2004. (Cited pages 25 and 71.)

T. Manzocchi, J. J. Walsh, P. Nell et G. Yielding : Fault transmissibility multipliers for flow simulation models. *Petroleum Geoscience*, 5(1):53–63, fév. 1999. (Cited page 28.)

E. Marchandise, C. Geuzaine et J. Remacle : Cardiovascular and lung mesh generation based on centerlines. *International Journal for Numerical Methods in Biomedical Engineering*, 29(6):665–682, juin 2013. (Cited page 35.)

U. T. Mello, J. R. P. Rodrigues et A. L. Rossa : A control-volume finite-element method for three-dimensional multiphase basin modeling. *Marine and Petroleum Geology*, 26(4):504–518, 2009. (Cited page 23.)

R. Merland : *Génération de grilles de type volumes finis : adaptation à un modèle structural, pétrophysique et dynamique.* Thèse, Université de Lorraine, avr. 2013. (Cited pages 12, 17, and 24.)

A. Mohamed et C. Davatzikos : Finite element mesh generation and remeshing from segmented medical images. *In Proc. IEEE International Symposium on Biomedical Imaging: Nano to Macro*, vol. 2, p. 420–423. IEEE, 2004. (Cited page 34.)

I. Moretti, F. Lepage et M. Guiton : Une nouvelle méthode de restauration 3D basée sur une approche couplée géométrie-mécanique. *Oil & Gas Science and Technology - Rev. IFP*, 61(2):277–289, 2006. (Cited page 25.)

I. Moretti : Working in complex areas: New restoration workflow based on quality control, 2D and 3D restorations. *Marine and Petroleum Geology*, 25(3):205–218, mars 2008. (Cited page 25.)

H. Mustapha, R. Dimitrakopoulos, T. Graf et A. Firoozabadi : An efficient method for discretizing 3D fractured media for subsurface flow and transport simulations. *International Journal for Numerical Methods in Fluids*, 67(5):651–670, 2011. (Cited page 28.)

H. Mustapha et K. Mustapha : A new approach to simulating flow in discrete fracture networks with an optimized mesh. *SIAM Journal on Scientific Computing*, 29(4):1439–1459, jan. 2007. (Cited page 25.)

V. Nivoliers : *Échantillonnage pour l'approximation de fonctions sur des maillages.* Thèse, Université de Lorraine, 2012. (Cited page 12.)

J. Nocedal : Updating quasi-newton matrices with limited storage. *Mathematics of computation*, 35(151):773–782, 1980. (Cited page 54.)

A. Okabe, B. Boots, K. Sugihara et S. N. Chiu : *Spatial tessellations: concepts and applications of Voronoi diagrams*, vol. 501. Wiley, 2009. (Cited pages 7, 8, and 10.)

S. J. OWEN et T. R. SHELTON : Validation of grid-based hex meshes with computational solid mechanics. *In Proceedings of the 22nd International Meshing Roundtable*, p. 39–56. Springer, 2014. (Cited page 25.)

J. PELLERIN, B. LÉVY et G. CAUMON : Topological control for isotropic remeshing of nonmanifold surfaces with varying resolution: application to 3D structural models. *In Proc. IAMG*. cogeo@oeaw-giscience, sept. 2011. (Cited pages 6, 51, and 85.)

J. PELLERIN, B. LÉVY et G. CAUMON : A voronoi-based hybrid meshing method. *In International Meshing Roundtable, Research Notes*, oct. 2012. (Cited pages 6, 71, and 85.)

J. PELLERIN, B. LÉVY, G. CAUMON et A. BOTELLA : Automatic surface remeshing of 3D structural models at specified resolution: A method based on voronoi diagrams. *Computers & Geosciences*, 62(0):103 – 116, 2014. (Cited pages 6, 51, and 85.)

G. PEYRÉ et L. D. COHEN : Geodesic remeshing using front propagation. *International Journal of Computer Vision*, 69(1):145–156, mai 2006. (Cited page 36.)

M. PRÉVOST, F. LEPAGE, L. J. DURLOFSKY et J.-L. MALLET : Unstructured 3D gridding and upscaling for coarse modelling of geometrically complex reservoirs. *Petroleum Geoscience*, 11(4):339–345, oct. 2005. (Cited page 34.)

W. R. QUADROS et S. J. OWEN : Defeaturing CAD models using a geometry-based size field and facet-based reduction operators. *Engineering with Computers*, 28 (3):211–224, fév. 2012. (Cited pages 27 and 28.)

W. R. QUADROS, S. J. OWEN, M. L. BREWER et K. SHIMADA : Finite element mesh sizing for surfaces using skeleton. *In Proc. 13th International Meshing Roundtable*, p. 389–400, 2004. (Cited pages 29, 40, and 50.)

L. RINEAU et M. YVINEC : A generic software design for delaunay refinement meshing. *Computational Geometry*, 38(1–2):100–110, 2007. (Cited page 33.)

T. ROBINSON, C. ARMSTRONG et R. FAIREY : Automated mixed dimensional modelling from 2D and 3D CAD models. *Finite Elements in Analysis and Design*, 47 (2):151–165, fév. 2011. (Cited pages 28 and 86.)

J. RUPPERT : A delaunay refinement algorithm for quality 2-dimensional mesh generation. *Journal of Algorithms*, 18(3):548–585, 1995. (Cited page 14.)

Y. SAAD : *Iterative methods for sparse linear systems*. SIAM, Philadelphia, 2 édn, 2003. (Cited page 23.)

O. SAHNI, K. E. JANSEN, M. S. SHEPHARD, C. A. TAYLOR et M. W. BEALL : Adaptive boundary layer meshing for viscous flow simulations. *Engineering with Computers*, 24(3):267–285, avr. 2008. (Cited page 35.)

L. SALLES, M. FORD, P. JOSEPH, C. DE VESLUD et A. LE SOLLEUZ : Migration of a synclinal depocentre from turbidite growth strata: the annot syncline, SE france. *Bulletin de la Sociéte Géologique de France*, 182(3):199–220, 2011. (Cited page 62.)

W. SASSI, B. COLLETTA, P. BALÉ et T. PAQUEREAU : Modelling of structural complexity in sedimentary basins: The role of pre-existing faults in thrust tectonics. *Tectonophysics*, 226(1-4):97–112, nov. 1993. (Cited page 39.)

J. SCHÖBERL : NETGEN an advancing front 2D/3D-mesh generator based on abstract rules. *Computing and Visualization in Science*, 1(1):41–52, juil. 1997. (Cited page 32.)

A. SHEFFER : Model simplification for meshing using face clustering. *Computer-Aided Design*, 33(13):925–934, 2001. (Cited page 28.)

M. S. SHEPHARD, M. W. BEALL et R. M. O'BARA : Revisiting the elimination of the adverse effects of small model features in automatically generated meshes. *In Proc. 7th International Meshing Roundtable*, p. 119–132, 1998. (Cited page 28.)

M. S. SHEPHARD et M. K. GEORGES : Automatic three-dimensional mesh generation by the finite octree technique. *International Journal for Numerical Methods in Engineering*, 32(4):709–749, sept. 1991. (Cited pages 31 and 36.)

J. R. SHEWCHUK : Tetrahedral mesh generation by delaunay refinement. *In Proceedings of the fourteenth annual symposium on Computational geometry*, p. 86–95. ACM, 1998. (Cited page 33.)

J. R. SHEWCHUK : Constrained delaunay tetrahedralizations and provably good boundary recovery. *In Proc. 11th International Meshing Roundtable*, p. 193–204, 2002a. (Cited page 33.)

J. R. SHEWCHUK : Delaunay refinement algorithms for triangular mesh generation. *Computational Geometry*, 22(1):21 – 74, 2002b. (Cited page 33.)

J. R. SHEWCHUK : *Lecture notes on Delaunay mesh generation*. Department of Electrical Engineering and Computer Science, University of California at Berkeley, 2012. (Cited pages 27, 32, and 99.)

H. SI : Adaptive tetrahedral mesh generation by constrained delaunay refinement. *International Journal for Numerical Methods in Engineering*, 75(7):856–880, août 2008. (Cited page 33.)

H. SI et K. GÄRTNER : 3D boundary recovery by constrained delaunay tetrahedralization. *International Journal for Numerical Methods in Engineering*, 85(11):1341–1364, mars 2011. (Cited page 33.)

H. SI : Constrained delaunay tetrahedral mesh generation and refinement. *Finite Elements in Analysis and Design*, 46(1–2):33 – 46, 2010. (Cited page 33.)

O. SIFRI, A. SHEFFER et C. GOTSMAN : Geodesic-based surface remeshing. *In Proc. 12th International Meshing Roundtable*, p. 189–199, 2003. (Cited page 36.)

J. M. SULLIVAN, G. CHARRON et K. D. PAULSEN : A three-dimensional mesh generator for arbitrary multiple material domains. *Finite Elements in Analysis and Design*, 25(3–4):219–241, 1997. (Cited page 34.)

V. Surazhsky, P. Alliez et C. Gotsman : Isotropic remeshing of surfaces: a local parameterization approach. *In Proc. 12th International Meshing Roundtable*, p. 215–224, 2003. (Cited page 37.)

C. Sword, B. Mallison, W. Milliken, T. Viard et A. Cheng : Unstructured cut-cell grids for modeling complex reservoirs. *In SPE Reservoir Simulation Symposium*, The Woodlands, TX, USA, fév. 2013. Society of Petroleum Engineers. (Cited page 24.)

Z. Tavassoli, J. N. Carter et P. R. King : An analysis of history matching errors. *Computational Geosciences*, 9(2-3):99–123, nov. 2005. (Cited page 42.)

A. Thakur, A. G. Banerjee et S. K. Gupta : A survey of CAD model simplification techniques for physics-based simulation applications. *Computer-Aided Design*, 41 (2):65–80, fév. 2009. (Cited page 28.)

J. F. Thompson, B. K. Soni et N. P. Weatherill : *Handbook of grid generation.* CRC Press, Boca Raton, Fla., 1999. (Cited page 29.)

J. Tournois : *Optimisation de maillages.* Thèse, Université Nice Sophia Antipolis, nov. 2009. (Cited page 33.)

J. Tournois, C. Wormser, P. Alliez et M. Desbrun : Interleaving delaunay refinement and optimization for practical isotropic tetrahedron mesh generation. *ACM Transactions on Graphics*, 28(3):1, juil. 2009. (Cited page 33.)

D. L. Turcotte : *Geodynamics.* Cambridge University Press, Cambridge ; New York, 2 édn, 2002. (Cited page 23.)

S. Valette et J.-M. Chassery : Approximated centroidal voronoi diagrams for uniform polygonal mesh coarsening. *Computer Graphics Forum*, 23(3):381–389, sept. 2004. (Cited page 37.)

S. Valette, J.-M. Chassery et R. Prost : Generic remeshing of 3D triangular meshes with metric-dependent discrete voronoi diagrams. *IEEE Transactions on Visualization and Computer Graphics*, 14(2):369–381, 2008. (Cited pages 37, 38, and 100.)

O. Vidal-Royo, N. Cardozo, J. A. Munoz, S. Hardy et L. Maerten : Multiple mechanisms driving detachment folding as deduced from 3D reconstruction and geomechanical restoration: the Pico del Águila anticline (External Sierras, Southern Pyrenees). *Basin Research*, 24(3):295–313, juin 2012. (Cited pages 25 and 71.)

G. Voronoï : Nouvelles applications des paramètres continus à la théorie des formes quadratiques. Deuxième mémoire. Recherches sur les parallélloèdres primitifs. *Journal für die reine und angewandte Mathematik*, 134:198–287, 1908. (Cited page 7.)

J. Wang et Z. Yu : Feature-sensitive tetrahedral mesh generation with guaranteed quality. *Computer-Aided Design*, 44(5):400–412, mai 2012. (Cited page 31.)

D. R. WHITE, S. SAIGAL et S. J. OWEN : Meshing complexity: predicting meshing difficulty for single part CAD models. *Engineering with Computers*, 21(1):76–90, nov. 2005. (Cited page 40.)

D.-M. YAN, B. LÉVY, Y. LIU, F. SUN et W. WANG : Isotropic remeshing with fast and exact computation of restricted voronoi diagram. *ACM/EG Symposium on Geometry Processing / Computer Graphics Forum*, 28(5):1145–1454, 2009. (Cited pages 12, 17, 37, and 54.)

J. ZHANG, M. EMELIANENKO et Q. DU : Periodic centroidal voronoi tessellations. *International Journal of Numerical Analysis and Modeling*, 9(4):950–969, 2012. (Cited page 17.)

Y. ZHANG, T. J. HUGHES et C. L. BAJAJ : An automatic 3D mesh generation method for domains with multiple materials. *Computer Methods in Applied Mechanics and Engineering*, 199(5-8):405–415, jan. 2010. (Cited page 34.)

List of Figures

List of Tables

List of Algorithms

Accounting for the geometrical complexity of geological structural models in Voronoi-based meshing methods

Abstract: Depending on the specific method used to build a 3D structural model, and on the exact purpose of this model, its mesh must be adapted so that it enforces criteria on element types, maximum number of elements, and mesh quality. Meshing methods developed for applications others than geomodeling forbid any modification of the input model, that may be desirable in geomodeling to better control the number of elements in the final mesh and their quality.

The objective of this thesis is to develop meshing methods that fulfill this requirement to better manage the geometrical complexity of B-Rep geological structural models. An analysis of the sources of geometrical complexity in those models is first proposed. The introduced measures are a first step toward the definition of tools allowing objective comparisons of structural models and permit to characterize the model zones that are more complicated to mesh. We then introduce two original meshing methods based on Voronoi diagrams: the first for surface remeshing, the second for hybrid gridding. The key ideas of these methods are identical: (1) the use of a centroidal Voronoi optimization to have a globally controlled number of elements of good quality, and (2) combinatorial considerations to locally build the final mesh while sometimes modifying the initial model. The surface remeshing method is automatic and permits to simplify a model at a given resolution. The gridding method generates a hybrid volumetric mesh. Prisms and pyramids fill the very thin layers of the model while the remaining regions are filled with tetrahedra.

Keywords: B-Rep geological model, centroidal Voronoi diagram, restricted Voronoi diagram, restricted Delaunay triangulation

---

Prise en compte de la complexité géométrique des modèles structuraux dans des méthodes de maillage fondées sur le diagramme de Voronoï

Résumé : Selon la méthode utilisée pour construire un modèle structural en trois dimensions et selon l'application à laquelle il est destiné, son maillage, en d'autres termes sa représentation informatique, doit être adapté afin de respecter des critères de type, de nombre et de qualité de ses éléments. Les méthodes de maillage développées dans d'autres domaines que la géomodélisation ne permettent pas de modifier le modèle d'entrée. Ceci est souhaitable en géomodélisation afin de mieux contrôler le nombre d'éléments du maillage et leur qualité.

L'objectif de cette thèse est de développer des méthodes de maillage permettant de remplir ces objectifs afin de gérer la complexité géométrique des modèles structuraux définis par frontières. Premièrement, une analyse des sources de complexité géométrique dans ces modèles est proposée. Les mesures développées constituent une première étape dans la définition d'outils permettant la comparaison objective de différents modèles et aident à caractériser précisément les zones plus compliquées à mailler dans un modèle. Ensuite, des méthodes originales de remaillage surfacique et de maillage volumique fondées sur l'utilisation des diagrammes de Voronoï sont proposées. Les fondements de ces deux méthodes sont identiques : (1) une optimisation de type Voronoï barycentrique est utilisée pour globalement obtenir un nombre contrôlé d'éléments de bonne qualité et (2) des considérations combinatoires permettant de construire localement le maillage final, éventuellement en modifiant le modèle initial. La méthode de remaillage surfacique est automatique et permet de simplifier un modèle à une résolution donnée. L'originalité de la méthode de maillage volumique est que les éléments générés sont de types différents. Des prismes et pyramides sont utilisés pour remplir les zones très fines du modèle, tandis que le reste du modèle est rempli avec des tétraèdres.

Mots-clés : modèle géologique défini par frontières, diagramme de Voronoï barycentrique, diagramme de Voronoï restreint, triangulation de Delaunay restreinte